University of Turin
PhD Programme in Complex Systems for Life Sciences
Department of Oncology

XXXIV cycle

Academic Years 2018/2021

Preclinical exploration of a novel cellular immunotherapy with CAR-redirected cytokine-induced killer lymphocytes (CIK) against soft tissue sarcomas

Coordinator:
Prof. **Enzo Medico**

Tutor:
Prof. **Dario Sangiolo**

Co-tutor:
Dr. **Valeria Leuci**

PhD student:
Dr. **Chiara Donini**

TABLE OF CONTENTS

Abstract

Purpose

Cellular immunotherapy based on Cytokine-Induced Killer lymphocytes (CIK) has become a promising therapeutic approach against cancer. CIK are ex-vivo expanded lymphocytes, with a mixed T/NK phenotype with HLA-independent antitumor activity. The advent of Chimeric Antigen Receptor (CAR) therapies has marked a new immuno-oncology era. Engineering of CAR.CIK has the intent of generating bi-potential killers that conjugate the CAR-specificity with the intrinsic NKG2D-mediated antitumor capacity, providing an intriguing approach for treating solid tumors, including advanced incurable soft tissue sarcomas (STS).

We explored a novel cellular immunotherapy with CAR.CIK specific for the tumor-promoting antigen CSPG4 against multiple histotypes of STS, exploiting also TME-resembling challenging metabolic conditions to study CAR.CIK in energetic hostile environment and exploring progressively more complex 3D STS models to visualize CAR.CIK migration, invasion and to characterize the STS TME.

Experimental Design

Both CAR.CIK and STS of multiple histotypes were derived from patients. The functional activity of CSPG4-CAR.CIK was explored *in vitro*, in 2D and 3D models, and *in vivo*, in xenograft models. In selected experiments, challenging culture conditions of glucose deprivation ([Glucose]=5 and 0,5 mM) ± hypoxia (O_2=1%) were used to mimic the hostile TME of solid tumors.

Results

CSPG4-CAR.CIK were efficiently generated by STS patients (n=9).

Mean anti-CSPG4 CAR expression was 47%±6. CAR.CIK *ex vivo* expansion rates (159 fold, range 27-348) and phenotype (e.g. CD8: 70%±4; CD56: 38%±4, NKG2D: 68%±6) were comparable to paired unmodified CIK.

The membrane expression of CSPG4 was confirmed and quantified in all patient-derived STS cell lines (n=16).

CSPG4-CAR.CIK demonstrated a potent *in vitro* tumor-specific killing activity, significantly superior to paired unmodified CIK (n=24; $p<0.0001$). Importantly, the superiority of CSPG4-CAR.CIK anti-tumor activity was particularly evident at very low effector:target (E:T) ratios (up to 1:64; n=7; $p<0.001$). At clinically relevant E:T ratios, CSPG4-CAR.CIK spared human keratinocytes with low CSPG4 membrane expression (n=5).

CAR.CIK anti-tumor activity was not impaired by challenging metabolic conditions *in vitro*. Tumor killing by CAR.CIK was 2-fold higher than unmodified CIK in each metabolic condition (E:T 1:1, n=4, $p \leq 0.001$) and CAR.CIK demonstrated higher glucose uptake capability (about 2-fold) compared with unmodified CIK (n=2).

In 3D STS spheroids CSPG4-CAR.CIK showed higher penetration ability through Matrigel matrix (n=5, $p \leq 0.05$), tumor infiltration (n=8, $p \leq 0.01$) and killing (n=3, $p < 0.0001$) compared with paired unmodified CIK.

In the attempt of identifying and describing STS TME elements, we characterized STS infiltrating immune cells from fresh surgical samples (n=7) and patient-derived organotypic spheroids (n=7), reporting tumor-infiltrating lymphocytes (26%±6), NK cells (35%±11), immunosuppressive T_{regs} (13%±6), PMN-MDSCs (37%±11) and monocyte-MDSC (21%±6).

In vivo, CAR.CIK significantly delayed or reversed tumor growth in three STS xenograft models ($p < 0.0001$), with tumor infiltration by CAR.CIK confirmed by IHC. In dedicated cohorts, we did not observe any significant synergism by the simultaneous PD-1 blockage.

Conclusions

We successfully generated and characterized anti-CSPG4-CAR.CIK from patients with advanced STS, reporting their intense preclinical anti-tumor activity against multiple STS histotypes. Our findings support CIK as valuable platform for CAR redirection, providing reliable rationale to promote clinical studies with CAR.CIK in the challenging field of advanced incurable STS.

Introduction: State of art and rationale of the study

1. Soft Tissue Sarcomas: Pathology and treatment landscape

Sarcomas represent heterogeneous malignant tumors of mesenchymal origin including more than 50 distinct diagnoses. They are characterized by low incidence (1% of all adult malignancies and 10-15% of paediatric malignancies) but in most cases by poor prognosis (*1-3*). Sarcomas can be grouped into two main classes: soft tissue sarcomas (STS) and bone sarcomas or osteosarcomas.

The term soft tissue refers to tissue that connect, support or surround body structures and organs, including muscles, tendons, fibrous tissues, fat, blood vessels, nerves and synovial tissues (Figure 1). STS include different histotypes but are characterized by similar symptoms and treatment modalities.

Treatment options vary according to type, stage, grade of STS, possible side effects, patient comorbidities and performance status. Surgery is the first-choice for localized STS to obtain disease local control (*4, 5*).

Radiotherapy is indicated before surgery to reduce tumor size and improve the radicality of loco-regional surgery in case of voluminous masses or critical mass locations. After surgery chemo- or radio-therapy are often used to reduce risk of local recurrence.

Chemotherapy is used as neo-adjuvant therapy to reduce primary tumor size or after surgery as adjuvant therapy in presence of very aggressive forms to reduce risk of local and distant recurrence. Chemotherapy is the treatment of choice for metastatic disease.

Most active drugs include anthracyclines and ifosfamide alone or in combination, decarbonize, gemcitabine, taxanes, etoposide, vinorelbine and trabectedin (*6-9*).

Even if surgery together with pre- or post-operative radiotherapy or chemo-radiotherapy improved outcomes of patients with localized disease, 25-50% of patients develop recurrent and/or metastatic disease after surgery and complete responses to chemotherapy for metastatic STS are rare with a prognosis characterized by a median survival of 10-20 months (*6, 7, 10-12*).

One example of the greatest success in STS is targeted therapy with imatinib mesylate in Gastrointestinal Stromal Tumors (GIST) characterized by activating KIT and platelet-derived growth factor receptor (PDGFR) mutations in approximately 80% of cases (*13-15*). Imatinib treatment resulted in partial response or stable disease for more than 85% of patients, improving overall survival (*16, 17*).

Despite initial success, the mainstay of treatment in STS has no other breakthroughs.

For these reasons research and development of new and effective therapies to treat STS patients are needed.

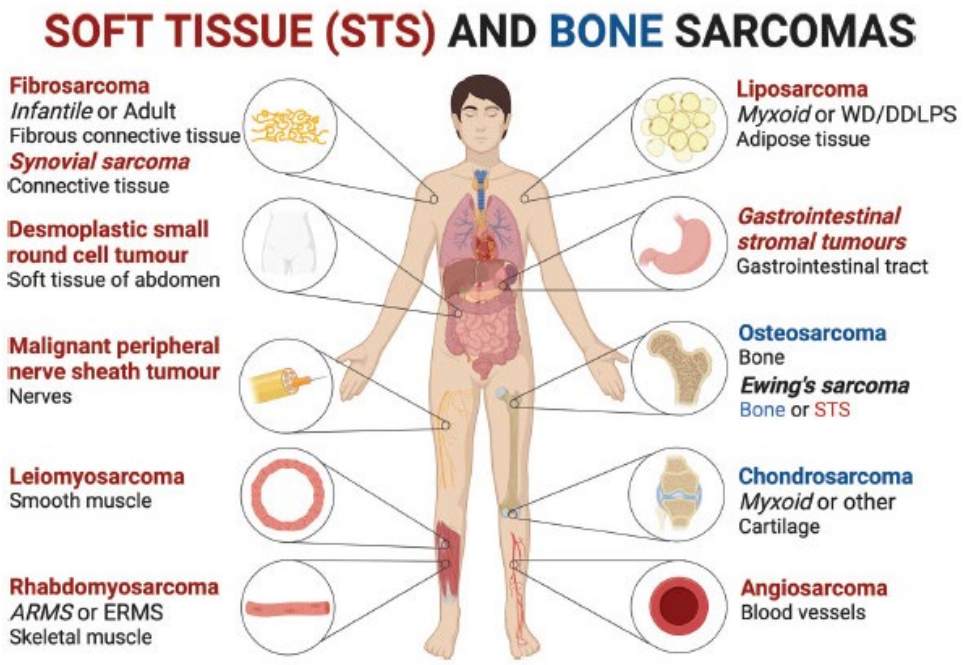

Figure 1. **Schematic representation of the most frequently occurring sarcomas**
Soft tissue sarcomas are highlighted in red and bone sarcomas are highlighted in blue. Related affected tissues are indicated.
Adapted from Damerell et al, *Molecular mechanisms underpinning sarcomas and implications for current and future therapy*, 2021.
Abbreviations: STS, Soft Tissue Sarcomas; ARMS, Alveolar Rhabdomyosarcoma; ERMS, Embryonal Rhabdomyosarcoma; WD/DDLPS Well-Differentiated/Dedifferentiated Liposarcoma.

2. The emerging role of immunotherapy for the treatment of STS

Immuno-oncology field has showed that immune system plays an important role in tumor surveillance, prevention, development and progression, while immune evasion by cancer cells has been established as a hallmark of cancer (*18*).

Impressive results are obtained by immunotherapy in melanoma, non-small cell lung cancer, prostate cancer and renal cell carcinoma *(2, 19-21)*. Lack of effective therapies in STS coupled with immunotherapy success in other tumors generates a growing interest in extending immunotherapy also to STS *(1, 2).* Like other types of malignant tumors, immunological approaches for STS treatment include: *i) cancer vaccines, ii) immune checkpoint inhibitors (ICIs), iii) adoptive cell therapies (ACT) (1, 2, 20, 21)*.

2.1 Cancer Vaccines

Despite many clinical trials have been carried out with cancer vaccines in different tumors, limited results have been obtained in STS and currently only a few vaccines have been approved by FDA (*22-24*).

A main critical point in cancer vaccines is the identification of tumor specific antigens, which are tumor-overexpressed proteins or specific mutated proteins on cell surface. Despite sarcoma heterogeneity, some STS showed specific genetic abnormalities (e.g. chromosomal translocations) or over-expressed specific cancer testis antigens (CTAs, e.g. NY-ESO-1, MAGE) that could be excellent candidates for cancer vaccines.

Different types of vaccines have been investigated for STS in clinical trials, based on: *i) tumor antigens (e.g. CTAs), ii) specific fusion proteins, iii) pulsed autologous antigen presenting cells (APCs) loaded with cancer antigens (e.g. dendritic cells (DCs)-based vaccines), iv) ganglioside (e.g. GD2).*

A clinical trial (*25, 26*) showed that the NY-ESO-1 vaccine was efficacy when combined with a saponin-based immunologic adjuvant, ISCOMATRIX, that induced a strong T-cell based immune response overcoming suppressive tumor microenvironment (TME) effects. Similar results were reported with NY-ESO-1 vaccine in combination with GM-CSF (sargramostim) that increased the number of immune cells in bone marrow and peripheral blood, improving vaccine efficacy (NCT00027911).

Overexpression of CTAs in STS seemed to be linked to epigenetic mechanisms such as hypomethylation of relative gene promoters (*25, 27*). Some clinical trials (NCT01241162, NCT01803152) (*28, 29*) are exploring combination therapy based on CTAs-derived cancer vaccines and epigenetic compounds (e.g. decitabine) in STS.

Synovial sarcoma is characterized by chromosomal translocation (X, 18; p11q11) that results in generation of SYT-SSX or SS18-SSX fusion protein. Combination of SYT-SSX fusion peptide fragment vaccine with IFNα showed increased disease control rate compared with the arm of vaccine as single agent (*30-32*).

Cancer vaccines can be build using autologous APCs (DCs-based vaccines), that can be obtained by leukapheresis, stimulated with tumor specific antigens and reintroduced into patients. They present tumor antigens through MHC class I and II to T lymphocytes triggering an immune response against cancer cells, circumventing immune evasion based on lacking of tumor antigen presentation and downregulation of MHC complex on cancer cells (*33-36*).

In a phase I clinical trial (*37*), STS patients were treated with DCs-based vaccine in combination with radiation that increases release of antigens to DCs inside the tumor site. Accumulation of $CD4^+$ T cells into tumor site positively correlated to clinical response. Another phase I clinical study (*38*) used engineered DCs to induced NY-ESO-1 expression obtaining 1 partial response and 14 stable diseases.
Ganglioside vaccines (GD2) were tested in STS in a phase II clinical trial but no significant outcomes were observed.
Summarizing, cancer vaccines induced tumor-specific immune response that resulted in clinical benefit in some STS patients with no radiographic improvements (*2*).

2.2 Immune checkpoint inhibitors (ICIs)

A way to manipulate immune system to induce an anti-tumor response is targeting molecules or interactions that suppress the immune response. Normally, inhibitory checkpoints are molecules expressed by immune cells to avoid attack of healthy autologous cells during immune response (autoimmune reaction). Cancer cells exploit these immune checkpoints as a way to evade immune recognition and elimination.
By blocking inhibitory immune checkpoints with monoclonal antibodies, immune system can overcome tumor immune evasion and anti-tumor immune response can be elicited.
CTLA-4 (Cytotoxic T-Lymphocyte Antigen 4) is a homologous receptor to CD28 expressed by T cells and it binds the co-stimulatory molecule B7 on APCs, mediating the inhibition of T cell priming (Figure 2A).
PD-1 (Programmed cell Death 1) is a receptor expressed on activated T cells and its ligands, PD-L1 and PD-L2 (Programmed cell Death Ligand 1-2), are expressed by DCs or macrophages and, in many cases, are overexpressed on tumor cells. PD-L1/2 engagement by PD-1 on activated T cells causes T cell exhaustion and anergy, having a leading role in cancer immune evasion (Figure 2B).
Encouraging results has obtained with ICIs in several cancer types.
Anti-CTLA-4 monoclonal antibody (ipilimumab) was FDA approved for treatment of melanoma in 2011. A phase II study (NCT00140855) of ipilimumab in advanced synovial sarcoma produced unsuccessful results and was closed prematurely because none of patients experienced an objective response (*39*).
Anti-PD-1 monoclonal antibodies (pembrolizumab, nivolumab) are indicated for the treatment of non-small cell lung cancer, Hodgkin lymphoma, B-cell lymphoma, urothelial carcinoma and it has been tested for STS but only few patients respond (*40, 41*).

SARC028 is a nonrandomized multi-cohort phase II study in which 86 patients with STS or bone sarcomas were treated with pembrolizumab (200 mg intravenously every 3 weeks). At a median follow up of 17.8 months, objective response rate was 18% and 12-week progression free survival was 55%. These results included 3 partial responses and 1 complete response of patients with undifferentiated pleomorphic sarcoma (UPS), 2 partial responses of patients with dedifferentiated liposarcoma and 1 partial response of patient with synovial sarcoma. No responses were seen in leiomyosarcoma patients.

Pre-treatment biopsies showed 5% of PD-L1^{+} and CD8^{+} TILs positive UPS. Generally, STS showed to be more responsive to pembrolizumab than bone sarcomas (*40*).

Lack of responses to PD-1 blockade (nivolumab) in leiomyosarcoma (12 patients) was confirmed also by a separate single-arm study (*42*).

A multicentre retrospective study (*43*) conducted on 88 patients with metastatic STS using nivolumab (6 patients), pembrolizumab (47 patients), ipilimumab (1 patient) or combination of nivolumab and ipilimumab (27 patients) showed 1 complete response in 1 UPS patient (treated with pembrolizumab), 20 partial response (7 UPS, 9 leiomyosarcoma) and disease stabilization in 28 patients with median progression free survival of 4.1 months and median overall survival of 19.1 months. Responses were observed with pembrolizumab or combination of pembrolizuman and ipilimumab.

A multicentre phase II randomized clinical trial (Alliance A091401 - NCT02500797) (*44*) in 76 patients with metastatic or unresectable STS investigated if nivolumab was more efficient in monotherapy (38) or in combination with ipilimumab (38). Results showed a response rate of 5% in monotherapy and 16% in combination therapy. Responses were seen in UPS, leiomyosarcoma, myxofibrosarcoma, angiosarcoma, alveolar soft part sarcoma (ASPS) and dedifferentiated liposarcoma. Combination therapy gave better results also in terms of median progression free survival and median overall survival. Clinical studies of combination immunotherapy are currently ongoing (nivolumab plus ipilimumab: NCT02879162).

A second phase II randomized clinical trial (NCT03307616) evaluated nivolumab and nivolumab plus ipilimumab clinical activity with or without radiation therapy in patients with surgically resectable UPS and dedifferentiated liposarcoma. The addiction of radiotherapy to nivolumab or nivolumab plus ipilimumab combination showed significant clinical activity in UPS.

A retrospective study (*41*) was conducted to explore anti-tumor activity of nivolumab on 28 patients with metastatic or unresectable STS (24) or bone sarcomas (4). All patients received a prior treatment with pazopanib, a tyrosine kinase inhibitor and at disease

progression some patients were treated with nivolumab alone while others with nivolumab and pazopanib combination. This study reported 3 partial responses (2/3 treated with combination therapy) and 9 disease stabilization. These data seem promising for nivolumab treatment alone or in combination with pazopanib but confirmation on a larger cohort is needed.

Several ongoing phase I/II clinical trials are assessing the role of PD-1 blockade in STS when combined with other immunomodulatory agents (pembrolizumab plus anti-VEGF agent: NCT03851614) or chemotherapy (pembrolizumab plus doxorubicin: NCT02888665). Some responses to ICIs were reported in clinical trials but the number of STS patients enrolled is too low to reach statistical significance. Anti-tumor efficacy of ICIs must be further evaluated in larger cohorts of patients.

Although limited by small numbers, these results highlight the potentialities of combinatorial approaches and the importance of STS subtype selection (e.g. UPS) to design future immunotherapy strategies in this challenging field.

Identification of potential responders through evaluation of predictive biomarkers, including PD-1/PD-L1 expression, and TILs presence is warranted and challenging at the same time for the extreme heterogeneity of STS and for the absence of standardized techniques for their evaluation and analysis.

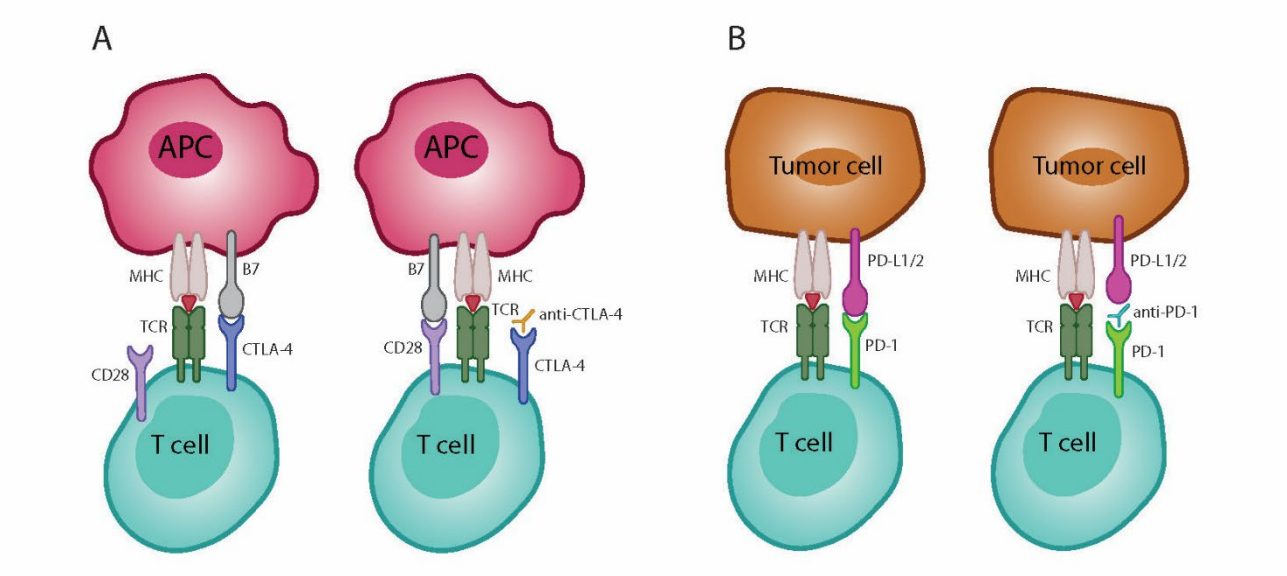

Figure 2. Mechanisms of action of CTLA-4/B7 and PD-1/PD-L1/2 pathways
Engagement of CTLA-4 by B7 on APCs impaired T cell priming (left) while CTLA-4 blocking prevent this binding in favour of CD28 engagement of B7 that induces T cell co-stimulation (right) **(A)**. Engagement of PD-1 by PD-L1/2^{+} tumor cells induces T cell apoptosis, anergy and functional exhaustion (left) while PD-1 blocking prevent T cell function impairment (right) **(B).**

Abbreviations: MHC, Major Histocompatibility Complex; TCR, T cell Receptor; CTLA-4, Cytotoxic T-Lymphocyte Antigen 4; PD-1, Programmed cell Death 1; PD-L1/2, Programmed cell Death Ligand 1-2.

2.3 Adoptive Cell Therapies (ACT)

ACT is an innovative and encouraging strategy in solid tumor treatment. This immunotherapy strategy is based on isolation, manipulation, expansion and reinfusion of immune cells into a donor patient to induce a more targeted and specific immune response and overcome the tolerance of evaded immune system to tumor cells (Figure 3).

ACT effectors can be harvested from TILs or obtained from peripheral blood. Effectors can be selectively expanded to recognize tumor antigens or genetically engineered to induce the expression of a transgenic T cell receptor (TCR) or a Chimeric Antigen Receptor (CAR) specific for a tumor antigen (*45-49*).

Therefore, ACT principal approaches exploit *i) TILs, ii) TCR-engineered effectors, iii) CAR-engineered effectors.*

Among these approaches, we can distinguish MHC-restricted and MHC-unrestricted strategies. MHC-restricted approaches are based on T lymphocytes and TCR-driven specificity (e.g. TILs, TCR-engineered T lymphocytes based approaches) while MHC-unrestricted strategies are based on innate immunity effectors (e.g. γδT, NK, NKT cells) with intrinsic anti-tumor activity not restricted to patients with a given MHC haplotype and on CAR-engineered lymphocytes.

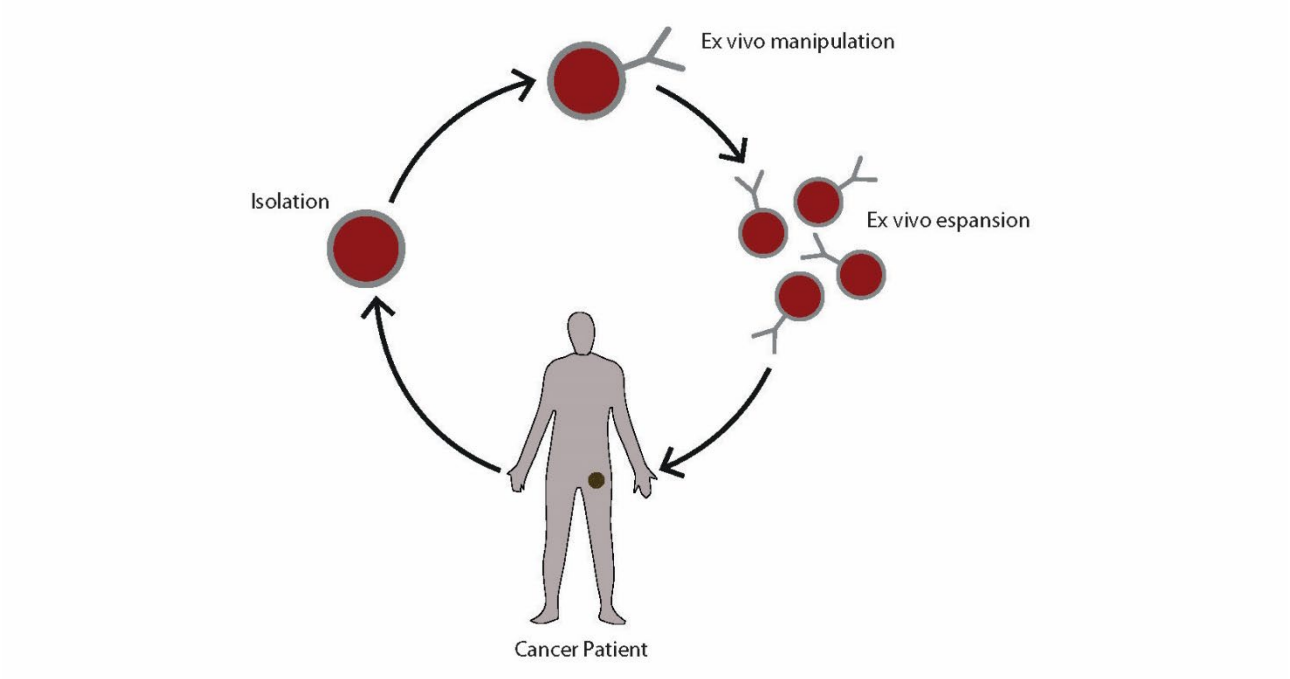

Figure 3. **General scheme of Adoptive Cell Therapy (ACT)**
ACT strategy is based on isolation, *ex vivo* manipulation, expansion and reinfusion of immune cells into a donor patient.
Abbreviations: ACT, Adoptive Cell Therapy.

2.3.1 TIL-based ACT and STS tumor microenvironment (TME)

TILs are collected from tumor, *ex vivo* activated and expanded to be re-infused into the patient to induce an effective anti-tumor response. The re-infusion is usually preceded by a lympho-depleting regimen with cyclophosphamide and fludarabine to deplete endogenous T cells and regulatory T cells that may suppress proliferation of infused T cells (Figure 4).
Efficacy of TIL therapy has been shown in metastatic melanoma by different clinical trials (*50*) but the use of TILs has never been investigated in STS-specific cohorts.
A study (*51*) reported TILs presence in about 35% of sarcoma patients, in particular in STS patients. Another interesting study (*52*) conducted on 70 STS patients demonstated the feasibility of expanding TILs extracted from STS biopsies and their reactivity against autologous tumors.
The potential role of TILs as predictive biomarker of STS response to immunotherapy is not clear at all (*53-55*).
In GIST patients, $CD3^+$ TIL number correlated with improved progression free survival, while infiltrating NK cells did not show any significant correlation presence (*56*). In non-GIST STS patients, $CD20^+$ TIL number correlated with better survival (*57*). Some studies (*58-60*) assessed presence of TILs, TAMs and PD-1 or PD-L1 expression in several samples from

STS patients. Multiplex immunohistochemical staining for CD3, CD4 (helper T cells), CD8 (cytotoxic T cells), FOXP3 (regulatory T cells), PD-1, PD-L1 and combinations were performed. Lymphocytes infiltration was observed in 98% of cases and macrophages infiltration in 90% of cases. Defining low TIL density below 5%, they showed that 54% of patients (mainly leiomyosarcoma, synovial sarcoma and chondrosarcoma) had low TIL density while 44% of patients (mainly GIST) high TIL density. The 80% of TILs were CD4 positive while 20% CD8 positive and 65% of $CD8^+$ TILs were PD-1 positive. 57% of STS samples expressed PD-L1 and 56% were PD-1 positive. Controversially, authors did not find significant association between TIL presence or PD-L1 expression and patient overall survival.

Previous studies have shown that the number of B lymphocytes is a key factor in tumor immunity, is associated with prolonged survival and has a dual effect on tumor recurrence and progression (*61*). Furthermore, a recent study (*62*) found that B lymphocytes infiltration correlated with an improved survival of STS patients, in tumors with both high or low infiltration of $CD8^+$ T cells.

Inflamed (“hot”) tumors are immunogenic and associated with high presence of TILs and tumor associated macrophages (TAMs). “Hot” tumors are the most likely to benefit from immunotherapy with checkpoint inhibitors. Tumor tissues that lack expression of many immunologic markers may indicate a non-immunogenic (“cold”) tumor microenvironment, which may require combination therapies consisting of an immunotherapy approach, such as ACT, to create an immunogenic tumor microenvironment plus an immune checkpoint therapy to further enhance the immune response (Figure 5).

Further investigations are necessary to better characterize distinct TME elements belonging to various STS histotypes and relative STS response to immunotherapy.

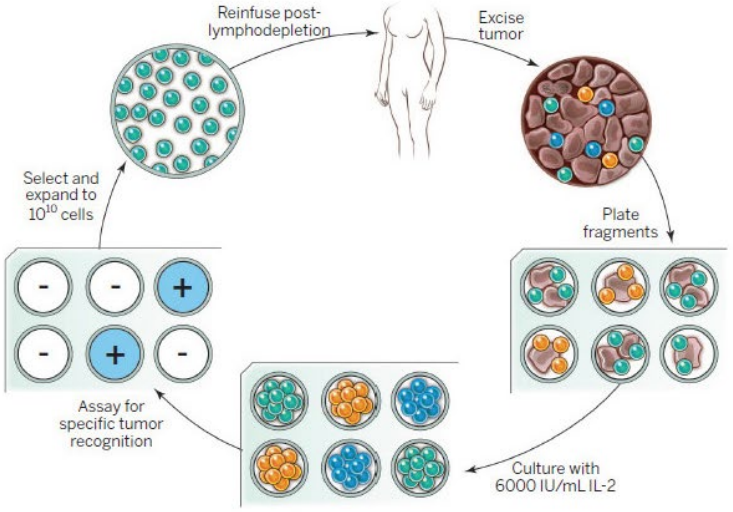

Figure 4. **General scheme for adoptive cell transfer of autologous TILs**
The resected cancer specimen is digested into a single-cell suspension or divided into multiple tumor fragments that are individually grown in IL-2. Lymphocytes overgrow, destroy tumors within 2 to 3 weeks, and generate pure cultures of lymphocytes that can be tested for reactivity in co-culture assays. Individual cultures are then rapidly expanded in the presence of OKT3 and IL-2. By approximately 5 to 6 weeks after resecting the tumor, up to 10^{10} lymphocytes can be obtained for infusion into patients.
Adapted from Rosenberg et Restifo, *Adoptive cell transfer as personalized immunotherapy for human cancer*, 2015.
Abbreviations: IL, interleukin.

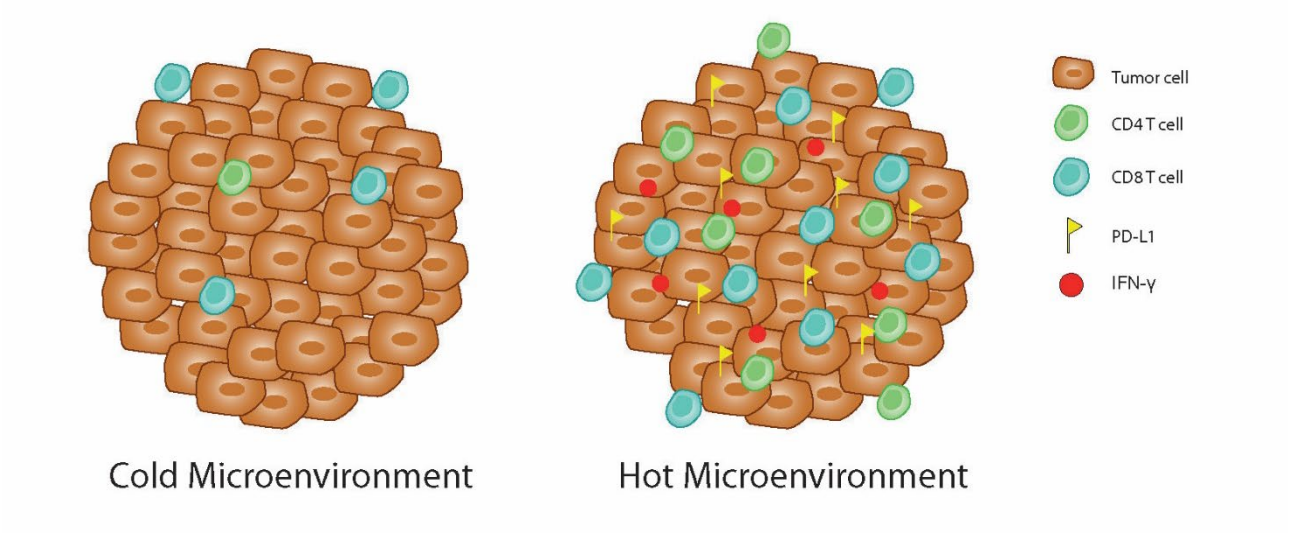

Figure 5. **Potential characteristics of immunogenic and non-immunogenic tumors**
Tumor tissues lacking expression of many immunologic markers may indicate a non-immunogenic ("cold") tumor microenvironment, which may require combination therapies to further enhance the immune response for clinical benefits **(A)**. Evaluation of tumor tissues may reveal an immunogenic tumor microenvironment consisting of many immunologic markers, including $CD8^+$ T cells, $CD4^+$ T cells, and PD-L1, which may be effectively treated with immune checkpoint to elicit clinical benefits **(B)**.
Abbreviations: PD-L1, Programmed cell Death Ligand 1; CD, Cluster of Differentiation.

2.3.2 TCR-based ACT

TCR-based ACT utilizes T lymphocytes engineered by a transgenic TCR to effectively target tumors.

Autologous T lymphocytes are obtained from leukapheresis or from Peripheral Blood Mononuclar Cells (PBMC), engineered *ex vivo* usually by retro- or lentiviral vector encoding a transgenic TCR and expanded to be re-infused into a cancer patient.

Transgenic TCR is specific for a tumor antigen and its antigen recognition is MHC-dependent (Figure 6).

A critical step in this approach is the identification of tumor specific antigens that are absent or low expressed in normal tissues. Selection of tumor specific antigens is important also to reduce off-tumor toxicities against healthy tissues.

Among interesting tumor antigens there are CTAs such as NY-ESO-1, expressed by the 80% of synovial sarcomas. In a phase I-II trial (NCT01343043) (*63*), 42 patients with advance synovial sarcoma were injected with genetically engineered T cells expressing anti-NY-ESO-1 TCR, achieving 1 complete response, 14 partial responses, 24 stable disease and only 3 disease progression. In a second phase I-II trial 4/6 patients with synovial sarcoma had partial responses and 38% of patients were alive at 5-years follow up with promising clinical efficacy comparing with standard chemotherapy (*45, 64*).

Crucial limitations of TCR-based ACT are unpredictable TCR toxicities related to mismatch of transgenic TCR chains with endogenous TCR chains and consequent generation of T cell with novel and paradoxical specificities (*64*).

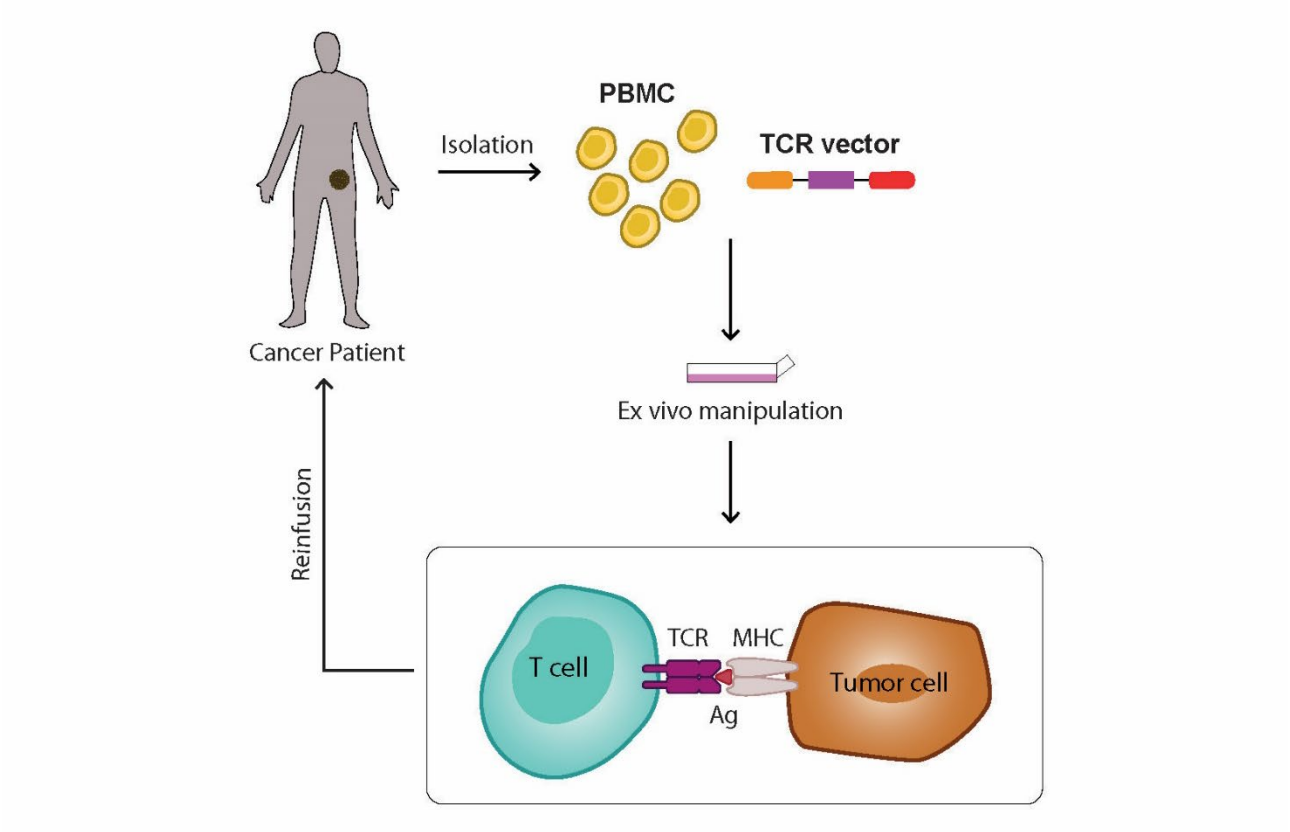

Figure 6. **TCR-engineering of lymphocytes**
PBMC are engineered *ex vivo* to insert a transgenic TCR and expanded to be re-infused into a cancer patient. Transgenic TCR is specific for a tumor antigen and its antigen recognition is MHC-dependent.
Abbreviations: PBMC, Peripheral Blood Mononuclear cells; MHC, Major Histocompatibility Complex; TCR, T cell Receptor.

2.3.3 CAR-based ACT

Chimeric Antigen Receptors (CAR)-strategy is one of the most promising approaches in cancer immunotherapy.

This strategy utilizes immune cells engineered by CAR specific for distinct tumor targets. Effector cells can be obtained from leukapheresis or from PBMC. CARs are then introduced into immune cells using viral vectors (e.g. adenovirus, retrovirus and lentivirus) or transposon vectors (e.g. Sleeping Beauty) or mRNA electroporation (*65-67*). Engineered immune cells were expanded and then re-infused into cancer patients (Figure 7).

A CAR is made by *i) an antigen recognition domain, most commonly a single-chain variable fragment (scFv) derived from a monoclonal antibody targeting a selected antigen, ii) a hinge that links recognition domain to transmembrane domain, iii) a transmembrane domain which bridges the membrane, iv) an intracellular domain that contains CD3z chain critical for TCR*

signalling (*68*). CARs are able to recognize antigens without MHC-presentation, circumventing immune evasion through MHC downregulation on cancer cells.

Since the initial development of CARs in 1989, CAR-T cells can be divided into four generations. The first generation of CAR were designed to mimic T cell activation and lead cytolysis, but it was not sufficient to direct a sustained, effective T cell response. Second and third CAR generations include one or two signalling domains, respectively, from co-stimulatory molecules such as more canonical CD28 and 4-1BB or OX40, CD27, ICOS to augment T cell function as well as redirect T cell specificity (Figure 8) (*69-75*). Normally, CARs provide a signal 1 of activation and a signal 2 of co-stimulation but not a signal 3 of proliferation. While activated CAR.T cells initially produced cytokines, they do not secrete sufficient amounts of cytokines after continuous exposure to antigen-positive target cells, leading to rapid reduction of their effector functions (*76-78*). The fourth-generation CARs were generated to increase CAR.T proliferation, and to rebalance cytokine milieu of the TME by providing additional immune-stimulatory cytokine signals. Fourth-generation CARs are known as “armored” CARs and include CAR.T cells redirected for universal cytokine-mediated killing (TRUCKs) which secrete cytokines to interfere with the immunosuppressive cytokine profile within solid tumor TME (*79*).

Optimizing CAR function remain a challenge also focusing on the interplay between functional domains (antigen binding and intracellular domains) and non-functional domains (hinge and transmembrane domains): antigen binding domains more proximal to plasma membrane induced greater CAR.T cell activation compared with distal antigen binding domains (*80-83*).

In addition, excessive CAR.T cell activation showed to be detrimental to T cell function (*84-86*), while tonic signalling in immunological synapse between CAR.T cells and target cells showed to support CAR.T cell effectiveness (*87-90*).

Encouraging results has been obtained in clinical trials against $CD19^+$ B cell malignancies and FDA approved CAR.T therapy for treatment of these diseases in 2017. Current efforts are dedicated at translating CAR-strategies in solid tumors. Unfortunately, no equivalent success has yet been achieved in treating solid tumors.

Therapeutic limitations of CAR-strategies in solid tumors are multifactorial and based on *i) presence of immunosuppressive tumor microenvironment (TME), ii) inefficient CAR effector homing and penetration in solid tumors, iii) limited effector fitness, iv) heterogeneous antigen expression* (*68*).

Despite CAR-therapy for solid tumors has not been nearly as successful as for hematologic malignancies, recently promising results at preclinical and clinical level against solid tumors and sarcomas are reported. Preclinical studies reported efficient anti-sarcoma activity of T cells redirected by CAR anti-HER2 against synovial sarcoma (*91*). Anti-VEGF CAR.T and anti-NKG2D^{ligands}-CAR.T demonstrated to be active against Ewing sarcomas (*92, 93*). Patient-derived IGF1R and ROR1-CAR.T cells reduced tumor growth in osteosarcoma xenografts prolonging animals survival (*94*). EphA2-CAR T cells showed potent *in vitro* and *in vivo* anti-tumor activity against osteosarcoma and Ewing sarcoma, eradicating also tumor deposits in mice liver and lung (*95*). GD2-CAR.T cell therapy combined with HGF neutralizing antibody synergistically inhibited tumor growth in Ewing sarcoma xenografts (*96*).

In a phase I clinical trial (NCT00902044) (*97*), initial results with autologous T cells redirected by HER2-specific CAR combined with chemotherapy in osteosarcoma patients showed 2 complete responses, 3 partial responses and only 5 disease progression with limited treatment-related toxicities. Phase I clinical trials (NCT02107963, NCT03635632, NCT04539366, NCT01953900, NCT00743496) (*2, 98-100*) using autologous T cells redirected by CAR targeting GD2, a disialoganglioside involved in signal transduction, proliferation and tumor cell migration, in sarcoma patients are currently ongoing.

Encouraging clinical responses in CAR-therapy have to face with important concerns about possible toxicities mostly due to “on target/off-tumor” toxicities, that could derive from CAR.T cell recognition of target antigen on normal tissues, and to cytokine release syndrome (CRS). CRS is a systemic inflammatory response deriving by release of large amounts of cytokines triggered by activated CAR.T cells and by subsequent activation of bystander immune and non-immune cells. To prevent possible toxicities investigators developed inducible safety switches to ablate CAR.T cells when the need arises (*68*). Safety switches can be based on suicide genes activated by drugs that eliminate genetically modified T cells (e.g. expression cassettes including either CAR structure and HSV-tk or iCA9 suicide gene) (*101-103*). Another approach is based on the expression of a targetable molecule (e.g. CD20, truncated EGFR) on CAR-engineered T cells, allowing a selecting CAR.T cells removal through administration of a specific monoclonal antibody (e.g. clinically approved mAb such as Rituximab or Cetuximab) (*104-108*).

New methods have been developed to augment the accuracy of CAR-immunotherapies by non-invasive and site-specific control of potency, specificity and safety of immune response based on *ii) endogenous and ii) exogenous switches (109)*.

Endogenous switches rely on introducing a second antigen specificity to potentially prevent “on-target/off-tumor” cytotoxicity. Some of these systems are based on two different intact CARs or tandem CARs (also known as dual CARs or TanCARs), made by two tandemly linked scFV domains on a single CAR molecule. The first CAR or scFV engagement provides a CD3ζ-mediated activation signal after recognition of the first antigen while the co-stimulatory signal is prepared by the second CAR or scFV engagement after recognition of a second antigen. CAR.T cells can be completely activated only by dual-antigen recognition (*110-114*).

Other approaches are derived from synNotch receptors that, after recognizing a tumor antigen, undergo trans-membrane cleavage, releasing the intracellular transcriptional domain that allows the expression of a specific CAR on T cells (*115, 116*).

Inhibitory CAR (iCAR) system includes a CAR specific to an antigens expressed exclusively on normal tissue (e.g. PSMA) with an inhibitory intracellular signalling domain (e.g. PD-1, CTLA-4) to restrict T cell activity. In presence of both normal tissue associated-antigen and tumor-associated antigen, iCAR suppresses CAR.T cell activity (*117*).

Exogenous switches are based on a secondary agent administration to induce CAR-activation.

Bispecific T-cell engagers are antibodies with different binding sites to bridge two or more cells with a physical link. This antibodies can be used to regulate more-secure CAR.T cell activity. Recently, a synthetic “universal” CAR was constructed to bind fluorescein isothiocyanate (FITC). This CAR is inactive and can not target cells in absence of the folate-FITC conjugate. After the administration of the conjugate, this bispecific T-cell engager redirects and regulates CAR activity to target folate receptor-positive tumor cells (*118*).

“On-switch” CAR recapitulates normal T lymphocytes activation. CAR key signalling modules (co-stimulatory domains and ITAMs) are distributed into physically separated molecules that can be conditionally reassembled when a heterodimerizing small molecule is added. CAR.T cells triggering occurs only after the administration of the heterodimerizing small molecule and the recognition of the antigen. This CAR provides a small molecule–dependent, titratable and reversible control of CAR.T cell activity (*119-121*).

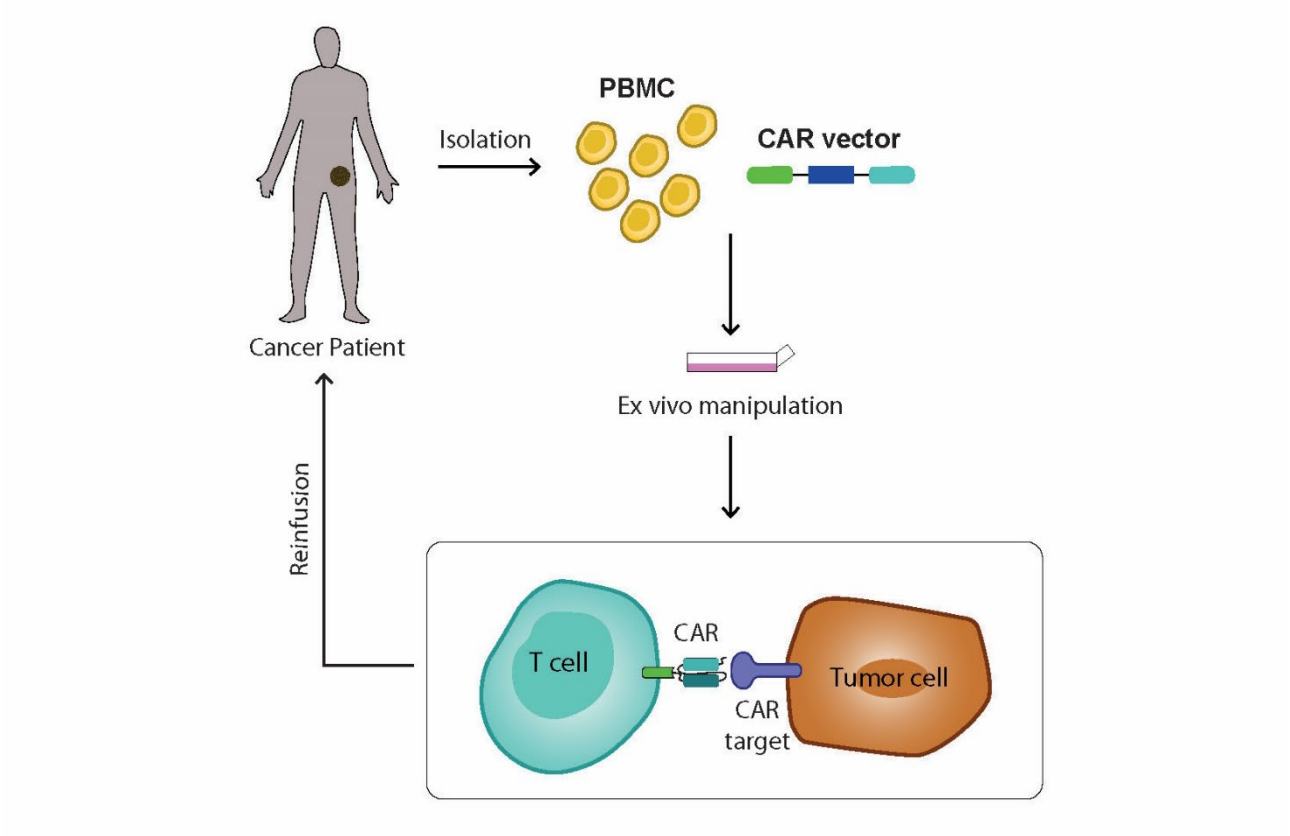

Figure 7. CAR-engineering of lymphocytes

PBMC are engineered *ex vivo* to express a CAR and expanded to be re-infused into a cancer patient. CARs recognize surface antigens without MHC-presentation.

Abbreviations: PBMC, Peripheral Blood Mononuclear cells; CAR, Chimeric Antigen Receptor.

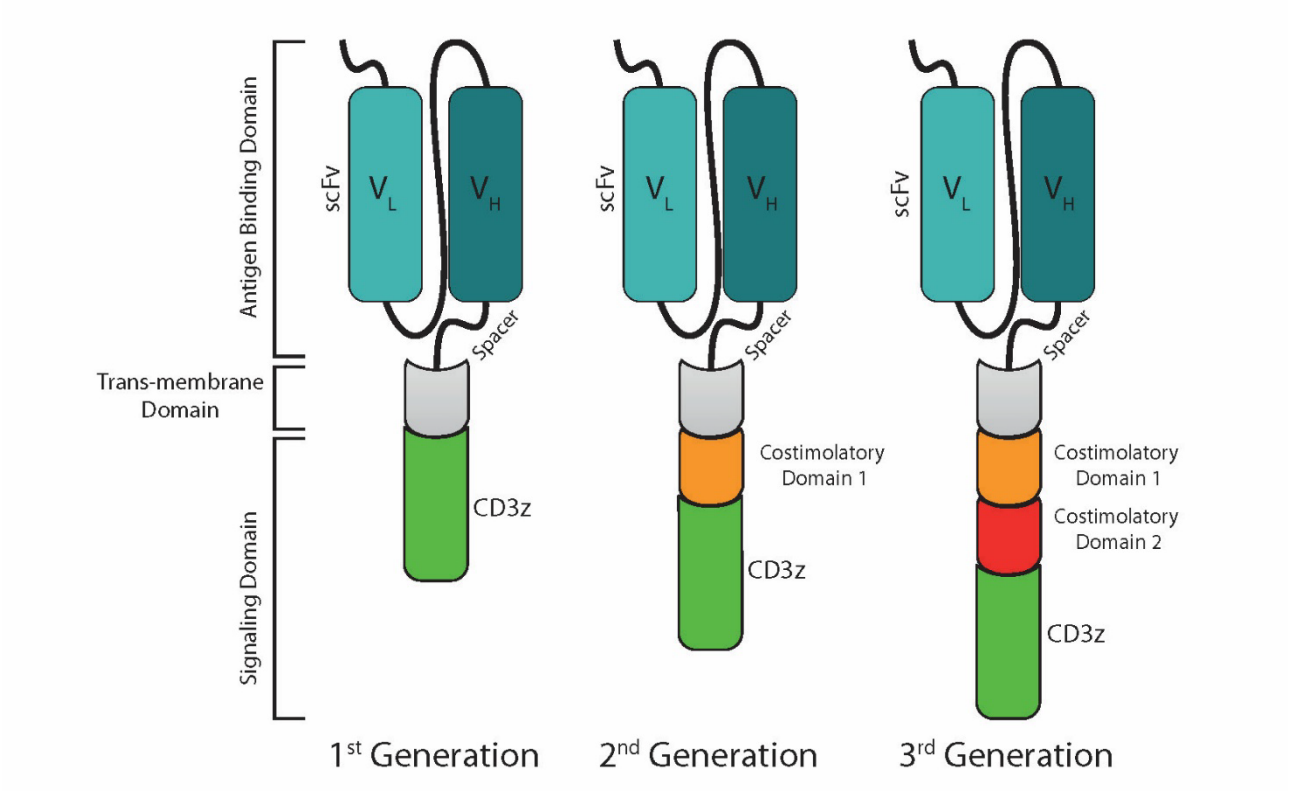

Figure 8. Schematic representation of CAR-generations
First-generation CARs contained only CD3z chain as activation domain while second and third CAR generations included other one or two signaling domains, respectively.
Abbreviations: ScFV, Single Chain Variable Fragment.

Within CAR-strategies, an intriguing approach is the alternative or integrative CAR engineering of innate immune effectors different from conventional T lymphocytes.
Preclinical data, and even initial clinical studies, are exploiting other types of lymphocytes, such as γδT, Natural Killer (NK), NKT and Cytokine-induced Killer (CIK) cells as innovative platforms for CAR engineering characterized by an intrinsic MHC-unrestricted and CAR-independent anti-tumor activity.
The biological features of such immune effectors may favourably contribute to the clinical development of CAR-strategies including their extension to the field of solid tumors (*122*).

3. CIK as immune effectors for CAR-therapy

Cytokine Induced Killer lymphocytes (CIK) are a heterogeneous *ex vivo* expanded lymphocytes with a mixed T-NK phenotype.
CIK are endowed with a MHC-unrestricted antitumor activity mainly mediated by their NKG2D membrane receptor, whose ligands are stress-inducible molecules expressed by a wide range of tumor, like MIC A/B and ULBP family (ULBP1, ULPB2/5/6, ULBP3). Final CIK killing is mediated by perforin and granzymes.
The biological features that makes CIK appealing for adoptive immunotherapy are *i) high ex-vivo expansion, ii) reduced alloreactivity, iii) MHC-unrestricted tumor-killing* (Figure 9) (*123*).
An important limitation for success of ACT strategies is the obtainment of sufficient numbers of anti-tumor immune effectors. CIK expansion is easy and cost-effective. CIK can be efficiently expanded *in vitro* starting from PBMC but also from bone marrow or umbilical cord blood precursors (*124-126*). Standard culture conditions require 3 to 4 weeks of expansion with timed addition of IFNγ (1000 U/ml), Ab-anti CD3 (50ng/ml) and IL2 (300U/ml). IFNγ is added on day 0 to activate monocytes present in initial culture and provides contact-dependent and soluble crucial signals for the acquisition of Th1 phenotype and cytotoxic power of CIK.
Ab anti-CD3 is added on day 1 and provides mitogenic signals, subsequently sustained by IL2 addiction that drives CIK expansion. After 3-4 weeks, expansion rates are variable from few to more than 1000 fold (Figure 10). Such CIK expansion level, considering precursor

availability, is encouraging for clinical applications. Additional experimental strategies (e.g. additional soluble factors) are under evaluation to increase expansion of “poor expanders” that may less benefit from this approach (*123*). Standard CIK culture conditions have been successfully validated under Good Manufacturers Practice (GMP) conditions (*127, 128*).

At the end of the expansion CIK are a heterogeneous $CD3^+$ T lymphocytes population characterized by two main subset: $CD3^+CD56^+$ fraction is the main responsible for MHC-unrestricted anti-tumor activity while $CD3^+CD56^-$ cells exhibit higher proliferative potential and more naïve phenotype. Mature CIK are mainly $CD8^+$ and the terminally differentiated late effector phenotype ($CD45RO^+CD62L^-CCR7^-$) is the most represented.

A second clinically relevant property of CIK is their reduced alloreactivity potential across MHC barriers that may result in a reduced risk for Graft Versus Host Disease (GVHD) (*129*).

In the last decade our group and others demonstrated the effective generation and antitumor activity of CIK in multiple tumor settings, including STS (Figure 11A, B) (*130-138*). Clinical studies confirmed the feasibility, efficacy and safety of adoptive immunotherapy with CIK against solid tumors like breast cancer, hepatocellular carcinoma, renal cancer carcinoma, non-small cell lung cancer, gastric cancer, colorectal cancer and non-Hodgkin lymphomas (*139-144*). A summary of main clinical findings was published in the International Registry on CIK Cells (IRCC).

We reported patient-derived CIK activity against STS but we observed that their function decreased at low effector/target (E:T) ratios, showing potential limitations in clinical perspective.

Adoptive immunotherapy with CIK may benefit from CAR–based approaches, thus CIK with their biological features might provide an intriguing platform for CAR-strategies with potential positive impact in the challenging translation to the field of solid tumors and favorable safety implications.

CAR engineered CIK generated bi-specific tumor killers, conjugating in the same effector CAR-specificity and NKG2D-mediated intrinsic anti-tumor activity. Advantages may derive by enhanced efficacy against tumors with heterogeneous antigen expression, contrasting tumor clonal selection events (*145, 146*).

CIK showed limited lifespan and *in vivo* persistence and their therapeutic administration requires multiple infusions, compared with long-time persistence of conventional T lymphocytes, mainly employed in low or single infusion protocols (*147*). However, this might represent a positive value in terms of safety for CAR.CIK. Preclinical studies exploring CAR.CIK anti-tumor efficacy reported promising results.

The first preclinical evidence of CIK as experimental platform for CAR-redirected immunotherapies have been provided against hematological malignancies, targeting CD19 and CD33/CD123 antigens, and clinical trials are currently ongoing (clinical trial numbers NCT03389035, NCT02944162) (*148-150*). Recent data presented by our group and others extended these proofs of concept against STS. Our group (*145*) reported the intense anti-STS activity of CAR.CIK redirected against CD44v6, a target expressed in about 40% of STS (Figure 12A-C). Anti-ErbB2 CAR.CIK showed promising preclinical activity against STS (*97, 151, 152*).

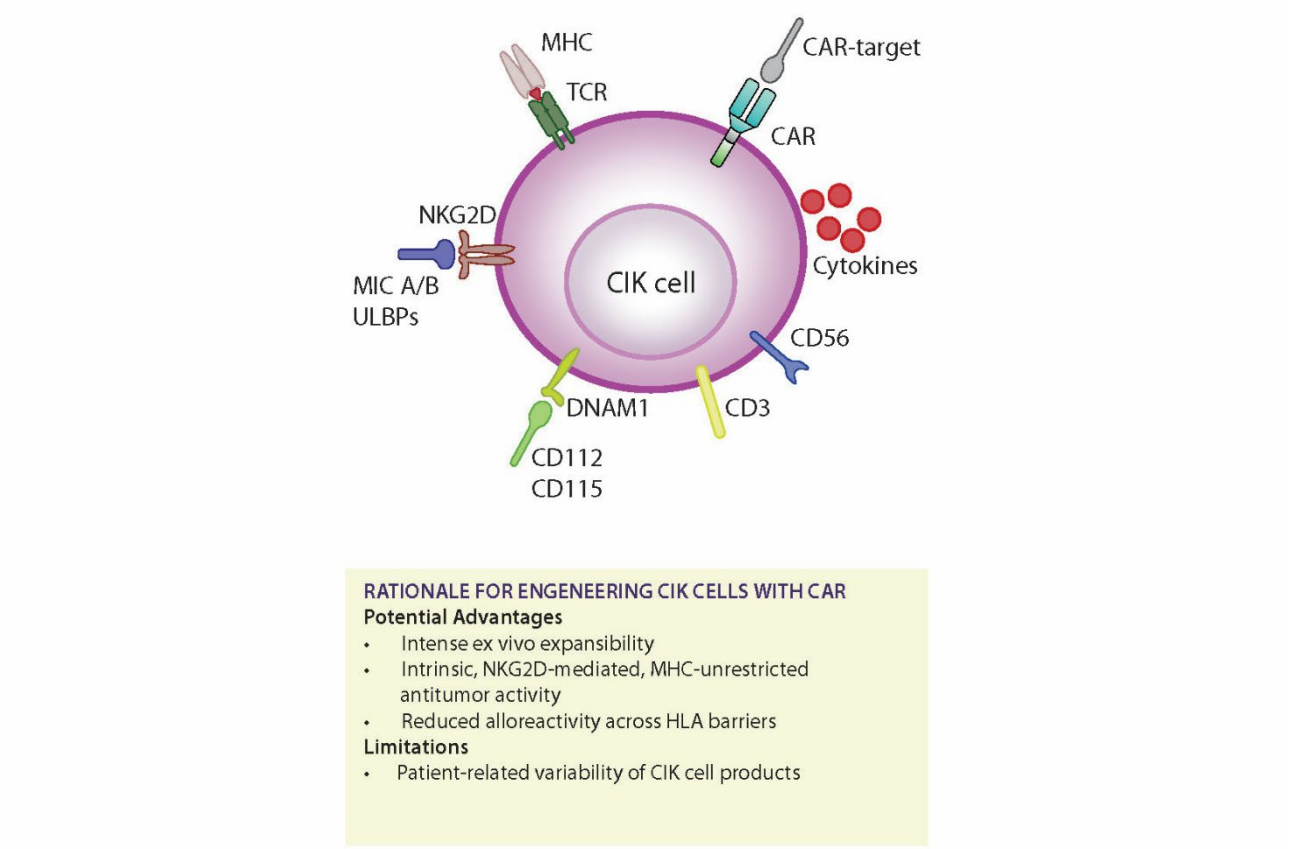

Figure 9. **Principal features of Cytokine Induced Killer lymphocytes (CIK)**
Main potential advantages and limitations of CIK for CAR engineering.
Adapted from Rotolo et al, *CAR-Based Strategies beyond T Lymphocytes: Integrative Opportunities for Cancer Adoptive Immunotherapy,* 2019.
Abbreviations: MHC, major histocompatibility complex; TCR, T cell Receptor; CAR, Chimeric Antigen Receptor; CD, Cluster of Differentiation; NKG2D, Natural Killer Group 2D receptor; MIC A/B, MHC class I chain-related gene A/B; ULBPs, UL16 binding proteins; DNAM-1, DNAX Accessory Molecule-1; CIK, Cytokine Induced Killer.

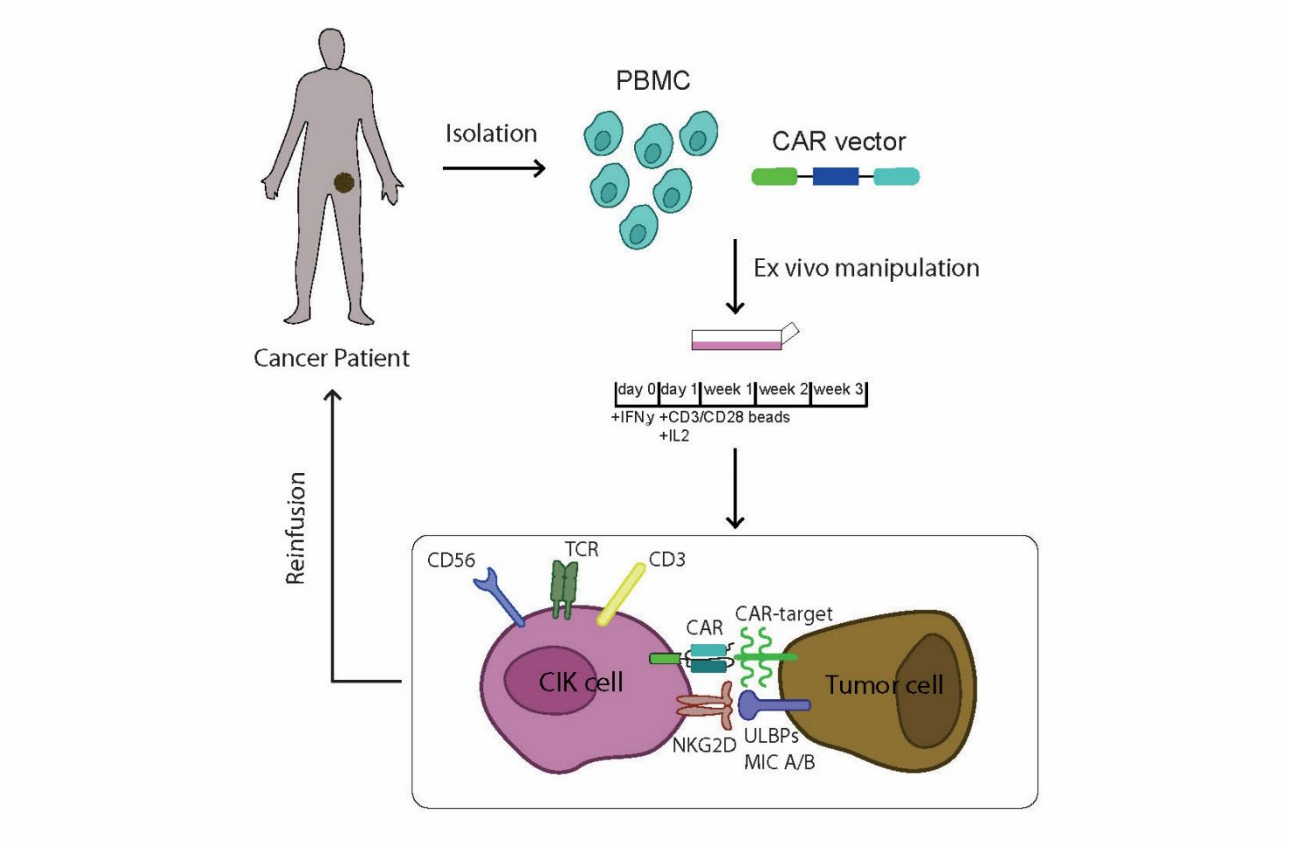

Figure 10. **Generation and CAR-engineering of Cytokine Induced Killer lymphocytes (CIK)**
PBMC are expanded with timed addition of IFNγ (1000 U/ml), Ab-anti CD3 (50ng/ml) and IL2 (300U/ml) and engineered to express a CAR and expanded to be re-infused into a cancer patient. CARs recognize surface antigens without MHC-presentation.
Abbreviations: TCR, T cell Receptor; CAR, Chimeric Antigen Receptor; CD, Cluster of Differentiation; NKG2D, Natural Killer Group 2D receptor; MIC A/B, MHC class I chain-related gene A/B; ULBPs, UL16 binding proteins; IL, interleukin; CIK, Cytokine Induced Killer.

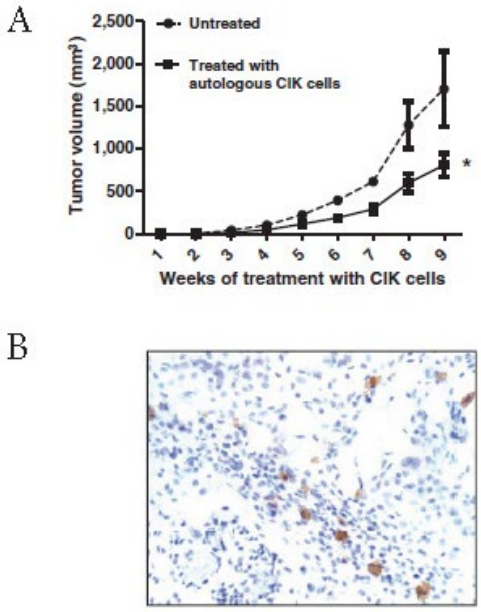

Figure 11. *In vivo* activity of CIK cells against sarcoma

NOD/SCID mice (n = 12) were subcutaneously implanted with 1 x 10^6 cells of pleomorphic undifferentiated sarcoma. Four days after tumor implantation, 1 x 10^7 autologous CIK cells were weekly infused by tail vein injection (n = 6). A significant delay of tumor growth was observed in treated mice compared with controls (n = 6), P = 0.017. Curve of tumor growth is reported in **A**. Infiltration of CIK cells at tumor sites were shown by immunohistochemistry (Ab anti-CD3) at the end of experiment **(B)**.

Adapted from Sangiolo et al, *Cytokine-Induced Killer Cells Eradicate Bone and Soft-Tissue Sarcomas,* 2013.

Abbreviations: CIK, Cytokine Induced Killer.

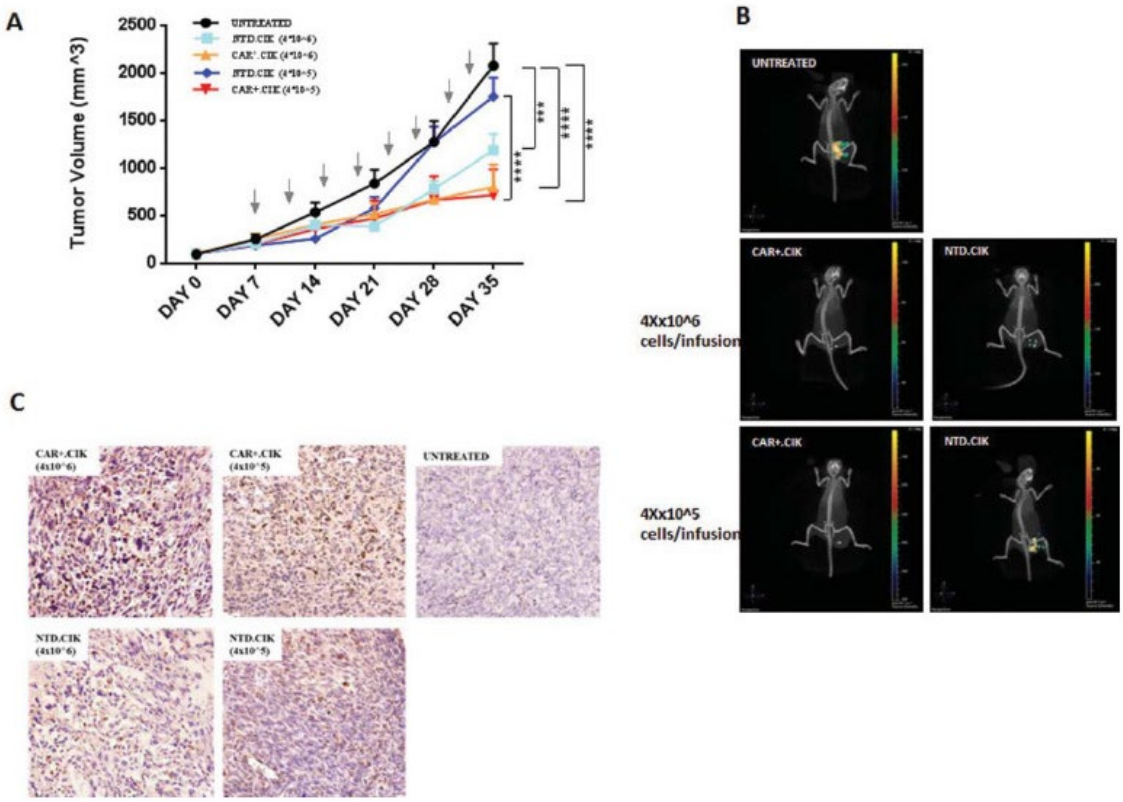

Figure 12. ***In vivo*** **anti-sarcoma activity of anti-CD44v6 CAR.CIK**
CAR.CIK were intravenously infused, every 3–4 days (total 8 infusions), in NOD/SCID mice bearing subcutaneous patient-derived UPS xenograft. Two different doses (4 x 10^5 and 4 x 10^6 per infusion) of CAR.CIK were explored. We observed a significant delay of tumor growth in mice (n = 6) treated with CAR.CIK cells (4 x 10^5), compared with untreated controls (n = 6, $p < 0.0001$) or treated with equivalent doses of paired NTD.CIK cells (n = 6, $p < 0.0001$). A similar antitumor activity was observed with 1 log-higher dose of CAR.CIK (4 x 10^6). Arrows indicate CIK cell infusions **(A)**. In selected cases (1 representative mouse per group, n = 5) results were confirmed by a 3D imaging analysis based of fluorescent glucose uptake **(B)**. Tumor homing of CAR.CIK was confirmed by IHC in explanted tumors by staining with anti-human CD3 antibody **(C)**.
Adapted from Leuci et al, *CD44v6 as innovative sarcoma target for CAR redirected CIK cells,* 2018.
Abbreviations: CAR, Chimeric Antigen Receptor; NTD, Not Transduced; NOD SCID mice, Non obese diabetic/severe combined

4. Chondroitin Sulfate Proteoglycan 4 (CSPG4) as CAR-target

The application of CAR-strategies for the treatment of solid tumors may represent the most innovative therapeutic approach for many tumors for which no effective therapy is nowadays available. The selection of the tumor-associated antigen (TAA) to be targeted by CAR engineered effectors is crucial to prevent deleterious side effects (*153*). The ideal CAR target should be homogeneously expressed by tumor cells, across different patients, with minimal or no expression in normal tissues.

Solid tumors tend to display a large degree of heterogeneity of antigen expression and it is common to find a TAA enriched on a subset of tumor cells but also expressed at low levels on normal tissues.

Chondroitin Sulphate Proteoglycan-4 (CSPG4, also known as High Molecular Weight (HMW) melanoma-associated Chondroitin Sulphate Proteoglycan (MCSP)) is a cell surface type I transmembrane proteoglycan, first identified on human melanoma cells (*153*).

Cell-surface proteoglycans are macromolecules that can be detected intracellularly, at the cell surface or in the extracellular matrix (ECM) and are critical in mediating cell-cell interactions and interaction with ECM components (*153*).

CSPG4 showed to be highly expressed on other solid tumors such us mesothelioma, head and neck squamous cell carcinoma and triple negative breast carcinoma with aggressive clinical course (*154, 155*) but its expression on normal tissues resulted negligible (*156*). In silico analysis detected CSPG4 overexpression in other solid malignancies including glioblastoma, clear cell renal carcinoma, osteosarcoma, STS and subset of acute leukemia suggesting that targeting this antigen may have a major impact on a broad array of solid tumors (*153, 157*).

In various type of cancers, CSPG4 showed to be expressed not only by differentiated malignant cells but also by a more “stem-like” cell subset, characterised by high tumorigenicity and chemo/radio-resistance and involved in tumor recurrence and metastatic spread (*158, 159*).

CSPG4 interacts with α4β1 integrins to directly modulate cell adhesion, motility and participates in tumor migration, invasion, angiogenesis and metastasis with its ectopic expression in tumor cells (*160, 161*), exploiting a crucial role in tumor progression by controlling cell adhesion processes.

CSPG4 in not an oncogene *per se* but its cytoplasmic domain contains multiple amino acid residues that can be phosphorylated promoting tumor cell proliferation, survival and migration pathways by activation of ERK1/2, PI3K and integrin-regulated focal adhesion kinases (*162-164*).

This role may account for the association of CSPG4 expression and poor clinical outcomes founded in melanoma, head and neck squamous cell carcinoma and breast cancer (*165-168*).

CSPG4 is also involved in angiogenesis and wound repair (*168*). In particular, it displayed a differential distribution on pericytes in different anatomic sites: it is upregulated on tumor-associated pericytes while is barely detectable on pericytes in anatomic site distant from

tumor site (*169*). Its upregulation on tumor-associated pericytes may be due to hypoxic conditions frequently present in TME. This peculiar expression of CSPG4 added an anti-angiogenic effect to CSPG4-targeted immunotherapy.

CSPG4 has been targeted with monoclonal antibodies (mAb) in melanoma, glioblastoma, head and neck squamous cell carcinoma, mesothelioma and breast carcinoma models resulting in the inhibition of tumor growth and preventing disease recurrence and metastatic capability of tumor cells (*170-175*).

The specificity of CSPG4-specific mAbs has been also exploited creating a humanized bi-specific T-cell engaging antibody (BiTE) that binds both CSPG4 and CD3 to engage cellular components of immune system. T cells co-cultured with melanoma cells in presence of this specific BiTE showed efficient cytotoxic activity, setting the basis for testing the BiTE-CSPG4-specific Ab in clinical trials (*176*).

Recent advantages of coupling mAb specificities to effector functions has allowed generating specific CARs. Given its restricted expression in normal tissues and high expression in various type of solid tumors with a relevant role in biology of tumor cells, CSPG4 is an attractive target for immunotherapy (*157, 177-179*).

Anti-CSPG4 CAR.T cells showed efficient anti-tumor growth *in vitro* and *in vivo* against melanoma, head and neck squamous cell carcinoma, mesothelioma and breast cancer cell lines (Figure 13A-C) (*157*). CSPG4-CAR.T cells efficiently controlled the growth of glioblastoma *in vitro* and *in vivo* upon intracranial tumor inoculation. Moreover, CSPG4-CAR.T cells were also effective against glioblastoma with moderate to low expression of CSPG4. This effect was mediated by the *in vivo* up-regulation of CSPG4 on tumor cells, induced by tumor necrosis factor-α (TNFα) released by the microglia surrounding the tumor (*180*).

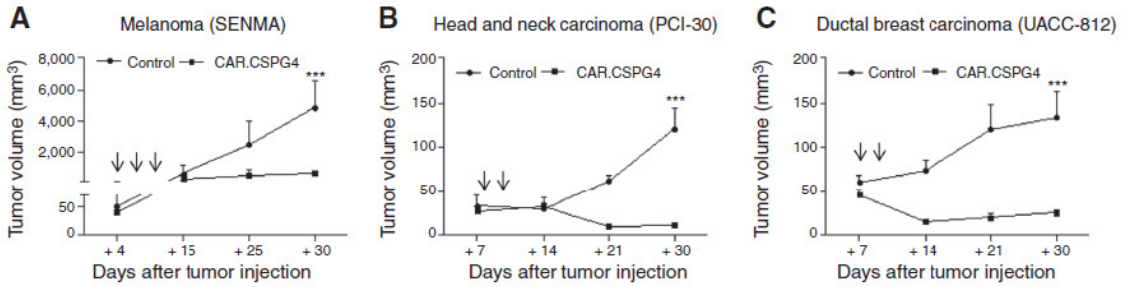

Figure 13. CSPG4-CAR.T lymphocytes control tumor growth *in vivo*

Tumor growth of NSG mice engrafted subcutaneously with melanoma (SENMA; **A)**, head and neck squamous cell carcinoma (HNSCC, PCI-30; **B)**, or breast carcinoma (UACC-812; **C)** cell lines and infused intravenously with either CSPG4-CAR (closed squares) or control (closed circles) T lymphocytes. Arrows indicate T-cell infusions. Shown are mean±SD from 15 mice per group (3 independent experiments) for the melanoma model and 10 mice per group (2 independent experiments) for the HNSCC model and breast carcinoma models (***, $P < 0.001$).

Adapted from Geldres et al, *T Lymphocytes Redirected against the Chondroitin Sulfate Proteoglycan-4 Control the Growth of Multiple Solid Tumors both In vitro and In vivo,* 2014.

Abbreviations: CAR, Chimeric Antigen Receptor; CSPG4, Chondroitin Sulfate Proteoglycan 4.

Aim of the work

Currently effective therapy is not available for unresectable and high-grade STS and survival rates of adults and children with STS remain extremely poor even in the era of immune checkpoint inhibitors. This unmet clinical need prompted us to test a novel approach of adoptive immunotherapy in this challenging field.

Aim of my PhD study is to investigate and explore the efficacy of a novel cellular immunotherapy with CIK lymphocytes redirected by a CSPG4-specific CAR against multiple STS histotypes. The experimental platform includes patient-derived CIK and cell lines established from distinct STS histotypes.

CIK were transduced with a second-generation CAR anti-CSPG4 with 4-1BB co-stimulation domain. CSPG4-CAR.CIK anti-tumor activity was explored *in vitro*, within bi- and three-dimensional STS models, and *in vivo* against STS xenograft models.

Specific objectives of my thesis project are: *i) generation and characterization of CSPG4-specific CAR.CIK, ii) CSPG4 prevalence and distribution on STS, iii) in vitro anti-sarcoma activity of CSPG4-CAR.CIK, iv) migratory and infiltrative abilities of CSPG4-CAR.CIK within 3D STS models, v) in vivo CSPG4-CAR.CIK anti-tumor activity against distinct STS xenografts.*

Progressively more complex 3D STS models allowed to better visualize CAR.CIK anti-tumor kinetics in term of migration, tumor homing and infiltration capacity and to characterize STS TME elements. In selected experiments, challenging culture conditions of glucose deprivation and low oxygen tension were used to mimic the impact of hostile TME on CAR.CIK activity.

Data from this thesis have been recently published by our group (*181*).

The final perspective of the project is to provide a strong rationale for the development and translation into clinical setting of a novel cellular immunotherapy with CSPG4-specific CAR-engineered CIK for the treatment of patients with advanced or relapsed high grade STS.

Materials and Methods

Data analysis of CSPG4 RNA expression in The Cancer Genome Atlas

RNA-sequencing expression data were selected and downloaded from the cBioPortal, TCGA PanCancer collections. The dataset included 251 STS samples: Leiomyosarcoma n=99, Dedifferentiated Liposarcoma n=58, UPS/Malignant Fibrous Histiocytoma/High-Grade Spindle Cell Sarcoma n=50, Myxofibrosarcoma n=25, Malignant Peripheral Nerve Sheath Tumor n=9, and Synovial Sarcoma n=10. Another 336 melanomas served as a positive expression control and various epithelial tumors (Breast Cancer n=1082, Pancreatic Cancer n=176, Lung Adenocarcinoma n=510, Lung Squamous Cell Carcinoma n= 482) were explored for comparison. RSEM expression values were plotted after Log_2 transformation with 0.5 jittering on the x-axis using Microsoft Excel.

Soft Tissue Sarcoma (STS) cell lines

Patient-derived STS cell lines were generated in our laboratory from surgical biopsies (*132*). We received approval for collection of patient samples and the associated informed consent document from the Institutional Review Board (IRB) per Declaration of Helsinki guidelines (Prot. Number 225/2015). Patient-derived STS were cultured in either KO DMEM F12 (KO Out Dulbecco's Modified Eagle Medium, Gibco BRL) or IMDM (Iscove's Modified Dulbecco Medium, Sigma Aldrich) medium, with 10% or 15% FBS, 25 mmol/L HEPES, 100 U/mL penicillin, and 100 U/mL streptomycin (Gibco BRL) in a humidified 5% CO_2 incubator at 37°C. Patient-derived melanoma cell line M14 (*182*), which does not express CSPG4 protein, was used as a specificity control and cultured in RPMI 1640 medium (Sigma Aldrich), supplemented with 10% heat inactivated FBS, 100 U/mL penicillin, and 100 U/ mL streptomycin (Gibco BRL) at 37°C in a 5% CO_2 incubator. The HT1080 cell line used in this study was originally obtained from the American Type Culture Collection (ATCC) and was authenticated by genotype analysis with the Cell ID system (Promega) that compared their profile with those published on the DMSZ database. Adult and neonatal keratinocytes were cultured with the Lonza KGM™ Gold Keratinocyte Growth Medium Bullet Kit™.

Soft Tissue Sarcoma (STS) spheroids

Three-dimensional STS spheroids were generated as a single spheroid per well using ultra-low attachment (ULA) 96-well round bottom plates (Corning) with no additional coating. A

STS cell suspension of 500 - 5000 cells/100 µl was plated into wells and then centrifuged at 1000 g for 10 min (*151*). STS spheroids were assembled in 1-4 days, depending on the histotypes. We generated GFP^+ STS spheroids from cells previously transduced with the pRRL.sin.PPT.PGK.eGFP.Wpre VSV-G pseudo-typed third-generation lentiviral vector.

Generation of CSPG4-CAR.CIK

Supernatants containing retroviral particles encoding CAR specific for the CSPG4 antigen (CSPG4-CAR) or the control vector encoding CAR specific for the CD19 antigen (CD19-CAR), both containing 4-1BB costimulatory endodomains, were available through an active collaboration with Prof. G. Dotti (University of North Carolina, USA) (*180, 183*). We generated CSPG4-CAR.CIK and CSPG4-CAR.T cells from peripheral blood mononuclear cells (PBMC) isolated from patients diagnosed with STS by density gradient centrifugation using Lymphosep (Aurogene). Approval was obtained from the IRB per the Declaration of Helsinki guidelines for the collection of biological samples (tumors and blood) and for patient informed consent releases (protocol no., 225/2015). For CAR.CIK, PBMCs from 8 patients with STS (Supplementary Table S1) were seeded on day 0 in cell culture flasks at a concentration of $2x10^6$ cells/mL with IFNg (Miltenyi Biotec; 1,000 U/mL) in RPMI1640 Medium (Gibco BRL), supplemented with 10% FBS (Sigma), 100 U/mL penicillin, and 100 U/mL streptomycin (Gibco BRL). Following a 24-hour incubation at 37°C, PBMCs were activated by anti-biotin MACSiBead particles loaded with anti-CD2, -CD3, and -CD28 mAbs (Miltenyi Biotec) and human IL2 IS (Miltenyi Biotec, 300 U/mL). To generate CAR.T cells, PBMCs were seeded on day 0 at a concentration of 2 $x10^6$ cells/mL and activated using anti-biotin MACSiBead particles. On day +1, human IL2 IS (Miltenyi Biotec, 50 U/mL) was added. On day +2, PBMCs were transduced with 0.5 mL of retroviral supernatants in retronectin coated plates by overnight incubation. Unmodified not transduced (NTD) NTD.CIK and NTD.T cells were used as a paired control. Both CAR.CIK and control NTD.CIK were expanded over 4 weeks, refreshed with IL2 medium (CIK, 300 U/mL) every 2–3 days as needed, and cultured at 1.8 $x10^6$ cells/mL. CAR.T cells were cultured at 1.8 $x10^6$ cells/mL for 1 week, and the IL2 (50 U/mL) medium was refreshed every 2–3 days as needed.

Glucose deprived medium preparation

We prepared STS glucose deprived medium diluting DMEM High Glucose (Thermo Scientific, Life Technologies) with [Glucose]=25 mM (4,5 mg/ml) 5 times ([Glucose]=5mM)

or 50 times ([Glucose]=0,5mM) with DMEM without glucose (Thermo Scientific, Life Technologies).
For CSPG-CAR.CIK glucose deprived medium we diluted RPMI 1640 medium (Sigma Aldrich) with [Glucose]=11 mM (2,3 mg/ml) 2 times [Glucose]=5mM and 20 times [Glucose]=0,5mM with RPMI without glucose.
Glucose deprived medium were added with 2% FBS (Euroclone S.p.A), 100 U/mL penicillin, and 100 U/ mL streptomycin (Gibco BRL).

Viability assays

We evaluated CSPG4.CAR-CIK viability after 24h and 72h in challenging ([Glucose]=5-0,5mM ± O_2=1%) and standard culture conditions ([Glucose]=25/11mM, O_2=21%) with a bioluminescence cell viability assay (CellTiter-Glo Luminescent Cell Viability Assay (Promega)). The number of viable and metabolically active cells was evaluated by quantifying the ATP in culture, according to manufacturer protocol. We confirmed viability data by flow cytometry, staining with DAPI and assessing the percentage of viable $DAPI^-$ cells.

Flow cytometry

Conjugated CD3, CD4, CD8, CD56, PD-1, CXCR3, CXCR4, and CCR7 mAbs (BD Pharmingen) and CD45RO, CD45RA, and CD62L mAbs (Miltenyi Biotec) were used to characterize lymphocytes. A mAb specific for the IgG1/CH2CH3 Spacer (Jackson ImmunoResearch) was used to detect CAR expression.
In selected experiments we performed immunophenotype characterization of CSPG4-CAR.CIK after 24h and 72h cultured in challenging metabolic conditions represented by glucose deprivation ([Glucose]= 5 – 0,5 mM) combined or not with hypoxia (O_2=1%) and comparing results with standard culture conditions ([Glucose]=11mM and O_2=21%). For these characterizations, we focused on nutrient transporters (GLUT1-APC (R&D Systems), MCT1-PE (R&D Systems), MCT4-FITC (Santa Cruz Biotechnology)) and immunecheckpoint receptors expression (PD-1-APC (BD PHarmingen™), TIM3-APC (MACS Miltenyi Biotec), LAG3-APC (BD PHarmingen™), CD96-PE (eBioscience), TIGIT-PerCp Cy5 (eBioscience)).
STS cells were stained with conjugated mAbs for the expression of CIK NKG2D ligands, MIC A/B (BD Pharmingen) and ULBPs (R&D Systems) and for the expression of HLA-ABC, PD-L1, and PD-L2 (BD Pharmingen). STS were stained for CSPG4 with mAbs 225.28,

763.74, and D2.8.5-C4B8 (*184*), kindly provided by Prof. S. Ferrone, which recognize distinct and spatially distant epitopes of CSPG4. Cells were first incubated with CSPG4-specific mAbs (1 mg/mL for all mAbs), then washed, and incubated with rabbit anti-mouse IgG-PE Secondary Antibody (Miltenyi Biotec). Alternatively, CSPG4 was detected with the conjugated anti-human CSPG4-APC mAb (Miltenyi Biotec). CSPG4 molecules expressed on the surface of STS and other cell lines were measured using a quantitative immunofluorescence assay (Bangs Laboratories, Inc.). Briefly, cells of interest and calibration beads with increasing amounts of antibody capture capability were labeled simultaneously with the anti-human CSPG4-APC mAb. Labeled cells and calibration beads were analysed on the same flow cytometer and a standard regression line was calculated between fluorescence intensity and antigen density, expressed as antibody-binding capacity in molecules per cell. We defined high CSPG4 expression as 2-fold increase as compared with normal keratinocytes.

In selected experiments we performed phenotype characterization of STS after 24h and 72h of cultures in challenging metabolic conditions represented by glucose deprivation ([Glucose]= 5 – 0,5 mM) combined or not with hypoxia (O_2=1%) and comparing results with standard culture conditions ([Glucose]=25mM and O_2=21%). For these characterizations, we focused on nutrient transporters (GLUT1-APC (R&D Systems), MCT1-PE (R&D Systems), MCT4-FITC (Santa Cruz Biotechnology)) and immunecheckpoint ligands expression (CD112-PE (R&D Systems), CD155-FITC (R&D Systems), HLA II-FITC (BD PHarmingen™), PD-L1-PE (BD PHarmingen™), PD-L2-APC (BD PHarmingen™), GAL9-APC (Invitrogen, Life Technologies)).

Labeled cells were acquired on FACS Cyan (Cyan ADP, Beckman Coulter SRL) and analyzed using Summit Software.

Fluorescent glucose (2-NBDG) uptake assays

To monitor CSPG4-CAR.CIK and STS glucose uptake we used a fluorescent glucose analog (2-NBDG, 7-nitrobenz-2-oxa-1,3-diazol-4-yl)amino)-2-deoxyglucose (ThermoFisher Scientific). Briefly, we plated CSPG4-CAR.CIK with STS cells directly in FACS tubes at E:T ratio 1:1 in glucose-lacking medium with 2-NBDG (50mM) for 15 minutes, both in normoxia and hypoxia. STS cells and CSPG4-CAR.CIK were also tested separately as control to assess their spontaneous uptake.

We stopped glucose uptake reaction washing cells with cold (4°C) PBS 1x, then we stained with anti-CD3 mAb (BD Pharmingen) to better identify effectors from target cells in co-

culture. CSPG4-CAR.CIK and STS cells glucose uptake was assessed as percentage of 2-NBDG$^+$ cells. Parallel unmodified CIK we used as control.

Tumor cell killing assays

We assessed the tumor-killing ability of patient-derived CSPG4-CAR.CIK and unmodified NTD.CIK *in vitro* against STS cell monolayers and STS 3D spheroids. In two cases, CIK and STS cell cultures were generated from samples collected from the same patient (S1 and S172), while in all other cases, cytotoxicity assays were performed with HLA-mismatched effector cells. Cytotoxicity assays against STS cell monolayers were performed using flow cytometry or a bioluminescence cell viability assay. In the first case, target cells were stained with either vital dye PKH26 (Sigma-Aldrich) or 5,6-carboxyfluorescein diacetate succinimidyl ester (CFSE; Molecular Probes), according to the manufacturer's protocols. Immune-mediated killing was analysed by Flow Cytometry (Cyan ADP, Dako) and measured by the DAPI permeability of target cells (PKH26$^+$ or CFSE$^+$ gate). For the bioluminescence method, cytotoxicity was measured with the CellTiter-Glo Luminescent Cell Viability Assay (Promega), in which the number of viable and metabolically active target cells was evaluated by quantifying the ATP in culture. CIK cells were cocultured at different effector to target cell (E:T) ratios (10:1, 5:1, 2.5:1, 1:1, 1:2, and 1:4) in cytotoxicity assays (300 U/mL IL2 medium at 37°C and 5% CO_2) for 5 hours (short-term assay) and 48 hours (long-term assay). In selected experiments, we tested the cytotoxic activity at very low E:T ratio (1:8, 1:16, 1:32, and 1:64). Target cells were also tested separately from CIK cells as control to assess their spontaneous mortality. The percentage of STS-specific lysis for each E:T ratio was calculated using the following formula: [(experimental - spontaneous mortality/100 - spontaneous mortality) x 100]. In selected experiments, growth of residual sarcoma cells was investigated 48 hours after the treatment with either CSPG4-CAR.CIK or NTD.CIK.

In selected experiments we evaluated CSPG4-CAR.CIK antitumor activity in challenging metabolic conditions ([Glucose]=5-0,5mM ± O_2=1%) comparing to standard conditions ([Glucose]=25/11mM, O_2=21%). We performed these dedicated cytotoxicity tests at E:T 1:1 for 24h.

In 3D assays, STS spheroids stably expressing GFP were seeded one per well in ULA 96-well round bottom plates. CSPG4-CAR.CIK and unmodified NTD.CIK were stained with PKH26 dye and plated at E:T ratio 2:1 in culture medium with 300 U/mL IL2 at 37°C 5% CO_2. Fluorescence images were acquired at 12-hour intervals over 96 hours under the same magnification (10x). Killing activity was determined as loss of GFP fluorescence spheroid

area (pixel) using fluorescence microscopy (Leica DMI 3000B equipped with Photometrics CoolSnap HQ CCD Camera). Untreated STS spheroids were used to evaluate spontaneous mortality. All images were analyzed with ImageJ software, and percentage of tumor cell lysis was determined by the formula: [100 - treated GFP^+ STS spheroid (pixel) - 100/untreated GFP^+ STS spheroid (pixel)].

Immunofluorescence analysis of CSPG4-CAR.CIK cell recruitment and infiltration in STS spheroids

GFP^+ STS spheroids were co-cultured with CSPG4-CAR.CIK or unmodified NTD.CIK cells stained with red dye PKH26 at E:T ratio 2:1 in culture medium (300 U/mL IL2 at 37C, 5% CO_2). Following a 16-hour co-culture at 37°C, CIK cells were removed and immunofluorescence acquisition was conducted on the remaining spheroids. Briefly, STS spheroids were washed twice, centrifuged at 300 g for 3 minutes in PBS, fixed in 4% paraformaldehyde for 1 hour, resuspended with mounting medium, and applied on either glass slides or glass bottom chamber slide wells. STS spheroids were observed using a Leica SP8 AOBS confocal microscope. Next, 80MHzpulsed white light laser (470–670 nm) was used to excite the fluorochromes in the spheroids. Fluorescence channels were scanned sequentially, and hybrid Spectral Detectors (HyD SP Leica Microsystems) revealed the emissions. Image acquisition of the STS spheroids was performed maintaining the same laser power, gain, offset, and magnification (20x). We generated maximum intensity projections for each analysed spheroid with LAS X Software (Leica) to quantify CIK cell recruitment and infiltration. Images of the total PKH26 red fluorescence area (mm^2) present either at the boundary or inside the spheroid were analysed using ImageJ software.

Live-cell imaging of cytotoxic assays against STS spheroids

We plated one single GFP^+ STS spheroid per well in a black-walled glass bottom 24-well (#1.5 Cellvis) to dynamically visualize the cytotoxic activity of CSPG4-CAR.CIK and unmodified NTD.CIK against the STS spheroids. We added CSPG4-CAR.CIK and unmodified NTD.CIK stained with the PKH26 dye at E:T ratio 2:1 in culture medium with 300 U/mL IL-2 at 37°C, 5% CO_2. The plate was placed onto a sample stage within an incubator chamber set to 37°C, in an atmosphere of 5% CO_2, 20% humidity. Imaging was recorded on a Hamamatsu EM-CCD camera (C9100-02, Hamamatsu, SZK, Japan) mounted on a Leica AF 6000LX workstation for 72 hours at identical positions in intervals of 15 min at 10x magnification [Suppl. Video 1-2]. Three-dimensional reconstructions of GFP^+ STS

spheroids infiltrated by CIK were performed by LAS X software Visualization module and THUNDER Imaging Systems (Leica) [Suppl. Videos 3-6].

CIK-cell penetration capability into Matrigel matrix

STS spheroids were collected, washed in PBS, resuspended in 20 mL of liquefied Matrigel (BD Pharmingen) at 4°C, and then plated as droplets in well centers of a 24-well tissue culture plate that had been prewarmed to 37°C. Plates were incubated at 37°C and 5% CO_2 for 15 minutes to allow the solidification of the Matrigel domes. Domes were then overlaid with 500 mL of prewarmed medium with 300 U/mL IL2 and cocultured with PKH2-stained CSPG4-CAR.CIK or unmodified NTD.CIK cells (50.000 cells/well) for 5 days. Empty domes were used as controls. At the end of the co-culture period, each well was washed twice with prewarmed PBS to eliminate any effector cells outside the domes. Fluorescence microscopy (Leica DMI 3000B with Photometrics CoolSnap HQ equipped with CCD camera) was used to visualize CSPG4-CAR.CIK or unmodified NTD.CIK cell migration at the Matrigel boundary and cells that penetrated into the Matrigel domes. Analysis of the PKH26 red fluorescence dye presence (mm^2) was performed with ImageJ software.

CIK-cell migration capability into 3D microfluidic system

GFP^+ STS spheroids were formed, collected, washed in PBS and placed into central “tumor” chamber of 3D microfluidic chip (AIM Biotech) in culture medium. CSPG4-CAR.CIK or unmodified NTD.CIK cells were stained with red dye PKH26 and placed into a side “immune” chamber of the same 3D microfluidic chip in standard or glucose deprived ([Glucose=5mM]) culture medium with 300 U/mL IL2. Microfluidic chip was incubated onto the motorized stage within an incubator chamber set to 37°C, in an atmosphere of 5% CO_2, 20% humidity.
Imaging was performed with Iris 15 camera (Photometrics) mounted on high content imaging system LIPSI (Nikon Instrument Inc.) for 7 days at identical positions in intervals of 4h at 10x magnification.
Analysis of the progressively increase of PKH26 red fluorescence dye presence (mm^2) in the central chamber was performed with NISElements software and quantification represented theCSPG4-CAR.CIK migration into central “tumor” chamber of 3D microfluidic system.

STS TME elements isolation

Human STS samples were obtained from surgical specimens. Patients provided consent under institutional review board–approved protocols and investigations were conducted after approval by a local Human Investigations Committee.

Fresh tumor specimens were mechanically dissociated in a 10-cm dish using sterile forceps and scalpel and partially digested in collagenase IV (100 U/mL, Worthington) in combination with the gentleMACS™ Octo Dissociator (Miltenyi Biotec). Samples were pelleted and resuspended in 10 mL of DMEM High Glucose (Sigma-Aldrich). Red blood cells were removed from visibly bloody samples using RBC lysis buffer (Pharm Lyse, BD Pharmingen). Sample were strained over 100-µm cell strainer (Falcon) to generate a single cells suspension. Non-tumoral cells were isolated by Tumor Cell Isolation Kit (Miltenyi Biotec) on MACS separation columns (Miltenyi Biotec), according to manufacturer instructions. Isolated cells were stained with conjugated antibodies anti-CD45-PerCP-Cy5 (BD Pharmingen), CD3-FITC (Miltenyi Biotec), CD4-APC (Miltenyi Biotec), CD8-PE (Miltenyi Biotec), CD56-APC (Miltenyi Biotec), PD-1-PE-CF594 (BD Pharmingen), HLA-DR-PE-Cy7 (BD Pharmingen), CD15-FITC (BD Pharmingen), CD14-PE (BD Pharmingen), CD11b-APC (BD Pharmingen), CD19-FITC (Dako), CD20-PE (BD Pharmingen), CD25-PE (Miltenyi Biotec), CD33-PE (Miltenyi Biotec), FOXP3-APC (Miltenyi Biotec), CD45RO-APC (Miltenyi Biotec), CD45RA-FITC (Miltenyi Biotec), CD62L-PE (Miltenyi Biotec), CCR7-PE (Miltenyi Biotec) and analysed by flow cytometry. For T_{regs} characterization, we employed T_{regs} detection kit (Miltenyi Biotec) according to manufacturer instructions.

Generation of 3D PDO STS spheroids

Human STS samples were obtained from surgical specimens.

Fresh tumor specimens were mechanically dissociated in a 10-cm dish using sterile forceps and scalpel and partially digested in collagenase IV (100 U/mL, Worthington) in combination with the gentleMACS™ Octo Dissociator (Miltenyi Biotec). Samples were pelleted and resuspended in 10 mL of DMEM High Glucose (Sigma-Aldrich). Red blood cells were removed from visibly bloody samples using RBC lysis buffer (Pharm Lyse, BD). Sample were strained by a 40 mm ⌀ 80 syringe (Braun) obtaining PDO-spheroids (*185, 186*).

PDO-spheroids were pelleted and resuspended in Cultrex (RGF BME type 2, R&D Systems) and the spheroid–collagen mixture was plated into the center region of a microscope 8 chamber polystyrene vessel tissue culture treated glass slide (Falcon).

Wells containing PDO spheroids were hydrated with 300 µl of medium after 10 minutes to achieve Cultrex solidification.
After 24h PDO spheroids were fixed in fixed in 4% paraformaldehyde for 30 min and stained with directly conjugated antibodies and DAPI, according to manufacturer instructions.
Conjugated antibodies used were specific for the following human markers: CD45-PE (R&D Systems), CD45RO-Alexa Fluor 488 (Biolegend), CD3-Alexa Fluor 555 (Abcam), CD4-Alexa Fluor 488 (Abcam), CD8-Alexa Fluor 660 (eBioscence, Invitrogen), CD56-Alexa Fluor 488 (Abcam), CD11b-Alexa Fluor 647 (Abcam), αSMA-Alexa Fluor 660 (eBioscence, Invitrogen), p-Ker (AE1/AE3)-Alexa Fluor 570 (eBioscence, Invitrogen), FOXP3-Alexa Fluor 570 (eBioscence, Invitrogen), GRZb-Alexa Fluor 647 (Biolegend), IFNγ Alexa Fluor 488 (Biolegend), PD-1-Alexa Fluor 647 (Abcam), PD-L1-Alexa Fluor 555 (Abcam), MHC-I-Alexa Fluor 647 (Abcam), CSPG4-APC (Miltenyi Biotec).
STS spheroids were observed using a TCS SPE Leica.
We generated maximum intensity projections for each analysed spheroid with LAS X Software (Leica) to quantify presence of distinct STS TME elements. Images were analysed using ImageJ software.

In vitro cytokine production

CSPG4-CAR.CIK and CSPG4-CAR.T cells, and unmanipulated NTD.CIK and NTD.T cells were cocultured alone or with tumor cells in RPMI1640 medium with 300 U/mL (CIK) or 50 U/mL IL2 (T cells) at a 2:1 E:T ratio and incubated at 37°C for 48 hours. Concentrations of cytokines in culture supernatant were measured using the Bio-Plex Pro Human Cytokine 9-plex Assay Kit (Bio-Rad Laboratories Inc.) according to the manufacturer's instructions. Each sample was measured in duplicate. Data were acquired and analyzed by Bioclarma (Analysis Service). Granzyme B concentration was measured in supernatants from mixed target/effector cell cultures (ELISA Granzyme B Kit, Diaclone SAS), as recommended by the manufacturer. In selected experiments, we quantified CSPG4-CAR.CIK IFNγ production in normoxia and hypoxia conditions by Quintikine ELISA Human IFNγ kit (R&D systems).

In vivo activity of patient-derived CSPG4-CAR.CIK

The antitumor activity of CSPG4-CAR.CIK and unmodified NTD.CIK was evaluated using STS xenograft models in immunodeficient mice. *In vivo* experiments received approval by the competent committee and internal review board (auth. no., 178/2015-PR). STS xenografts were established in 7- to 8-week-old NOD/SCID/$\gamma c^{-/-}$ (NSG) or NOD/SCID

(Charles River Laboratories, SRL) female mice by subcutaneous injection with 1 x 10^6 cells obtained from three STS [fibrosarcoma (HT1080), leiomyosarcoma (S172), and UPS (S1)]. Autologous CSPG4-CAR.CIK and unmodified NTD.CIK were available for S172 and S1 xenografts. Allogeneic CSPG4-CAR.CIK from unrelated patients with STS were generated following the same protocol used to generate autologous CIK identical and used in the HT1080 xenograft model. When tumors were approximatively 50 mm^3 in volume, mice were infused twice a week with 1 x 10^6 CSPG4-CAR.CIK or unmodified NTD.CIK resuspended in PBS (200 mL), for a total of four infusions. Mice injected with PBS only were used as controls. Treatment and control cohorts included 6 mice each for the leiomyosarcoma (S172) group. For the fibrosarcoma (HT1080) and UPS (S1) xenografts and control groups, each group included 3 mice. Dedicated mice cohorts (n=3/cohort) were treated with intravenous infusion of 1x10^6 CSPG4-CAR.CIK or unmodified CIK twice a week combined with intraperitoneal anti-PD-1 antibody (200 μg/mouse; inVivoMAb) three times a week for 2 weeks.

In the experiments with fibrosarcoma (HT1080) and leiomyosarcoma (S172), mice were sacrificed at the end of treatment. In the experiment with UPS (S1), mice were sacrificed 14 days after the last CIK infusion. Mice were monitored daily for possible toxicities, while tumor growth was measured weekly with manual caliper. Mice were sacrificed at the end of treatment or if tumor reached 2 cm along the main diameter.

In additional experiments, mice engrafted with the S172 cell line (n = 4 mice per treatment) or the HT1080 cell line (n = 5 mice per treatment) were infused with CSPG4-CAR.CIK and unmodified NTD.CIK generated from unrelated donors. In these models, when the tumor volume was approximatively 20 mm^3, mice received two infusions (on days 0 and +4) of 3 x 10^6 CSPG4-CAR.CIK or unmodified NTD.CIK. Mice were sacrificed 11 days after the last dose of cells. Tumor volume was calculated by the following formula: V ¼ 4/3 x π x $(a/2)^2$ x (b/2), where a is the length and b is the width of the tumor.

IHC

STS xenografts were analyzed by IHC. Samples (5-mm thick) were cut from formalin-fixed, paraffin-embedded tissue sections, mounted on slides, and treated per standard IHC procedures. Tissue sections were deparaffinized with 100% xylene and rehydrated with decreasing concentrations of ethyl alcohol. Antigen retrieval was performed by boiling the sections in 1 mmol/L EDTA (pH 9.0) for 60 minutes. Slides were treated with 3% hydrogen peroxide, 1% BSA (Invitrogen), and 5% normal horse serum in TBS [25 mmol/L Tris (pH

7.4) and 150 mmol/L NaCl] containing 0.1% Tween 20 (Sigma-Aldrich, Inc). To confirm CSPG4 expression, slides were incubated in a closed humid chamber overnight at 4°C with the CSPG4-specific mAb 225.28, 763.74, and D2.8.5-C4B8 (4 mg/mL each) pool. After washing, a secondary anti-mouse IgG xeno-antibody was added. Secondary antibodies conjugated to horseradish peroxidase (HRP) were generated and IHC signals were detected with the EnVision1 System-HRP (Dako North America, Inc) and chromogen Diaminobenzidine (DAB) Substrate (DakoCytomation Liquid DABþ Substrate Chromogen System, Dako). Tissue sections were counterstained with Mayer Hematoxylin (Bio-Optica). We also explored the presence of infiltrated CSPG4-CAR.CIK, unmodified NTD.CIK cells, and apoptotic tumor cells in explanted tumors from treated mice. Tissues were stained according to the manufacturer's protocols with the primary polyclonal antibody anti-CD3 (DAKO) and anti-cleaved caspase 3 (Cell Signaling Technology). Tissue sections were mounted on glass slides and visualized with a DM750 Leica Microscope equipped with Leica ICC50W CCD Camera (LAS EZ3.4.0 software).

Statistical analysis

All experiments were performed at least twice. Data were analyzed using GraphPad Prism 8.0 (GraphPad Software). Descriptive data are presented as mean values ± SE. To find statistical significance in the comparison of two groups, we used two-tailed Student t tests; for comparison of three or more groups, the data were analyzed by two-way ANOVA with Bonferroni multiple comparison post hoc tests. A $P < 0.05$ was considered significant. Significance is represented on graphs as *, $P \leq 0.05$; **, $P \leq 0.01$; ***, $P \leq 0.001$; ****, $P \leq 0.0001$.

Results

1. Anti-CSPG4 CAR-redirected Cytokine Induced Killer Cells (CIK)

1.1 Generation and characterization of patient-derived CSPG4-CAR.CIK

CIK were efficiently generated from Peripheral Blood Mononuclear Cells (PBMCs) obtained from 9 patients, with diagnosis of STS. We genetically engineered CIK to express the CSPG4-specific CAR, including the 4-1BB costimulatory molecule, by oncoretroviral transduction of PBMCs at day +3 of culture with the retroviral vector MoMLV-RV-CSPG4.CAR.

Three weeks after transduction and *ex vivo* expansion, the mean membrane CAR expression in CAR-engineered CIK (CSPG4-CAR.CIK) was 47% ± 6% as assessed by flow cytometry (Fig. 1A). The CSPG4-CAR expression was comparable to that obtained transducing CIK with the control retroviral vector MoMLV-RV-CD19.CAR (CD19-CAR). The median *ex vivo* expansion of CSPG4-CAR.CIK was 159 fold (27-348).

The main cellular subset of CSPG4-CAR.CIK were $CD3^+CD8^+$ (70% ± 4%) with a relevant subset (38% ± 4%) co-expressing the CD56 molecule ($CD3^+CD56^+$). The mean membrane expression of NKG2D receptor was 68% ± 5% and the effector memory (EM: $CD62L^+CD45RA^-$) was the most represented phenotype (47% ± 0.1%) (Fig. 1B).

The membrane expression of the immune-checkpoint receptor PD-1 in mature CSPG4-CAR.CIK was low (12% ± 2%). In selected experiments (n=3), we explored the expression of other immune-checkpoints, reporting relevant levels of TIM3 and CD96 receptor on CSPG4-CAR.CIK.

Ex vivo expansion rates and phenotypic characterization of CSPG4-CAR.CIK were comparable to that observed with paired control unmodified NTD.CIK ($p>0.05$), ruling out possible detrimental effects by retroviral transduction on CSPG4-CAR.CIK and CAR expression.

All CIK phenotype data were summarized in Table 1.

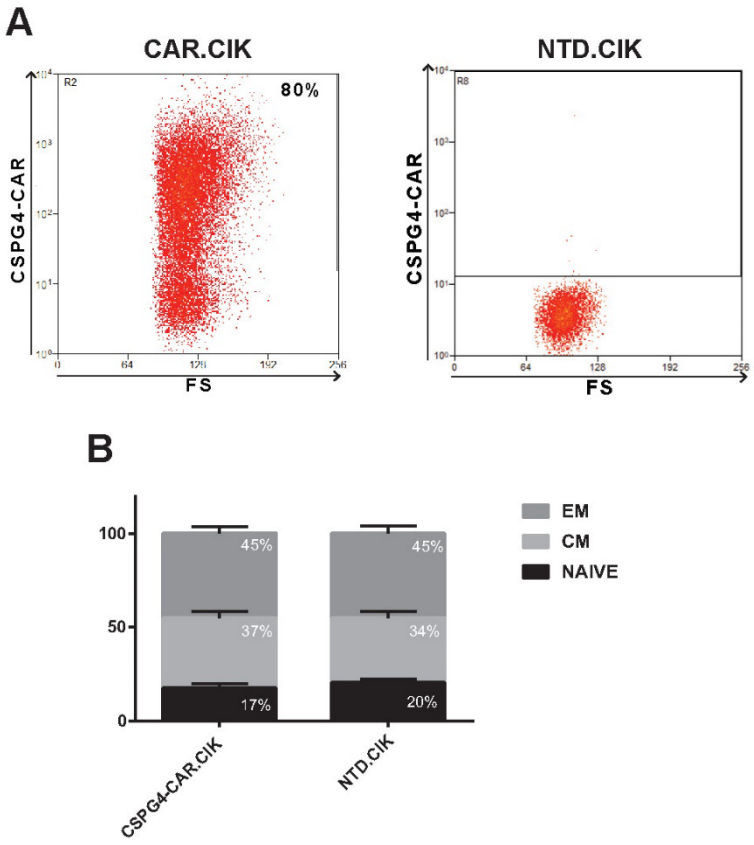

Figure 1. **Phenotypic characterization of CSPG4-CAR.CIK**
Representative flow-cytometry dot-plots showing that patient-derived CAR.CIK express the CSPG4-CAR as compared to paired control unmodified CIK **(A).** CSPG4-CAR.CIK were mostly composed by effector memory (EM), followed by central memory and naive cells. Cell subset composition of CSPG4-CAR.CIK was comparable with that of unmodified NTD.CIK (paired t test, p>0.05) **(B).**
Abbreviations: CIK, Cytokine Induced Killer cells; CSPG4, Chondroitin Sulfate Proteoglycan 4; Chimeric Antigen Receptor (CAR); Not Transduced (NTD); Effector Memory (EM: $CD45RA^{-}/CD62L^{-}$); Central Memory (CM: $CD45RA^{-}/CD62L^{+}$); NAÏVE: $CD45RA^{+}/CD62L^{+}$.

#Pt	Diagnosis		CD3 (%)	CD3/CAR (%)	CD3/CD56 (%)	CD3/CD8 (%)	NKG2D (%)	CXCR3 (%)	CXCR4 (%)	CCR7 (%)	PD-1 (%)
#Pt1	Low Grade Myofibroblastic Sarcoma	CAR.CIK	99	44	50	81	88	60	39	3	2
		NTD.CIK	99	/	67	77	86	76	39	11	3
#Pt2	Synovial Sarcoma	CAR.CIK	99	83	64	71	70	90	39	19	18
		NTD.CIK	99	/	58	62	81	93	39	45	5
#Pt3	Liposarcoma	CAR.CIK	99	30	40	70	89	78	38	28	4
		NTD.CIK	99	/	31	75	55	90	22	26	4
#Pt4 *	UPS	CAR.CIK	98	37	40	64	64	77	35	22	12
		NTD.CIK	97	/	26	59	64	80	41	26	11
#Pt5 *	Leiomyosarcoma	CAR.CIK	98	39	16	55	46	72	60	34	15
		NTD.CIK	99	/	24	51	54	71	52	26	23
#Pt6	UPS	CAR.CIK	99	65	43	88	60	87	32	9	17
		NTD.CIK	99	/	34	80	88	97	10	23	10
#Pt7	Chondrosarcoma	CAR.CIK	98	68	39	83	73	86	31	26	10
		NTD.CIK	98	/	46	91	83	91	34	37	18
#Pt8	Endometrial Stromal Sarcoma	CAR.CIK	99	65	20	78	55	90	82	72	15
		NTD.CIK	99	/	20	62	60	97	66	47	5
#Pt9	GIST	CAR.CIK	99	10	49	71	95	79	45	28	8
		NTD.CIK	99	/	38	61	81	83	40	23	7
Mean±SEM (%)		CAR.CIK	99±0,2	47±6	38±4	70±4	68±5	79±5	45±7	28±7	12±2
		NTD.CIK	98±0,4	/	35±4	66±4	70±4	84±5	40±7	29±3	11±2

Table 1. **Phenotypic characterization of patient-derived CSPG4-CAR.CIK and unmodified NTD.CIK**
The immunophenotype of all patient-derived CSPG4-CAR.CIK and paired unmodified NTD.CIK is reported in the table.
*CIK from #Pt4 and #Pt5 are autologous with STS S1 and S172, respectively.
Abbreviations: CIK, Cytokine Induced Killer cells; Chimeric Antigen Receptor (CAR); Not Transduced (NTD).

1.2 Challenging metabolic conditions did not significantly affect CSPG4-CAR.CIK viability and phenotype

In selected experiments (n=3), we cultured CAR.CIK in challenging metabolic conditions resembling the hostile features of solid tumor microenvironment (TME), to assess their viability and characterize immunophenotype and functional capabilities.

Challenging metabolic conditions were represented by glucose deprivation ([Glucose]= 5 – 0,5 mM) in the culture medium combined or not with hypoxia (O_2=1%) and results were compared to standard conditions ([Glucose]=11mM and O_2=21%) after 24h of culture (Fig. 2A). We compared data from CSPG4-CAR.CIK with paired unmodified NTD.CIK as control.

The tested challenging metabolic conditions did not significantly impair CSPG4-CAR.CIK viability. NTD.CIK viability was comparable to CSPG4-CAR.CIK viability at all the culture conditions tested ($p \geq 0.05$) (Fig 2B). Only after extending the culture time at 72h, we started to observe a progressive decrease in both CAR-CIK and NTD-CIK viability, especially at very low ([Glucose]=0,5mM) glucose concentrations.

We assessed potential variations in CSPG4-CAR.CIK immunophenotype caused by challenging metabolic conditions, focusing on cytotoxic receptors (CAR, NKG2D), glucose and lactate transporters (GLUT1, MCT1, MCT4), immunecheckpoint receptors (PD-1, LAG3, TIM3, CD96, TIGIT). CIK phenotype (mean±SEM) in standard culture conditions is reported in Fig. 2C. In the explored challenging conditions (after 24h and 72h), we did not observe any relevant phenotype variations as compared to standard conditions ($p > 0.05$).

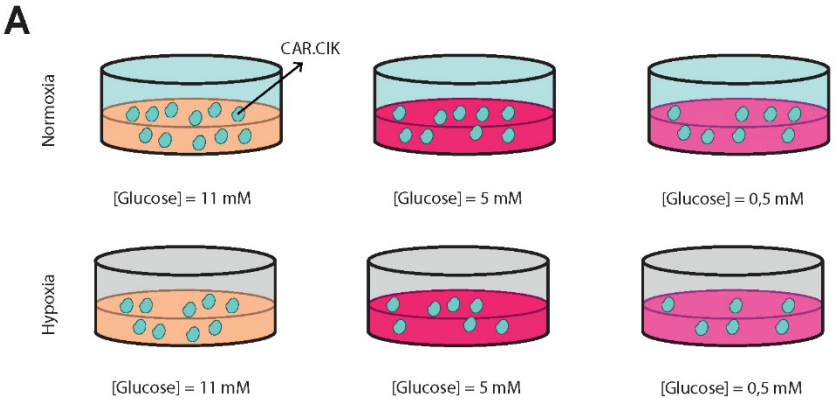

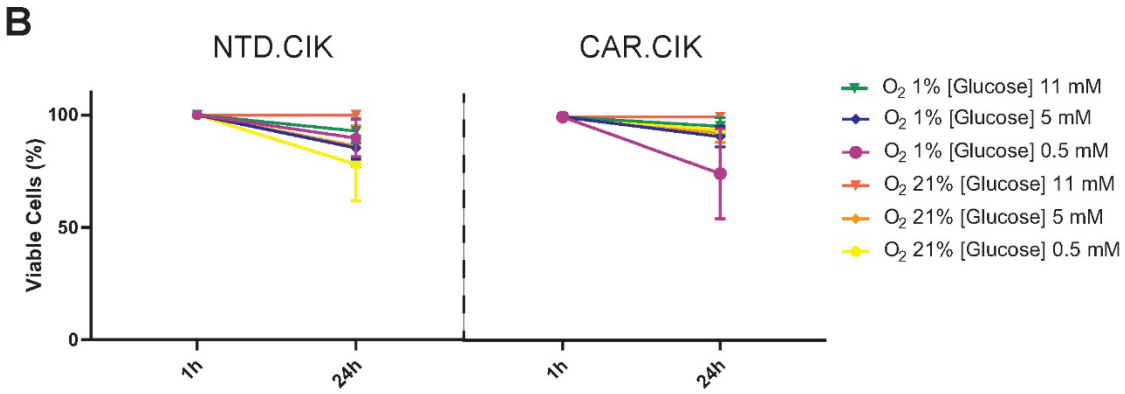

C

	CAR (%) Mean±SEM	CD3/CD56 (%) Mean±SEM	NKG2D (%) Mean±SEM	CD3/CD8 (%) Mean±SEM	PD-1 (%) Mean±SEM	TIM3 (%) Mean±SEM	LAG3 (%) Mean±SEM	CD96 (%) Mean±SEM	TIGIT (%) Mean±SEM	GLUT1 (%) Mean±SEM	MCT1 (%) Mean±SEM	MCT4 (%) Mean±SEM
CAR.CIK	47±14	36.5±12.5	85.5±9.5	71±0	7.0±1.0	52.5±46.5	25.5±25.5	93.5±0.5	22±2	67.5±7.5	9±8	60±0
NTD.CIK	/	32±6	88±7	66±5	6.5±0.5	62±33	17.5±15	94±3	21.5±6.5	65±5	9.5±8.5	58.5±2.5

Figure 2. **Challenging metabolic conditions did not significantly affect CSPG4-CAR.CIK**
Schematic representation of challenging metabolic conditions tested for CSPG4-CAR.CIK viability and immunephenotype assessment **(A).** CSPG4-CAR.CIK and NTD.CIK viability in challenging metabolic conditions ([Glucose]=5mM - 0,5 mM ± O_2 1%) compared to standard culture conditions ([Glucose]=11mM + O_2 21%) **(B).** Phenotypic characterization of patient-derived CSPG4-CAR.CIK and unmodified NTD.CIK in standard culture conditions. The immunophenotype of selected patient-derived CSPG4-CAR.CIK and paired unmodified NTD.CIK in standard culture conditions is reported in the table **(C)**.
Abbreviations: CIK, Cytokine Induced Killer cells; Chimeric Antigen Receptor (CAR); Not Transduced (NTD), CAR, Chimeric Antigen Receptor; CD, Cluster of Differentiation; NKG2D, Natural Killer Group 2D receptor; PD-1, Programmed cell Death 1; PD-L1/2, Programmed cell Death Ligand 1-2; TIM3, T cell immunoglobulin and mucin domain-containing protein 3; LAG3, Lymphocyte Activation Gene-3; TIGIT, T cell immunoreceptor with Ig and ITIM domains; GLUT1, Glucose transporter 1; MCT1, lactate transporter monocarboxylate transporter 1; MCT4, lactate transporter monocarboxylate transporter 4.

2. Soft Tissue Sarcoma (STS)

2.1 Characterization of STS

We characterized by flow-cytometry a panel of 16 STS cell lines obtained from biopsies of patients affected by different histotypes of advanced STS (UPS, n=3; gastrointestinal stromal tumor (GIST), n=5; liposarcoma, n=4; leiomyosarcoma, n=2; and Malignant Peripheral Nerve Sheath Tumors (MPNST), n=1; Fibrosarcoma, n=1 (HT1080 cell line from ATCC)). We confirmed that patient-derived STS cell lines express the main known ligands recognized by NKG2D at variable levels (MIC A/B, 30% ± 8%; ULBP1, 1% ± 0.7%; ULBP2/5/6, 71% ± 6%; and ULBP3, 25% ± 9%). HLA class I expression was retained by all STS cell lines tested (95% ± 2%), along with variable levels of immune-checkpoints, PD-L1 (32% ± 9%) and PD-L2 (65% ± 6%).
All STS phenotype data were summarized in Table 2.

#Pt	Diagnosis	MIC A/B (%)	ULBP1 (%)	ULBP2/5/6 (%)	ULBP3 (%)	HLA (%)	PD-L1 (%)	PD-L2 (%)	CSPG4 (%)
S1	UPS	13	0	100	90	100	10	76	95
S3	UPS	90	0	100	100	100	90	99	98
S5	UPS	3	0	100	75	100	0	45	95
S234	MPNST	7	0	16	0	86	2	42	97
S23	LIPOSARCOMA	67	9	88	1	100	0	78	52
S24	LIPOSARCOMA	3	0	70	3	99	0	86	83
S25	LIPOSARCOMA	100	0	83	0	100	85	98	98
S309	LIPOSARCOMA	69	0	26	1	98	24	63	92
S047	GIST	35	0	74	56	93	13	15	95
S061	GIST	3	0	38	2	79	31	90	95
S175	GIST	27	7	87	31	95	64	50	100
S181	GIST	29	0	79	31	82	18	17	100
S188	GIST	19	0	54	4	100	80	56	100
S088	LEIOMYOSARCOMA	17	1	83	1	100	2	84	62
S172	LEIOMYOSARCOMA	6	0	55	1	96	15	69	72
HT1080	FIBROSARCOMA	0	0	80	3	90	85	75	23
	Mean±SEM	30,5±8,2	1,1±0,7	70,8±6,5	24,9±8,9	94,9±1,8	32,4±8,8	65,2±6,5	84,8±5,5

Table 2. Phenotypic characterization of STS cell lines
Patient diagnosis and CIK NKG2D ligands, HLA-I, PD-1, PD-L1/2 and CSPG4 expression are reported for all STS cell lines used in the study.
Abbreviations: UPS, Undifferentiated Pleomorphic Sarcoma; MPNST, Malignant Peripheral Nerve Sheath Tumors; MIC A/B, MHC class I chain-related gene A/B; ULBPs, UL16 binding proteins, HLA, human leukocyte antigens; PD-L1/2, Programmed cell Death Ligand 1-2; CSPG4, Chondroitin Sulfate Proteoglycan 4.

2.2 CSPG4 as a potential CAR target in STS

First, we reported, by in silico analysis of RNA-sequencing expression data from TCGA database, that CSPG4 is expressed in multiple STS histotypes (leiomyosarcoma, dedifferentiated liposarcoma, undifferentiated pleomorphic sarcoma (UPS), malignant fibrous histiocytoma, high-grade spindle cell sarcoma, myxofibrosarcoma, MPNST and synovial sarcoma) at levels similar to those found in melanoma cells (Fig. 3A).

We confirmed CSPG4 membrane expression by flow-cytometry in a panel of 15 STS cell lines obtained from biopsies of patients affected by different histotypes of advanced STS (UPS, n=3; gastrointestinal stromal tumor (GIST), n=5; liposarcoma, n=4; leiomyosarcoma, n=2; and MPNST, n=1) and in the HT1080 cell line (fibrosarcoma) from the ATCC. CSPG4 resulted expressed in all 16 (100%) STS cell line analyzed (Fig. 3B).

We quantified CSPG4 density on STS cell lines on a per cell basis by beads-based quantitative flow cytometry. CSPG4 resulted to be expressed with variable density in our STS samples (mean of 321 ± 47 molecules/cell). Notably, normal keratinocytes showed detectable CSPG4 expression (92%) but low CSPG4 density (105 molecules/cell) (Fig. 3C).

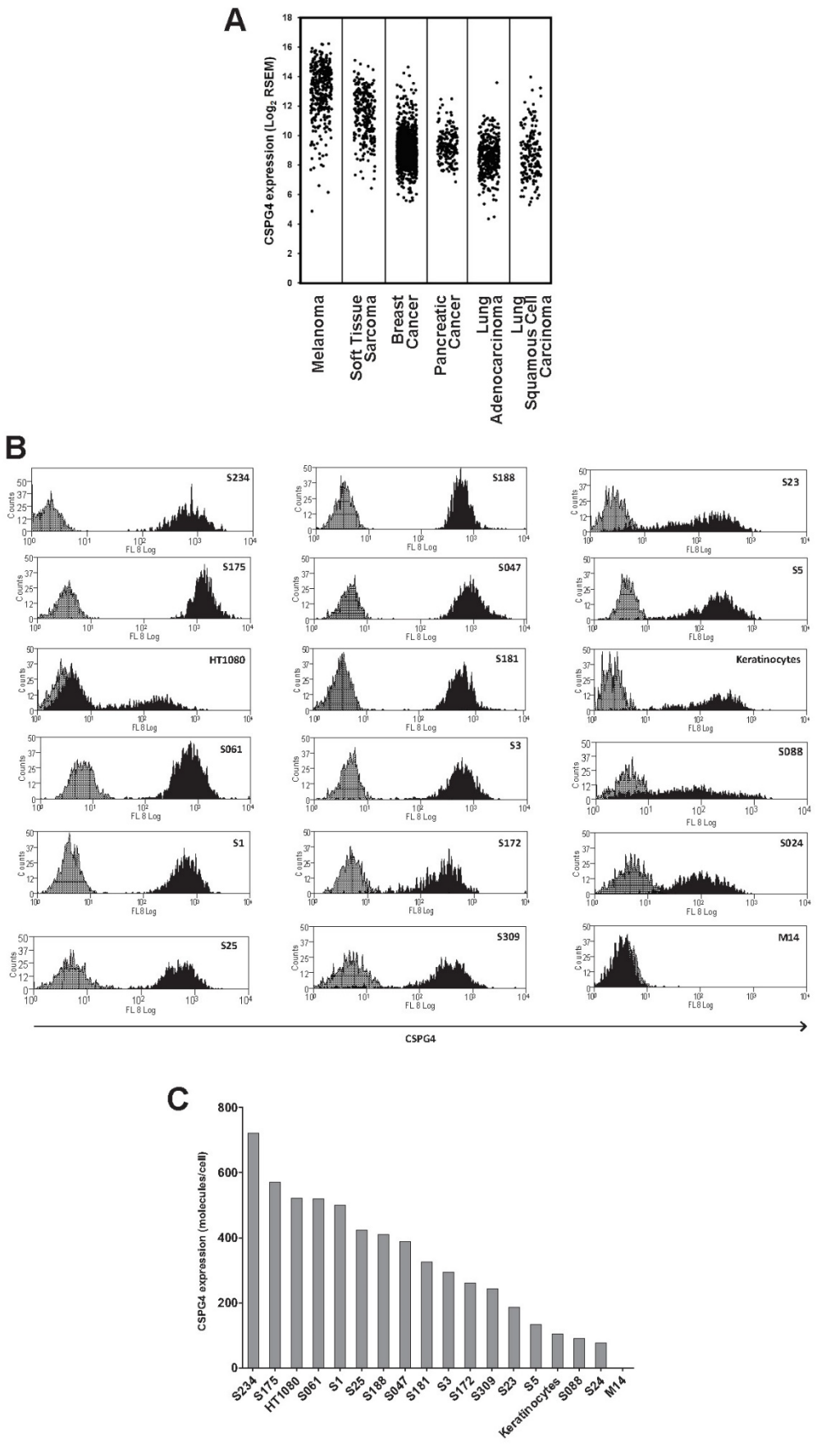
A
CSPG4 expression (Log2 RSEM)
Melanoma
Soft Tissue Sarcoma
Breast Cancer
Pancreatic Cancer
Lung Adenocarcinoma
Lung Squamous Cell Carcinoma
B
S234
S188
S23
S175
S047
S5
HT1080
S181
Keratinocytes
S061
S3
S088
S1
S172
S024
S25
S309
M14
Counts
FL 8 Log
CSPG4
C
CSPG4 expression (molecules/cell)
S234
S175
HT1080
S061
S1
S25
S188
S047
S181
S3
S172
S309
S23
S5
Keratinocytes
S088
S24
M14

Figure 3. CSPG4 is highly expressed in multiple STS histotypes
CSPG4 mRNA expression in multiple STS histotypes (Leiomyosarcoma; Dedifferentiated Liposarcoma; Undifferentiated pleomorphic sarcoma (UPS), Malignant Fibrous Histiocytoma, High-Grade Spindle Cell Sarcoma; Myxofibrosarcoma; Malignant Peripheral Nerve Sheath Tumor; Synovial Sarcoma). CSPG4 expression in STS was comparable to that observed in melanoma. RNA-sequencing expression data were selected and downloaded from the cBioPortal of the TCGA Pan-Cancer Collections. RSEM expression values were plotted after Log_2 transformation with 0.5 jittering on the x-axis, using Microsoft Excel®. **(A)**. CSPG4 expression was confirmed in patient-derived STS cell lines of various histologic types by flow cytometry. A representative flow-cytometry histogram is reported for each STS. The M14 melanoma cell line that lacks CSPG4 expression and normal keratinocytes were used for comparison. Isotype controls are shown in grey **(B)**. Grey histograms show the number of CSPG4 molecules expressed on the cell surface of various patient-derived STS cell lines quantified as the CSPG4-specific mAb-binding capacity (sABC) on a per cell basis **(C)**.
Abbreviations: CSPG4, Chondroitin Sulfate proteoglycan 4; STS, Soft Tissue Sarcoma.

2.3 Challenging metabolic conditions affected STS viability and phenotype

We cultured STS patient-derived cell lines from distinct histotypes (N=7: UPS n=2; Liposarcoma n=1; Gastrointestinal Stromal Tumor (GIST) n=2; Leiomyosarcoma n=1, Malignant Peripheral Nerve Sheath Tumors (MPNST) n=1) in challenging metabolic conditions resembling the hostile features of solid tumor microenvironment (TME), to assess their viability and characterize the main phenotype variations.

Challenging metabolic culture conditions were represented by glucose deprivation ([Glucose]=5 – 0,5 mM) combined or not with hypoxia (O_2=1%) and results were compared to standard culture conditions ([Glucose]=25mM and O_2=21%) within 24h of culture (Fig. 4A).

Distinct STS histotypes (n=7) showed different sensibility in their viability to the challenging metabolic conditions tested. Among our STS samples the most resistant to both glucose deprivation and hypoxia were MPNST and UPS, while GIST displayed the highest sensitivity.

We assessed variation in STS phenotype caused by challenging metabolic conditions, focusing on CSPG4 CAR-target, NKG2D ligands, glucose and lactate transporters (GLUT1, MCT1, MCT4), immunecheckpoint ligands (HLA II, PD-L1, PD-L2, GAL9).

STS phenotype (mean±SEM) in standard culture conditions is reported in Fig. 4B.

We did not observe any variation after 24h in challenging metabolic conditions as compared to controls. Extending the culture time at 72h, glucose deprivation increased immunecheckpoint ligand expression (PD-L1 2,2 fold ±1,5; PD-L2 4 fold ±2,8; GAL-9 2,6 fold ±0,9; HLA-II 6 fold ±4,8; mean±SEM, $p \leq 0.0001$) and nutrient transporters (GLUT1 2,2 fold ±0,3; MCT1 11,3 fold ±3,5; MCT4 1,6 fold ±0,5; mean±SEM, $p \leq 0.0001$). The combination with hypoxia conditions further increased nutrient transporter expressions (GLUT1 5,8 fold ±2,3; MCT1 14 fold ±7,8; mean±SEM, $p \leq 0.0001$) (Fig. 4C, D).

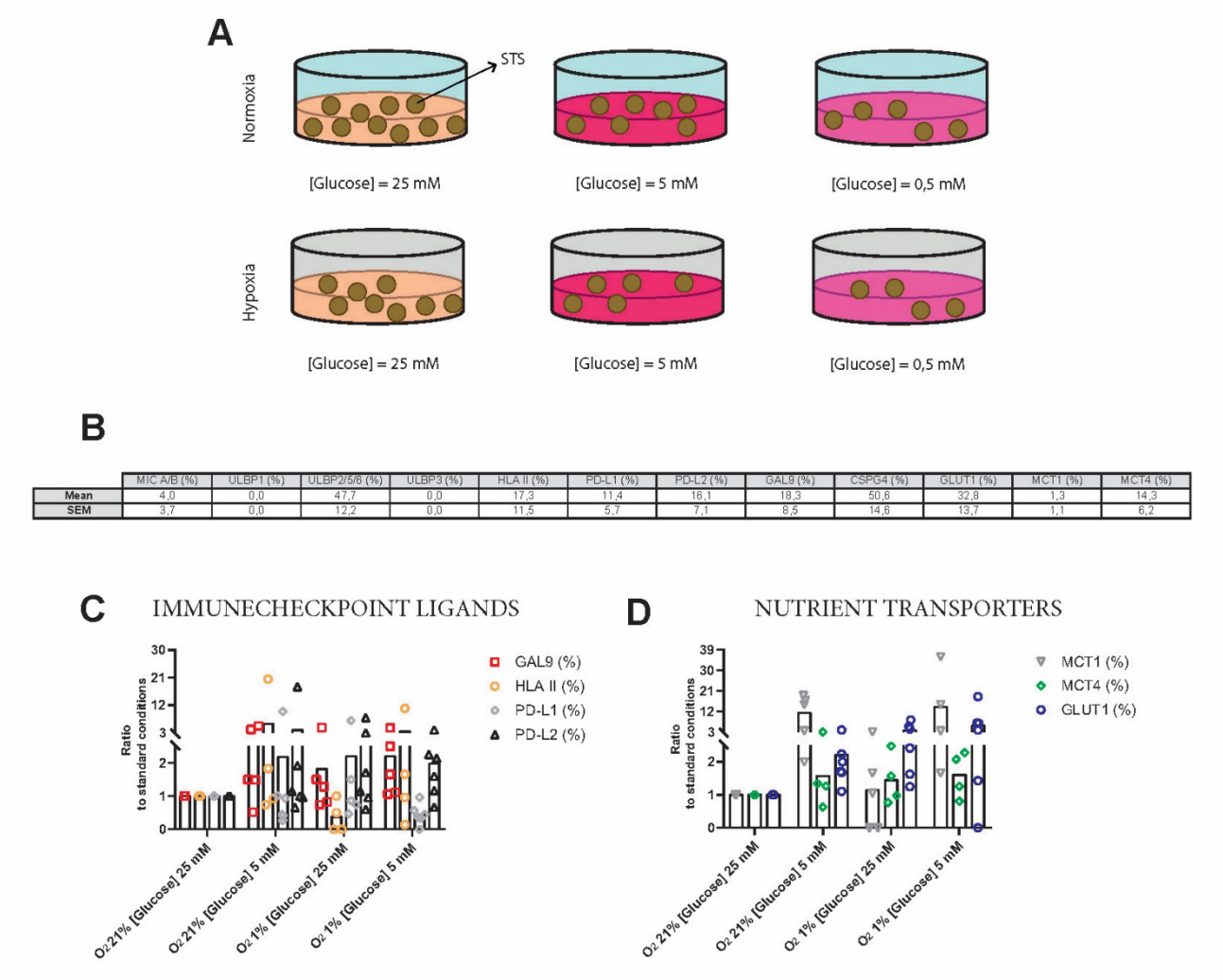

	MIC A/B (%)	ULBP1 (%)	ULBP2/5/6 (%)	ULBP3 (%)	HLA II (%)	PD-L1 (%)	PD-L2 (%)	GAL9 (%)	CSPG4 (%)	GLUT1 (%)	MCT1 (%)	MCT4 (%)
Mean	4,0	0,0	47,7	0,0	17,3	11,4	16,1	18,3	50,6	32,8	1,3	14,3
SEM	3,7	0,0	12,2	0,0	11,5	5,7	7,1	8,5	14,6	13,7	1,1	6,2

Figure 4. Challenging metabolic conditions affected STS

Schematic representation of challenging metabolic conditions tested for STS viability and phenotype assessment **(A)**. Phenotypic characterization of patient-derived STS in standard culture conditions. The immunophenotype of selected STS in standard culture conditions is reported in the table **(B).** Expression levels (ratio) of **C)** immunecheckpoint ligands (GAL9, HLA II, PD-L1, PD-L2) **D)** nutrient transporters (GLUT1, MCT1, MCT4) in challenging metabolic conditions ([Glucose]=5mM - 0,5 mM ± O_2 1%) compared to standard culture conditions ([Glucose]=25mM + O_2 21%; n=7, p≤0.0001).

Abbreviations: STS, Soft Tissue Sarcoma; MIC A/B, MHC class I chain-related gene A/B; ULBPs, UL16 binding proteins; PD-L1/2, Programmed cell Death Ligand 1-2; TIM3, LAG3, TIGIT MIC A/B, GLUT1, MCT1/4; CSPG4, Chondroitin Sulfate proteoglycan 4; GAL9, Active Galectin 9; GLUT1, Glucose transporter 1; MCT1, lactate transporter monocarboxylate transporter 1; MCT4, lactate transporter monocarboxylate transporter 4.

3. CSPG4-CAR.CIK *in vitro* anti-tumor activity within 2D STS models

3.1 CSPG4-CAR.CIK are effective *in vitro* 2D STS models

We explored the *in vitro* antitumor activity of CSPG4-CAR.CIK against 12 distinct STS. In 2 cases (S1 UPS, S172 Leiomyosarcoma) PBMCs and STS cell lines from the same patient were available and we could reproduce the autologous setting.

CSPG4.CAR.CIK showed potent *in vitro* cytotoxic activity against STS, significantly superior to that reported by unmodified NTD.CIK at effector-to-target cell ratios (E:T) from 10:1 to 1:4 (n=24; p<0.0001) (Fig. 5A).

In selected experiments (n=7) we assessed that anti-STS activity of CSPG4-CAR.CIK was retained even when challenged at extremely low E/T ratios (up to 1:64; p<0.001) (Fig. 5B).

CSPG4-CAR.CIK and paired unmodified NTD.CIK showed comparable cytotoxic activity between autologous and allogenic settings (n=2) (Fig. 5C).

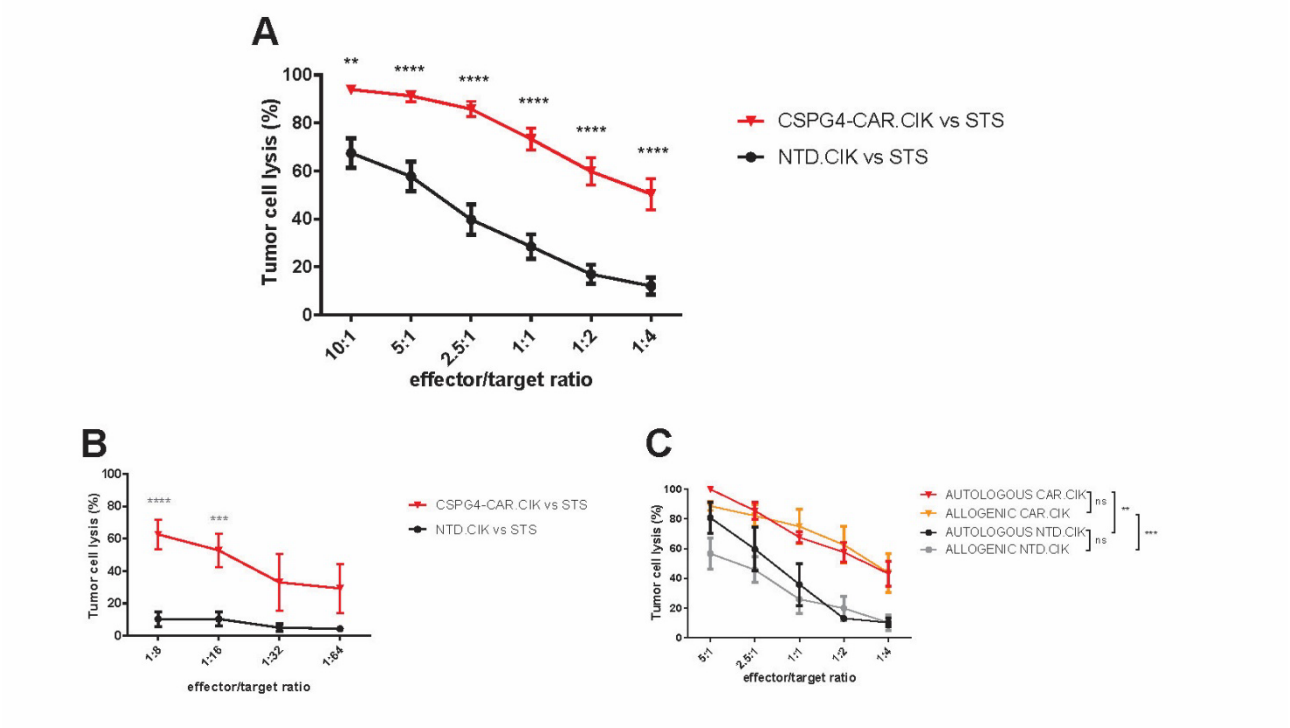

Figure 5. CSPG4-CAR.CIK effectively target STS cells *in vitro*

Patient-derived CSPG4-CAR.CIK efficiently targeted STS cells *in vitro* when using either HLA mismatched (10 samples) or matched CIK (2 samples). Specific cytotoxicity of CSPG4-CAR.CIK was significantly higher than that obtained with unmodified NTD.CIK. Tumor cell-specific cytotoxicity values from 29 experiments are reported (mean ± SEM) **(A)**. CSPG4-CAR.CIK retained their antitumor activity when challenged at very low E:T ratios (n=8) **(B)**. In two cases (S1 e S172) we performed cytotoxicity assays in the autologous setting against S1 e S172 STS. The S1 and S172 CSPG4-CAR.CIK and paired unmodified NTD.CIK showed comparable cytotoxic activity in autologous and allogeneic settings (n=2) **(C)**. All cytotoxicity assays were analyzed by two-way ANOVA and Bonferroni's post-test analysis; statistical significance is reported as * P ≤ 0.05, ** P ≤ 0.01, *** P ≤ 0.001, and **** P ≤ 0.0001; "n" refers to the number of separate experiments.

Abbreviations: CIK, Cytokine Induced Killer cells; CSPG4, Chondroitin Sulfate proteoglycan 4; CAR, Chimeric Antigen Receptor; NTD, Not Transduced; STS, Soft Tissue Sarcoma.

3.2 CSPG4-CAR.CIK *in vitro* cytotoxic activity is specific against CSPG4-expressing STS targets

We evaluated the specificity of CSPG4-CAR.CIK testing *i) CD19-CAR.CIK killing activity against STS, ii) CSPG4-CAR.CIK cytotoxicity against CSPG4-negative target, iii) CSPG4-CAR.CIK cytotoxicity against normal keratinocytes.*

In selected experiments, CIK were transduced to express CAR against CD19, to obtain a CAR.CIK population against an irrelevant target in STS. CSPG4-CAR.CIK antitumor activity was superior to that of control CD19-CAR.CIK ($n=6$, $p<0.05$), whose cytotoxicity was comparable to that of unmodified NTD.CIK (Fig. 6A).

Consistently, CSPG4-CAR.CIK and unmodified NTD.CIK killed at comparable levels a control melanoma cell line not expressing CSPG4 ($n=3$, $p>0.05$) (Fig. 6B).

We observed that, at clinically relevant E:T ratios, CSPG4-CAR.CIK spared human keratinocytes that show low CSPG4 membrane expression ($n=5$), supporting the hypothesis that antigen density may be important in triggering the antitumor activity and the potential off-tumor toxicities of CAR.CIK (Fig. 6C). Furthermore, we confirmed that tumors within the higher range of CSPG4 density were more intensely killed by CSPG4-CAR.CIK than tumors with lower CSPG4 expression levels ($n=7$, $p<0.05$) (Fig. 6D).

Following treatment with CSPG4-CAR.CIK, we evaluated the recovery of residual tumor cells spared by the cytotoxic effects of CSPG4-CAR.CIK. We observed significant delayed *in vitro* in the recovery of STS cells exposed to CSPG4-CAR.CIK (followed for 48 hours after treatment) compared with tumor cells exposed to unmodified NTD.CIK ($n=2$, $p<0.05$) (Fig. 6E).

We evaluated the double killing potential of CAR.CIK platform *i) testing CSPG4-CAR.CIK cytotoxicity against NKG2D-ligands negative STS, ii) comparing CSPG4-CAR.CIK killing activity with conventional CSPG4-CAR.T lymphocytes.*

In control experiments ($n=3$), we tested CSPG4-CAR.CIK cytotoxic activity against a STS culture expressing CSPG4 but lacking NKG2D ligands. In this case, the killing activity was retained by CSPG4-CAR.CIK while the cytotoxicity by unmodified NTD.CIK was negligible, confirming that CAR expression, *per se*, promotes antitumor activity of redirected CIK independently from NKG2D CIK receptor engagement ($p<0.001$) (Fig. 6F).

We generated CSPG4-CAR.T and CSPG4-CAR.CIK lymphocytes from PBMCs collected from the same patient with comparable expression levels of CSPG4-CAR. CSPG4-CAR.CIK displayed a significant and superior (3,8 fold E:T 5:1) STS killing activity compared with

paired “non-cytokine induced”, minimally activated, CAR.T lymphocytes (n=2, p<0.001) (Fig. 7A-C).

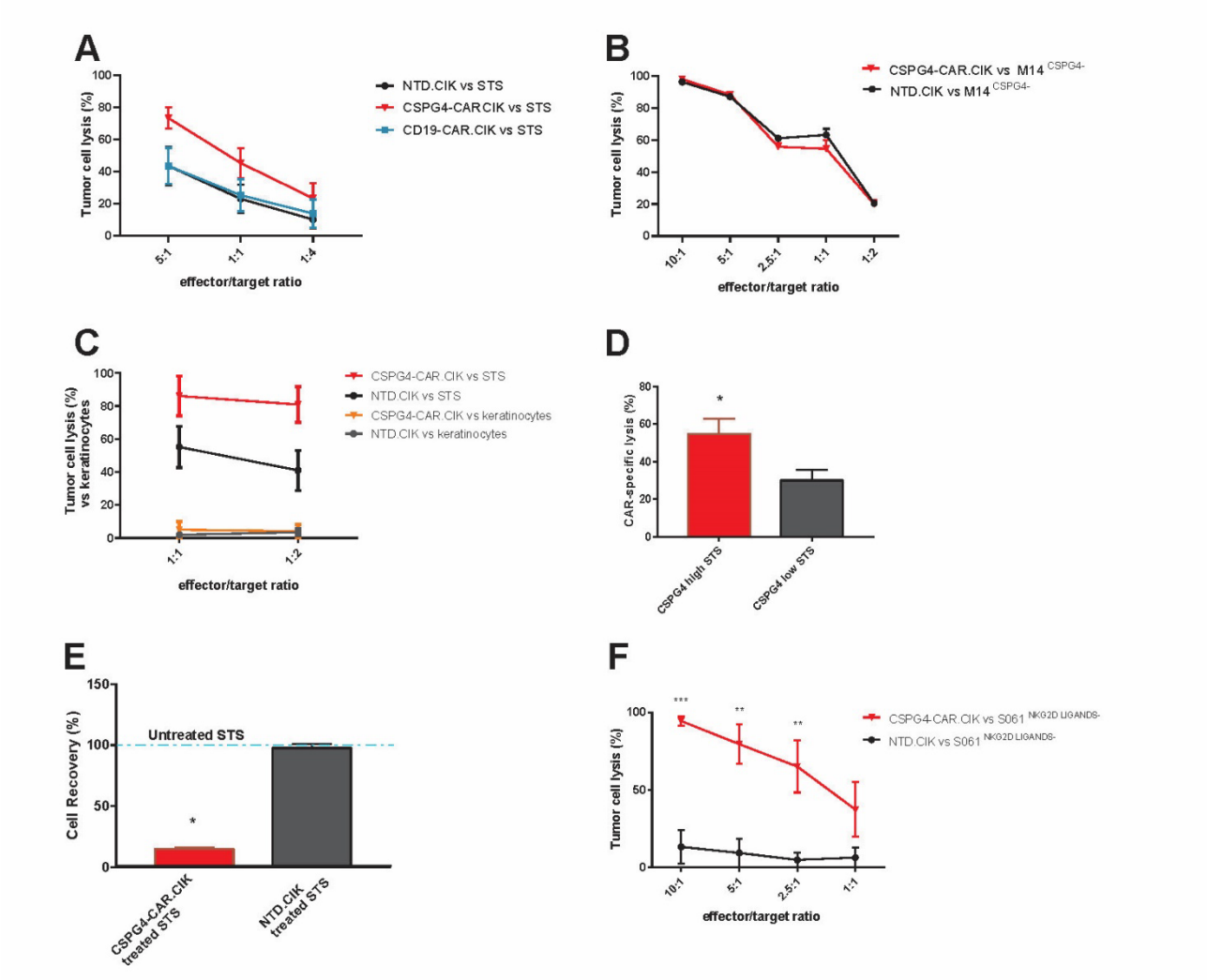

Figure 6. CSPG4-CAR.CIK specifically target CSPG4⁺ STS cells *in vitro*

In vitro cytotoxic activity of control CD19-CAR.CIK against STS was comparable to that of unmodified NTD.CIK (n=5) **(A)**. CSPG4-CAR.CIK and paired unmodified NTD.CIK showed similar cytotoxic activity against the M14 control cell line that lacks CSPG4 expression (n=3) **(B)**. Both CSPG4-CAR.CIK and paired unmodified NTD.CIK did not lyse normal keratinocytes (n=5) **(C)**. CSPG4-CAR.CIK exhibited more intense killing of STS cells with high CSPG4 expression as compared with STS cells with low CPSG4 expression (n=7, * P ≤ 0.05 by t-test) **(D)**. STS cell growth assessed 48 hours following *in vitro* treatment was significantly delayed in STS exposed to CSPG4-CAR.CIK, as compared with unmodified NTD.CIK. The dashed line represents the control parallel growth of untreated STS cells (n=2, * P ≤ 0.05 by unpaired t-test) **(E)**. CSPG4-CAR.CIK, but not paired unmodified NTD.CIK, retained cytotoxic activity against a STS sample expressing CSPG4, but lacking NKG2D ligands (S061) (n=3; two-way ANOVA and Bonferroni’s post-test analysis) **(F)**. All cytotoxicity assays were analyzed by two-way ANOVA and Bonferroni’s post-test analysis; statistical significance is reported as * P ≤ 0.05, ** P ≤ 0.01, *** P ≤ 0.001, and **** P ≤ 0.0001; “n” refers to the number of separate experiments.

Abbreviations: CIK, Cytokine Induced Killer cells; CSPG4, Chondroitin Sulfate proteoglycan 4; CAR, Chimeric Antigen Receptor; NTD, Not Transduced; STS, Soft Tissue Sarcoma.

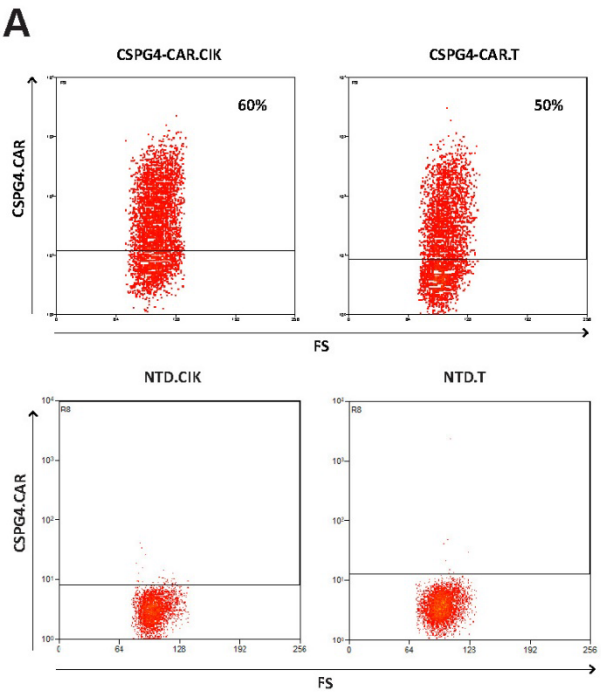

B

#Pt	Diagnosis		CD3 (%)	CD3/CAR (%)	CD3/CD56 (%)	CD3/CD8 (%)	PD-1 (%)	NAIVE (%)	CM (%)	EM (%)
CIK #Pt6	UPS	CAR	99	65	88	60	17	10	25	65
		NTD	99	/	80	88	10	10	15	75
T #Pt6	UPS	CAR	99	50	3	40	60	14	58	28
		NTD	99	/	3	46	50	16	57	26

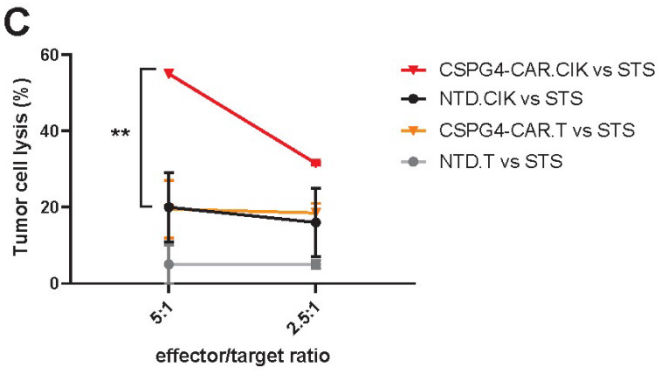

Figure 7. <u>CIK platform increased anti-tumor potential of CAR-strategies compared with CAR.T</u>

Representative flow-cytometry plots showing the expression of CSPG4.CAR in paired CIK and T lymphocytes **(A)**. The immunophenotype of paired patient-derived CSPG4-CAR.CIK, CSPG4-CAR.T and respective unmodified NTD controls is reported in the table **(B)**. CSPG4-CAR.CIK displayed significant and superior STS killing activity compared to paired "non-cytokine-induced", but minimally activated with IL-2 (50U/ml) CAR.T expressing comparable membrane levels of CSPG4-specific CAR molecules (n=2, two-way ANOVA and Bonferroni's post-test analysis) **(C).** All cytotoxicity assays were analyzed by two-way ANOVA and Bonferroni's post-test analysis; statistical significance is reported as * $P \leq 0.05$, ** $P \leq 0.01$, *** $P \leq 0.001$, and **** $P \leq 0.0001$; "n" refers to the number of separate experiments.

<u>Abbreviations</u>: CIK, Cytokine Induced Killer cells; CSPG4, Chondroitin Sulfate proteoglycan 4; CAR, Chimeric Antigen Receptor; NTD, Not Transduced; STS, Soft Tissue Sarcoma; Effector Memory (EM: $CD45RA^{-}/CD62L^{-}$); Central Memory (CM: $CD45RA^{-}/CD62\ L^{+}$); NAÏVE: $CD45RA^{+}/CD62L^{+}$.

3.3 CSPG4-CAR.CIK retained their anti-sarcoma activity in challenging metabolic conditions

In selected experiments (N=4: GIST n=1, UPS n=2, Leiomyosarcoma n=1) we evaluated CSPG4-CAR.CIK *in vitro* cytotoxic activity in the challenging metabolic conditions as described above. (Fig. 8A).

CSPG4-CAR.CIK retained their higher antitumor activity compared to parallel unmodified NTD.CIK in glucose deprivation both in normoxia (E:T 1:1: 80% vs 40% [Glucose]=25 mM; 68% vs 50% [Glucosio]=5 mM; 67% vs 31% [Glucosio]=0,5 mM; n=4, p≤0.001) and hypoxia (E:T 1:1: 78% vs 35% [Glucosio]=25 mM; 83% vs 43% [Glucosio]=5 mM; 81% vs 35% [Glucosio]=0,5 mM; n=4, p≤0.001) (Fig. 8B).

To support the intrinsic higher metabolic activity by CAR.CIK, in selected experiments (N=2: Leiomyosarcoma n=1, GIST n=1), we assessed their glucose uptake capability within competitive assays with STS cells, both in normoxia and hypoxia. (Fig. 9A).

CSPG4-CAR.CIK showed to uptake more glucose than control NTD.CIK when in co-culture with STS, both in normoxia (64% vs 37%) and hypoxia (65% vs 38%) (Fig. 9B).

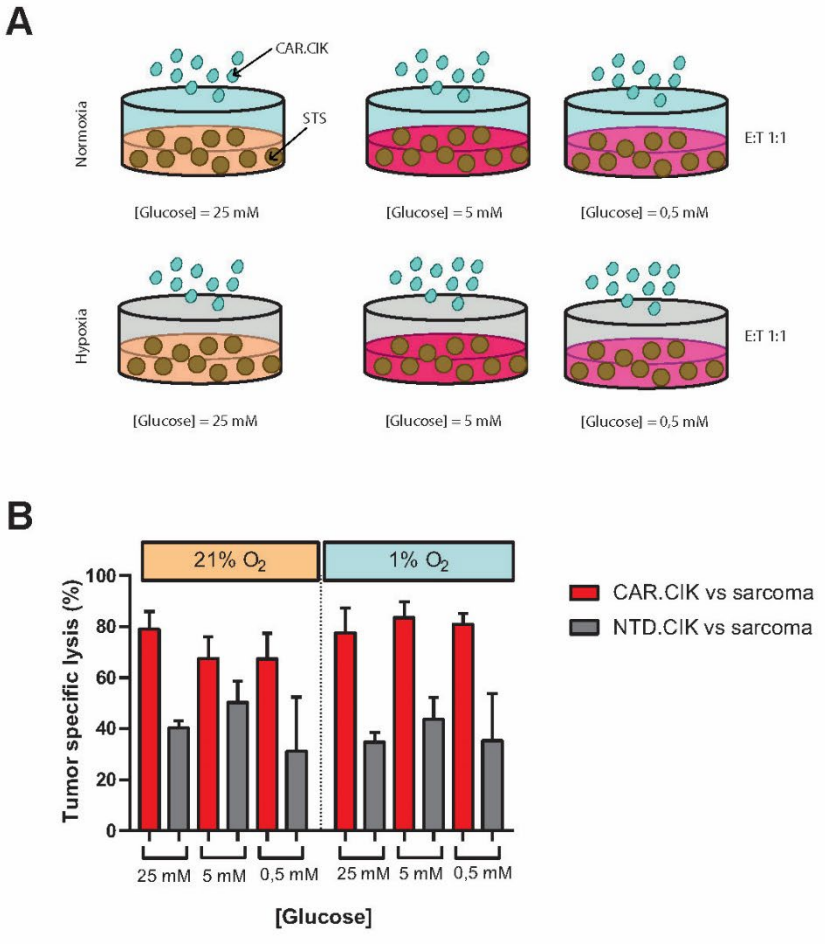

Figure 8. **CSPG4-CAR.CIK retained their anti-sarcoma activity in challenging metabolic conditions**
Schematic representation of challenging metabolic conditions tested for CSPG4-CAR.CIK antitumor activity evaluation **(A).** CSPG4-CAR.CIK retained efficient anti-sarcoma activity superior to paired NTD.CIK also in challenging metabolic conditions (n=4, p≤0.001) **(B)**.
Abbreviations: CIK, Cytokine Induced Killer cells; CAR, Chimeric Antigen Receptor; NTD, Not Transduced; STS, Soft Tissue Sarcoma.

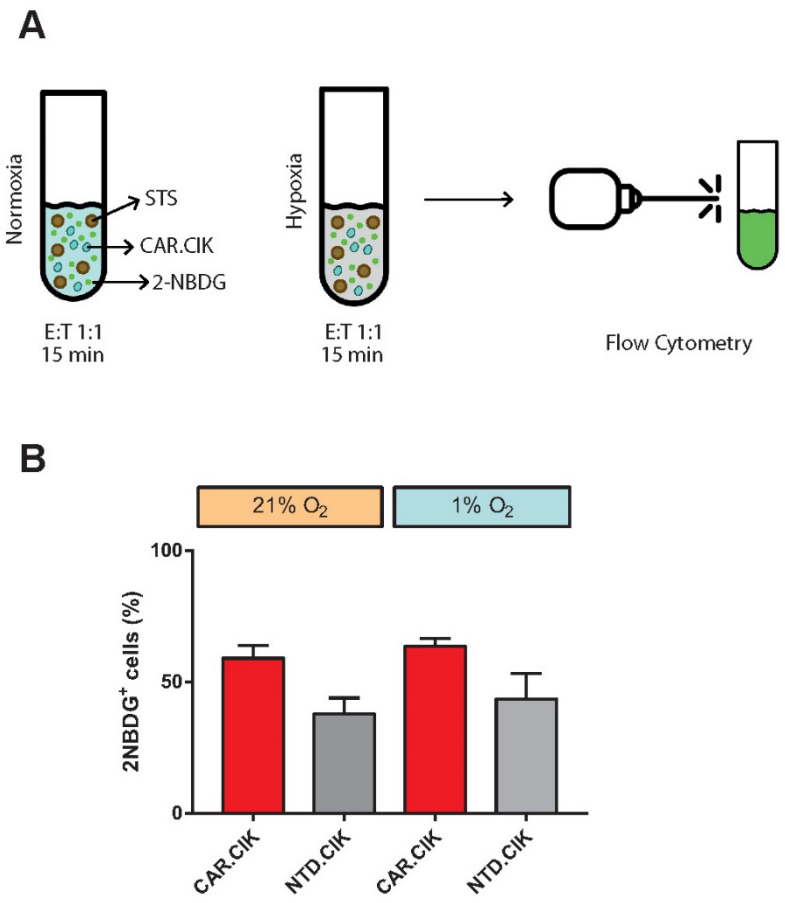

Figure 9. **CSPG4-CAR.CIK displayed higher glucose uptake than NTD.CIK**
Schematic representation of glucose uptake competition test with fluorescent 2-NBDG. CSPG4-CAR.CIK were co-cultured with STS cells directly in FACS tubes at E:T 1:1 in glucose-lacking medium added with 2-NBDG (50mM) for 15 minutes, both in normoxia (O_2=21%) and hypoxia (O_2=1%) . STS cells and CSPG4-CAR.CIK were also tested separately as control to assess their spontaneous uptake. **(A).** CSPG4-CAR.CIK showed to uptake more glucose than NTD.CIK both in normoxia and hypoxia (n=2) **(B).**
Abbreviations: CIK, Cytokine Induced Killer cells; CAR, Chimeric Antigen Receptor; NTD, Not Transduced; STS, Soft Tissue Sarcoma; 2-NBDG, 2-(N-(7-nitrobenz-2-oxa-1,3-diazol-4-yl)amino)-2-deoxyglucose).

3.4 CSPG4-CAR.CIK cytokine production

In selected experiments, we explored the production of Th1- and Th2-type cytokines and granzyme B by CSPG4-CAR.CIK at baseline and following exposure to STS CSPG4-positive targets. Overall, we observed higher baseline productions of IFNγ, IL1β, TNFα, GM-CSF, IL-8, IL-6, IL-4 , IL-10, and granzyme B by CSPG4-CAR.CIK compared with paired

unmodified NTD.CIK, that was intensely enhanced following engagement with STS CSPG4-positive targets (n=4). The positive ratios with the unmodified NTD.CIK for each cytokine, following engagement of STS targets, were: IFNγ (8-fold), IL-1b (4.2-fold), IL-6 (1.3-fold), TNFa (7.6-fold), GM-CSF (88-fold), IL-10 (15.6-fold), IL-8 (1.3-fold), IL-4 (7-fold), and granzyme B (20-fold) (Fig. 10A, B).

We compared CSPG4-CAR.CIK cytokine production with parallel CSPG4-CAR.T lymphocytes. We found that cytotoxic cytokines IFNγ and granzyme B were produced at similar levels by CSPG4-CAR.CIK and CSPG4-CAR.T lymphocytes while CSPG4-CAR.T lymphocytes showed higher levels of cytokines IL-6 and IL1-b related to cytokine release syndrome (Fig. 10C, D).

In selected cases (n=4) we compared CSPG4-CAR.CIK IFNγ production in normoxia and hypoxia. CSPG4-CAR.CIK showed a superior (3,5 log) IFN-γ production compared with unmodified NTD.CIK (99 ng/ml vs 51 pg/ml; $p<0.0001$) and this intense IFN-γ production was retained even in hypoxia (3,2 log; 58 ng/ml vs 20 pg/ml; $p<0.0001$) (Fig. 10E).

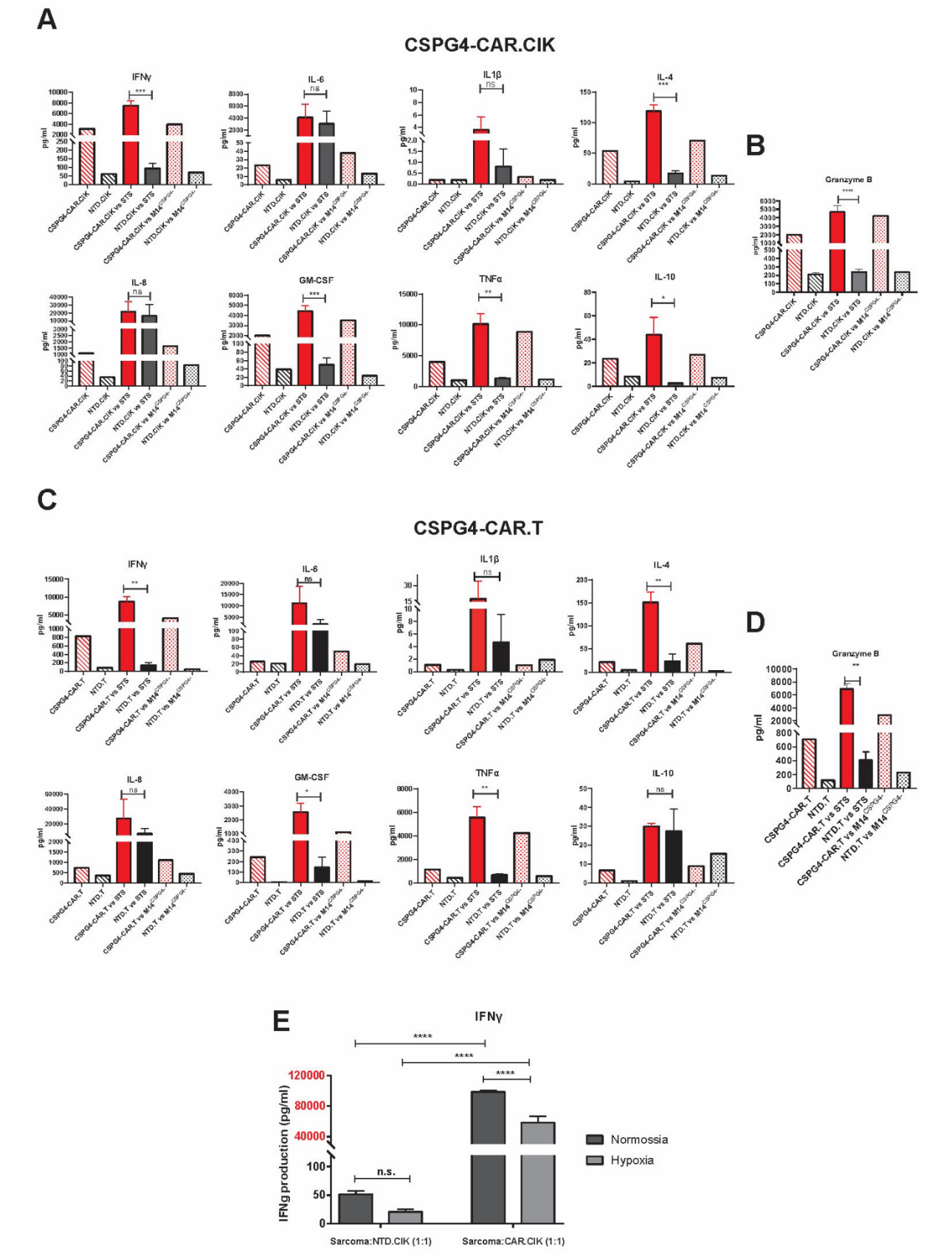

Figure 10. **Th1 and Th2 cytokine production by CSPG4-CAR.CIK and CSPG4-CAR.T**
Cytokine production by CSPG4-CAR.CIK and CSPG4-CAR.T was measured with and without engagement with the STS targets. The M14 melanoma cell line that lacks CSPG4 expression was used as control. CSPG4-CAR.CIK (IL-2 300U/ml) **(A, B)** and CSPG4-CAR.T lymphocytes, minimally activated with IL-2 (50U/ml), **(C, D)** produced higher

baseline amounts of IFNγ, IL1β, TNFα, GM-CSF, IL-8, IL-6, IL-4, IL-10 and granzyme B as compared with paired unmodified NTD.CIK or NTD.T. In both cases the cytokine production increased following engagement with STS CSPG4-positive targets. CSPG4-CAR.CIK IFNγ production in normoxia and hypoxia compared to NTD.CIK **(E)**. Each sample was measured in duplicate and results are reported as pg/ml (according to manufacturer instructions). Statistics were calculated using unpaired t-test and statistical significance is reported as * P ≤ 0.05; ** P ≤ 0.01; *** P ≤ 0.001; **** P ≤ 0.0001.
Abbreviations: CIK, Cytokine Induced Killer cells; CSPG4, Chondroitin Sulfate Proteoglycan 4;Chimeric Antigen Receptor (CAR); Not Transduced (NTD).

4. CSPG4-CAR.CIK *in vitro* anti-tumor activity within 3D STS models

4.1 CSPG4-CAR.CIK effectively target STS cells within 3D models

We developed STS spheroid models that could mimic the three-dimensionality of tumors and allow the exploration of dynamic parameters of CAR.CIK activity in a multidimensional structure. We successfully (success rate 100%) generated spheroid from distinct STS histotypes (N=21: UPS n=3; GIST n=10; Leiomyosarcoma n=3; Liposarcoma n=3; Fibrosarcoma n=1; MPNST n=1) (Fig 11A, B).

STS cells in spheroids homogenously expressed GFP following lentiviral transduction, allowing visualization and tracking of their fate by confocal and live imaging.

Spheroids were generated by 3 different STS (S1, S5 and S172) expressing different levels of CSPG4 (S1 499; S5 134; S172 262 molecules/cell respectively).

Spheroids were co-incubated with effector cells at 2:1 E:T ratio and the loss of fluorescence over time was quantified as surrogate measure of tumor elimination by CSPG4-CAR.CIK (Fig. 12A).

CSPG4-CAR.CIK effectively eliminated STS spheroids (tumor specific lysis at 48h: 94% vs S1; 70% vs S5; 99% vs S172), more effectively than unmodified NTD.CIK (n=3; P < 0.0001) (Fig. 12B-D).

In selected experiments (n=2) we performed live imaging to visualize the antitumor kinetics of CSPG4-CAR.CIK activity against STS spheroids (Supplemental Video 1-2). Representative data from side-by-side comparison of image-based read-out are showed (Fig. 13A).

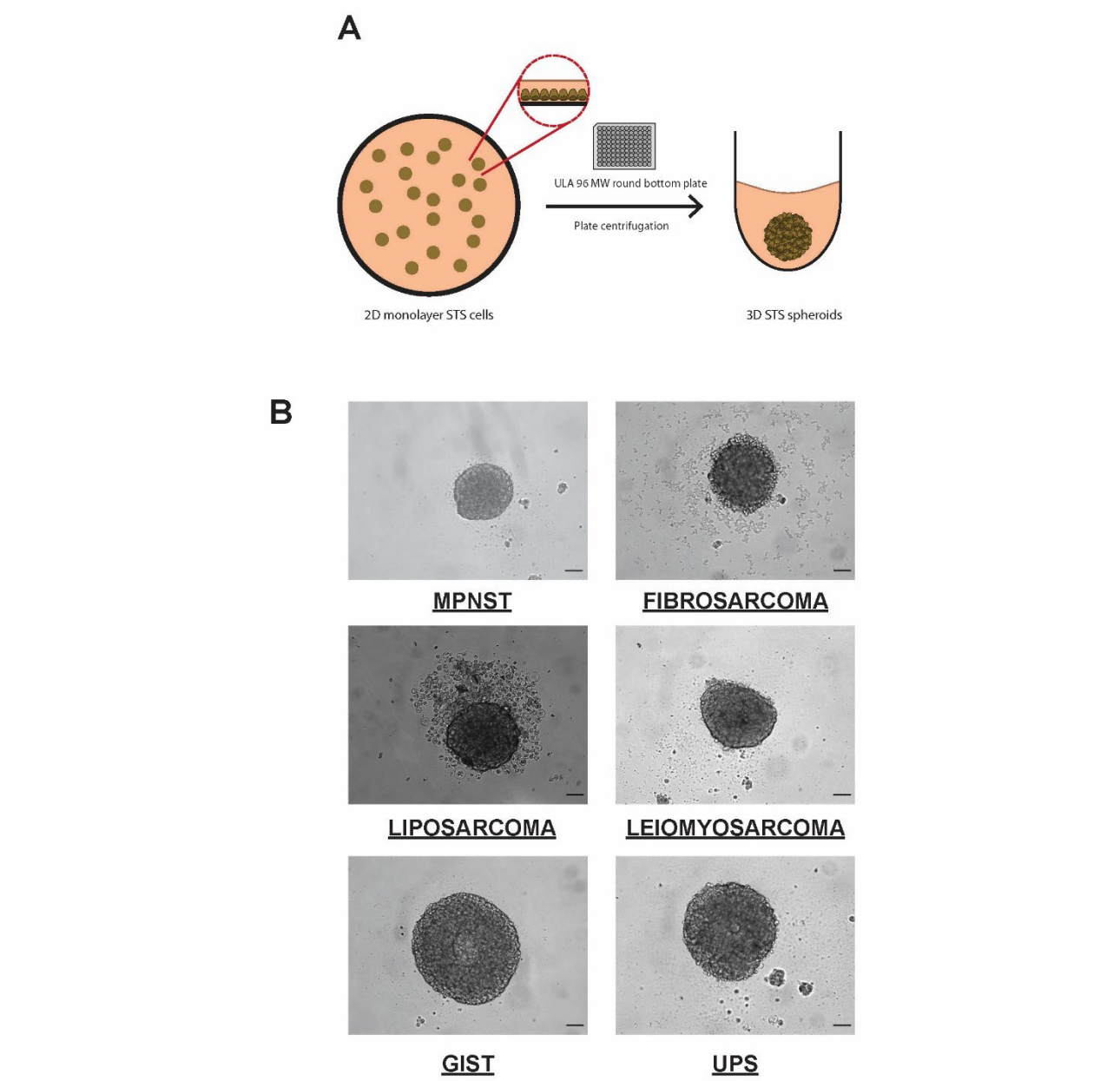

Figure 11. Successful generation of 3D STS spheroids
Schematic representation of 3D STS spheroid generation **(A)**. Representative microscope images of formed 3D spheroids from distinct STS histotypes **(B)**.
Abbreviations: STS: Soft Tissue Sarcoma.

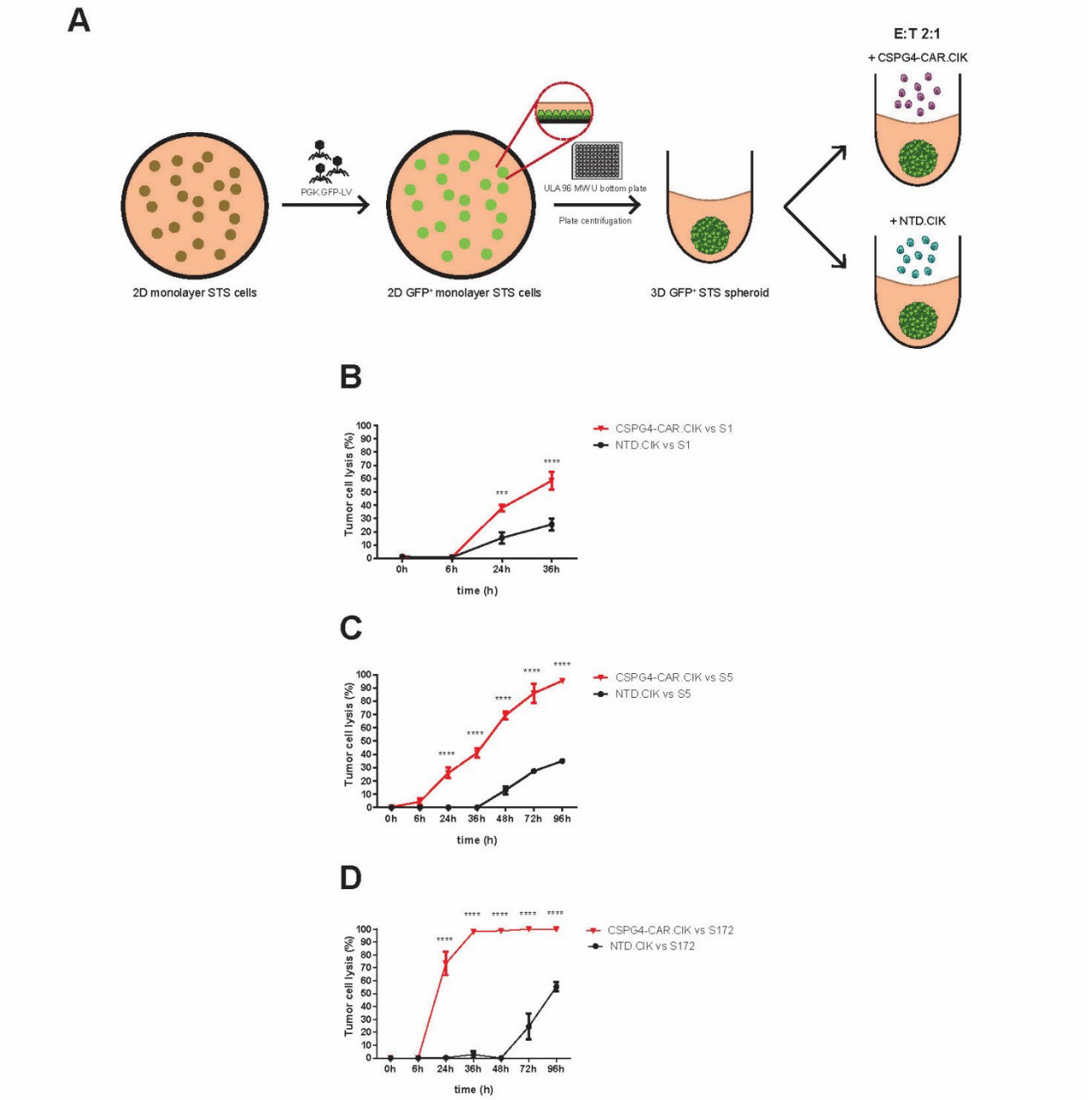

Figure 12. **CSPG4-CAR.CIK effectively target STS cells in 3D spheroids**

Schematic showing the 3D assay to test the cytotoxic activity of CSPG4-CAR.CIK against GFP-expressing STS spheroids (green) **(A)**. CSPG4-CAR.CIK displayed cytolytic activity against 3D STS spheroids. Tumor cell elimination mediated by CSPG4-CAR.CIK was quantified by measuring GFP fluorescence loss overtime of S1 **(B)**, S5 **(C)** and S172 **(D)** spheroids (pixel) by fluorescence microscopy. Values are reported as means (±SEM) from three independent wells (2:1 E:T ratio). Results were analyzed by two-way ANOVA and Bonferroni's post-test analysis; statistical significance is reported as * $P \leq 0.05$, ** $P \leq 0.01$, *** $P \leq 0.001$, and **** $P \leq 0.0001$.

Abbreviations: CIK: Cytokine Induced Killer cells; CSPG4: Chondroitin Sulfate proteoglycan 4; CAR: Chimeric Antigen Receptor; NTD: Not Transduced; STS: Soft Tissue Sarcoma; GFP: Green Fluorescent Protein.

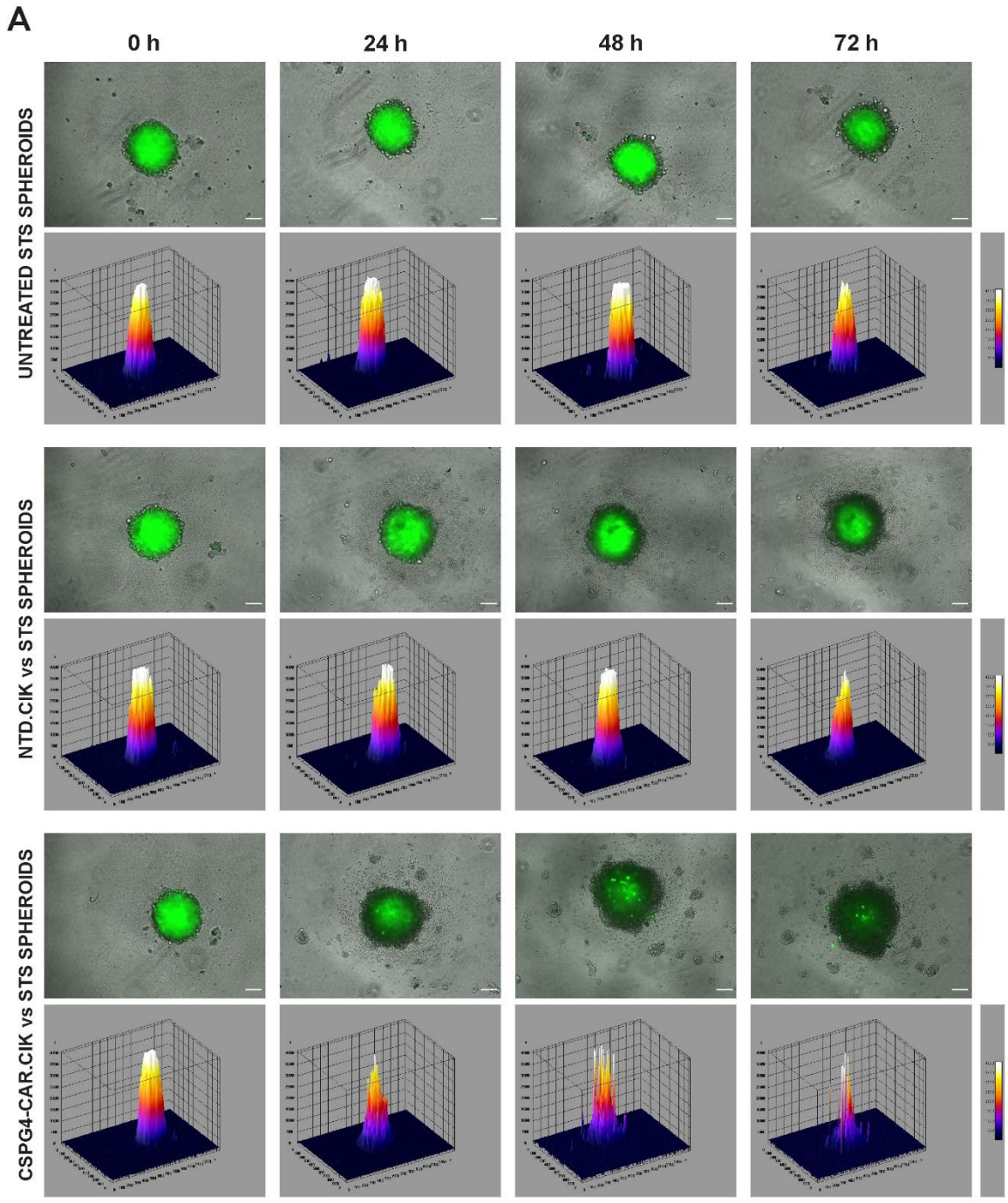

Figure 13. **Visualization of CSPG4-CAR.CIK cytotoxic activity against 3D STS spheroids**
CSPG4-CAR.CIK showed superior tumor elimination, as compared to paired unmodified NTD.CIK. Representative microscope fluorescence images and surface plot images of GFP-expressing STS spheroids (green) treated with CSPG4-CAR.CIK (up to 72 hours) and control CIK are shown. Magnification: 10X; Scale bars: 100 μm **(A)**.
Abbreviations: CIK: Cytokine Induced Killer cells; CSPG4: Chondroitin Sulfate proteoglycan 4; CAR: Chimeric Antigen Receptor; NTD: Not Transduced; STS: Soft Tissue Sarcoma; GFP: Green Fluorescent Protein.

4.2 CSPG4-CAR.CIK effectively infiltrated 3D STS spheroids

Maximum intensity projections and 3D-reconstruction of 2 STS spheroids (S172 and S5) visualized by confocal microscopy after 16h-incubation with CSPG4.CAR.CIK or unmodified NTD.CIK allowed to measure CIK recruitment and penetration capability (Fig. 14A). Results showed that CSPG4.CAR.CIK reached higher concentration within the inner layers STS spheroids as compared to unmodified NTD.CIK (n=8, $p<0.05$) (Fig. 14B-D; Supplemental Video 3-6).

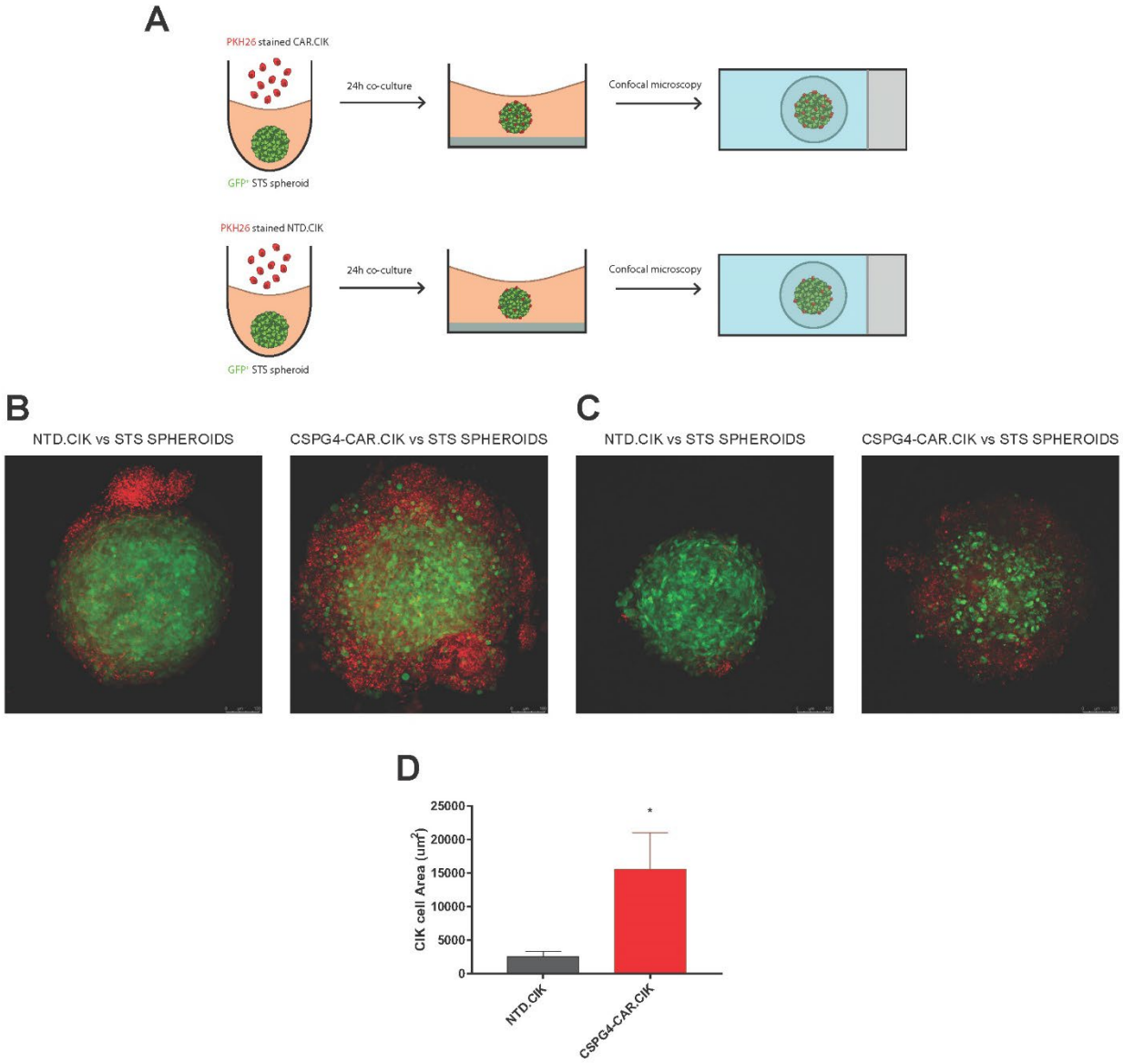

Figure 14. CSPG4-CAR.CIK infiltrate 3D STS spheroids
Schematic showing the 3D assay to test the infiltration of PKH26 stained CSPG4-CAR.CIK (red) within GFP-expressing STS spheroids (green) **(A)**. Representative maximum intensity projections of confocal microscopy images for S5 **(B)** and S172 **(C)** spheroids (green) treated with unmodified PKH26-stained (red) NTD.CIK and CSPG4-CAR.CIK (2:1 E:T ratio). Confocal microscopy images taken 16 hours after co-incubating CIK and STS

spheroids. 20X magnification and scale bars: 100 μm are shown. **(D)** CSPG4-CAR.CIK displayed superior infiltration within the STS spheroids (green) as compared with paired unmodified NTD.CIK (n=8, P≤0.05 by paired t-test). CSPG4-CAR.CIK density was determined as red fluorescent PKH26 area (μm^2).
Abbreviations: CIK: Cytokine Induced Killer cells; CSPG4: Chondroitin Sulfate Proteoglycan 4; CAR: Chimeric Antigen Receptor; NTD: Not Transduced; STS: Soft Tissue Sarcoma; GFP: Green Fluorescent Protein.

4.3 CSPG4-CAR.CIK showed effective migration abilities within 3D models

In selected assays we observed the capability of CSPG4-CAR.CIK to penetrate and migrate toward STS spheroids embedded in Matrigel domes, with the intent of mimicking their dynamics through the extracellular matrix (Fig. 15A). Microscopic inspection showed that CSPG4-CAR.CIK readily migrated to the membrane boundary and penetrate the Matrigel domes containing STS spheroids, more efficiently than unmodified NTD.CIK, ($n=5$, $p<0.01$) (Fig. 15B, C).

In selected experiments, we evaluated CSPG4-CAR.CIK migration abilities within a more complex 3D microfluidic system (AIM Biotech), where at the same time we placed STS spheroids in a central “tumor” chamber and CSPG4-CAR.CIK in a side “immune” chamber (Fig. 16A). CSPG4-CAR.CIK showed efficient and increased migration abilities compared with unmodified NTD.CIK ($n=3$, $p<0.01$) (Fig. 16B). CSPG4-CAR.CIK migration within 3D microfluidic chip was not impaired by challenging metabolic conditions ([Glucose]=5mM, $p>0.05$) (Fig. 16C).

Representative images comparing CSPG4-CAR.CIK migration at day 0 and day 5 are shown in Fig. 16D.

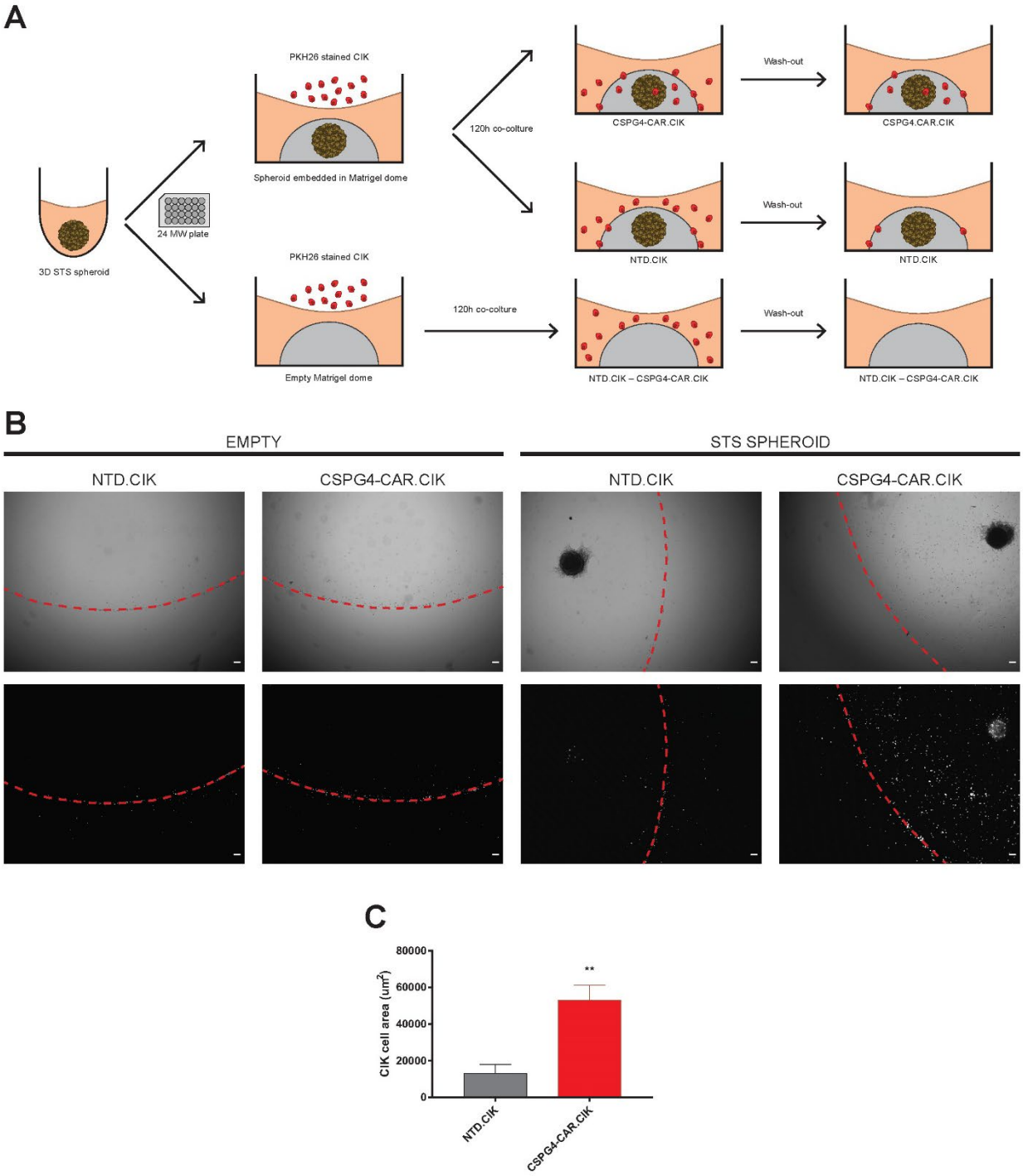

Figure 15. CSPG4-CAR.CIK penetrate Matrigel matrix toward the STS spheroids

Schematic showing the Matrigel® based penetration assay. STS spheroids were embedded into Matrigel® domes and co-cultured with either PKH26-stained CSPG4-CAR.CIK or unmodified NTD.CIK at E:T ratios 10:1. Empty domes served as controls. Fluorescence microscope images were acquired at day 5 of co-culture **(A).** Representative imagines of CSPG4-CAR.CIK and unmodified NTD.CIK empty or STS spheroids embedded in Matrigel® domes are displayed. Dashed lines represent Matrigel® boundaries. Top panel includes bright field microscope images; bottom panel includes fluorescent images. Magnification: 4X; Scale bars: 100 µm (**B).** Summary showing that CSPG4-CAR.CIK displayed superior ability in penetrating Matrigel® domes as compared to paired NTD.CIK (n=5, P≤0.01 by paired t-test). CSPG4-CAR.CIK density was defined as the fluorescent PKH26 area (μm^2) **(C).**

Abbreviations: CIK: Cytokine Induced Killer cells; CSPG4: Chondroitin Sulfate Proteoglycan 4; CAR: Chimeric Antigen Receptor; NTD: Not Transduced; STS: Soft Tissue Sarcoma.

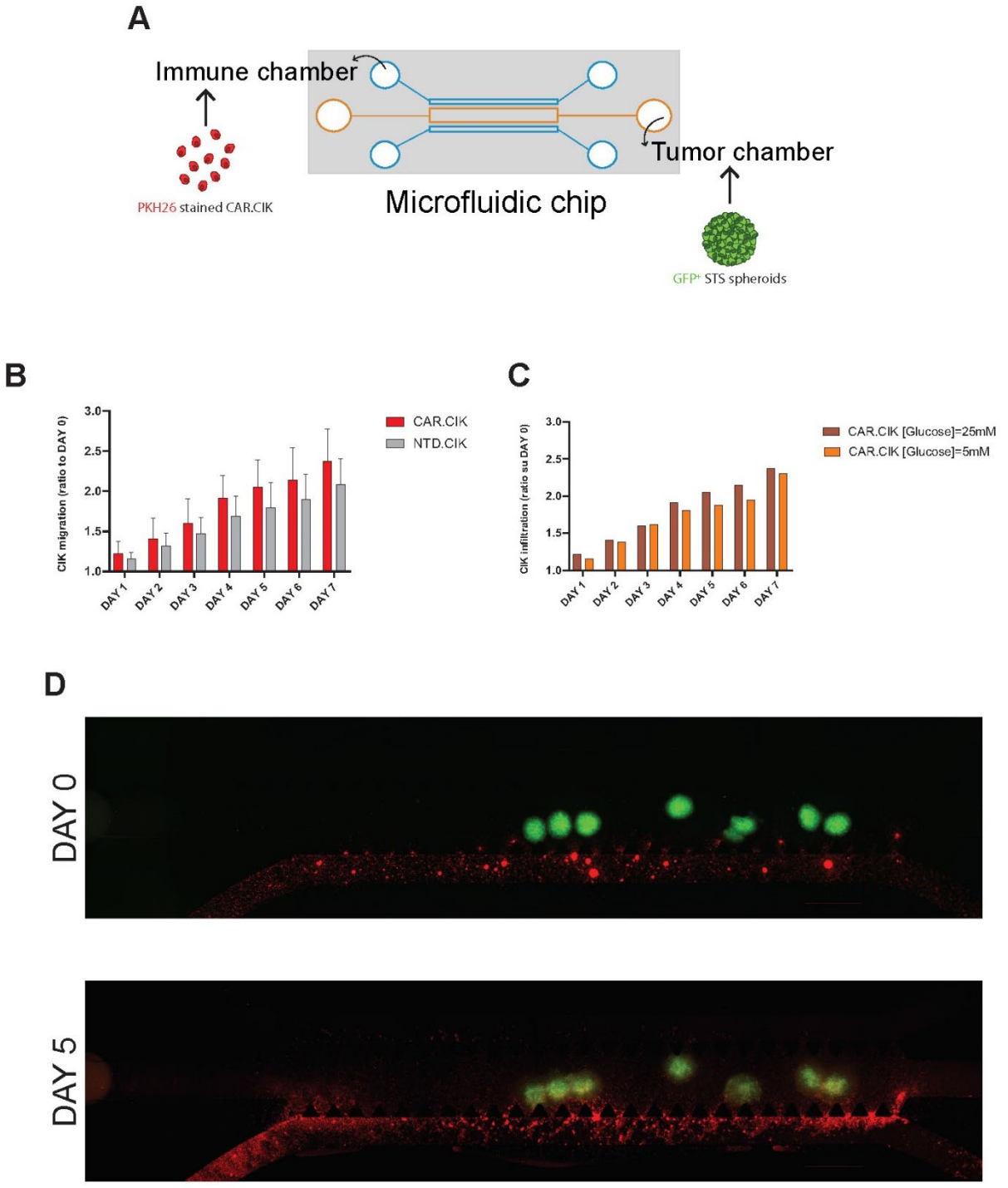

Figure 16. **CSPG4-CAR.CIK showed effective migration abilities within a 3D microfluidic system**
Schematic representation of 3D microfluidic chip (AIM Biotech) used for CSPG4-CAR.CIK migration ability assessment **(A)**. CSPG4-CAR.CIK showed efficient and increased migration abilities compared with unmodified NTD.CIK (n=3, $p<0.01$) **(B)**. CSPG4-CAR.CIK migration within 3D microfluidic chip was not impaired by challenging metabolic conditions ([Glucose]=5mM, $p>0.05$) **(C)**. Representative images comparing CSPG4-CAR.CIK migration at day 0 and day 5 **(D)**.
Abbreviations: CIK: Cytokine Induced Killer cells; CSPG4: Chondroitin Sulfate Proteoglycan 4; CAR: Chimeric Antigen Receptor; NTD: Not Transduced; STS: Soft Tissue Sarcoma; GFP: Green Fluorescent Protein.

4.4 Characterization of STS TME elements and generation of 3D PDO STS spheroids

With the intent of exploring the intrinsic nature of immune cells infiltrating STS, we set up an experimental platform to characterize TME elements of STS to study the interactions and activity of CSPG4-CAR.CIK in a more complex and realistic scenario.

Starting from fresh surgical samples (N=7: GIST n=4; Liposarcoma n=2, fibromixosarcoma n=1), we efficiently isolated non-tumoral elements and characterized STS infiltrating immune cells by flow cytometry (Fig. 17A). We identified immune infiltrating cells ($CD45^+$: 23%±8, mean±SEM). Interestingly, in 6/7 STS of our cohort we observed tumor-infiltrating T lymphocytes ($CD3^+$: 26%±6, mean±SEM) with a cut-off of greater than 5%, distinguishing the T cytotoxic subset ($CD8^+$: 51%±4, mean±SEM) and the T helper subset ($CD4^+$: 51%±3, mean±SEM). We also observed $PD1^+$ T cells ($CD3^+PD\text{-}1^+$: 40%±21, mean±SEM) and their subpopulations ($CD8^+PD\text{-}1^+$: 55%±15 and $CD4^+PD\text{-}1^+$: 40%±9, mean±SEM). We analysed the T cell differentiative subsets and the EM was the most represented phenotype (58%±28, mean±SEM). We identified NK and NKT cells ($CD56^+$: 35%±11, mean±SEM) in 6/7 STS TME and B lymphocytes ($CD19^+$: 18%±6, mean±SEM) in 5/7 out 7 STS. Additionally, we identified immunosuppressive regulatory T cells (T_{regs} $CD4^+FOXP3^+CD25^+$: 13%±6, mean±SEM), PMN-MDSCs ($HLA\text{-}DR^+CD11b^+CD15^+$: 37%±11, mean±SEM) and monocyte-MDSC ($HLA\text{-}DR^+CD11b^+CD14^+$: 21%±6, mean±SEM) (Fig. 17B).

Within our STS cohort, GIST resulted more enriched in immune infiltrating cells ($CD45^+$) compared to other STS hystotypes.

To visualize the distribution of described TME elements within STS tumors, we developed patient-derived organotypic (PDO) STS spheroids, a more exhaustive 3D model able to preserve original tumoral architecture with endogenous immune and non-immune stromal elements..We generated PDO STS spheroids from different STS histotypes (N=7: GIST n=4; Liposarcoma n=2, fibromixosarcoma n=1) with a success rate of 39% (7/18).

IF analysis were performed on PDO STS spheroids stained with distinct antibodies to visualize presence and distribution of TME elements. IF analysis allowed us to visualize the presence of the immune infiltrating populations, such as T cell subsets (cytotoxic T cell, helper T cells, T_{regs}), NK cells and macrophages, and also the pan-$Cytokeratin^+$ ($AE1/AE3^+$) malignant cells and αSMA^+ fibroblasts. We could observe the production of granzyme B granules by $CD56^+$ NK cells. We evaluated the expression of inhibitory checkpoint receptor PD-1 and its ligand PD-L1, MHC class I and CSPG4 in our PDO STS spheroids. Representative IF images of 3D PDO STS spheroids are shown (Fig. 17C).

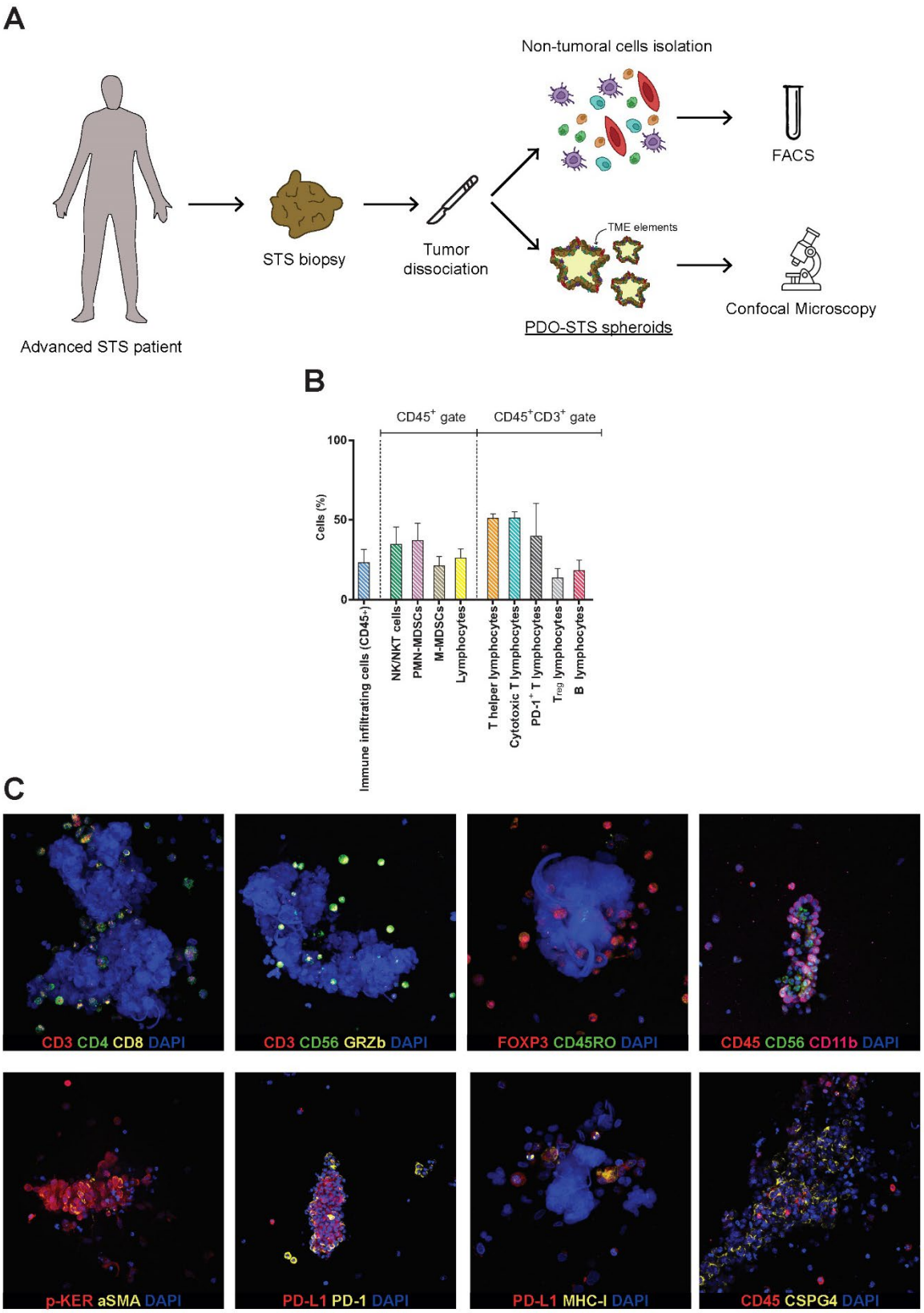

Figure 17. STS TME elements characterization and generation of 3D PDO STS spheroids
Schematic representation showing isolation of non-tumoral TME element and generation of 3D patient-derived organotypic (PDO) spheroids from fresh surgical STS samples **(A)**. Percentage of distinct TME elements isolated from fresh surgical STS samples and characterized by flow cytometry **(B)**. Representative maximum intensity projections of confocal microscopy images for PDO spheroids stained with distinct antibodies (CD45, CD45RO,

CD3, CD4, CD8, CD56, CD11b, FOXP3, GRZb, SMA, p-KER, PD-L1, PD-1, MHC-I, CSPG4) to visualize presence and distribution of different TME elements (infiltrating immune cells, T lymphocytes, NK cells, monocytes, fibroblasts) or markers **(C)**.
Abbreviations: STS: Soft Tissue Sarcoma; MDSC: Myeloid Dendritic Suppressor Cells; PMN-MDSC: Neutrophils and Polymorphonucler Myeloid Dendritic Suppressor Cells; M-MDSC: Monocytes Myeloid Dendritic Suppressor Cells; CSPG4: Chondroitin Sulfate Proteoglycan 4.

5. CSPG4-CAR.CIK *in vivo* anti-tumor activity

5.1 CSPG4-CAR.CIK controlled tumor growth *in vivo*

We explored the *in vivo* antitumor activity of CSPG4-CAR.CIK within three distinct patient-derived STS xenograft models (HT1080 Fibrosarcoma, S172 Leiomyosarcoma, S1 UPS) in immunocompromised mice, that were selected as representative of different levels of CSPG4 expression rates and density per cell. In two models (S1 and S172) CIK and tumor cells were autologous, while CAR.CIK tested in the HT1080 xenograft model were allogeneic as obtained from a third party STS patients.
The experimental plan included the treatment of engrafted xenograft tumors (starting at a tumor burden of 50 mm^3) with the intravenous infusion of $1x10^6$ CSPG4-CAR.CIK. Paired unmodified NTD.CIK were infused as control (Fig. 18A).
First, we explored the CAR.CIK immunotherapy treatment against a leiomyosarcoma xenograft (S172), with 72% and 262 molecule/cell of CSPG4 expression rate and density, respectively.
Treatment with autologous CSPG4-CAR.CIK, but not unmodified NTD-CIK, determined a significant delay of tumor growth compared with untreated controls ($p<0.05$; n=6 mice/group) (Fig. 18B).
Next, we treated a second cohort including fibrosarcoma (HT1080, n=3) and UPS xenografts (S1, n=3) showing 23% and 95% CSPG4 expression, respectively, but similar densities of target molecules (521 and 499 molecules/cell, respectively). In both cases CSPG4-CAR.CIK were effective in delaying tumor growth compared with untreated controls ($p<0.001$ vs HT1080; $p<0.0001$ vs S1; n=3 mice/group) and their antitumor effect was superior to that observed with paired unmodified NTD.CIK (Fig. 18C, D).
In the UPS xenograft group, we could confirm a significant persistent antitumor activity by CSPG4-CAR.CIK, but not NTD.CIK, up to 2 weeks after the end of treatments ($p<0.001$) (Fig. 18D).
The antitumor activity of CSPG4-CAR.CIK was explored in additional experiments, in which we started to treat mice with a smaller initial tumor burden (20 mm^3) for both HT1080 and

S172 tumors. We treated mice with 2 intravenous infusions (day 0, 3) of $3x10^6$ CSPG4-CAR.CIK (allogenic in both models) or paired unmodified NTD.CIK as control (Fig. 19A).
In these cohorts, CSPG4-CAR.CIK treatment resulted in significant delay of tumor growth up to 11 days after the end of treatment as compared with controls ($p<0.001$, HT1080 and $p<0.0001$, S172) (Fig. 19B, D). A complete tumor regression was observed in 2 of 4 mice bearing leiomyosarcoma and 1 of 5 mice bearing fibrosarcoma (HT1080) (Fig. 19C, E).
Tumor infiltration by CSPG4-CAR.CIK was confirmed in explanted tumors by IHC (Fig. 20A). Cleaved caspase 3 levels were confirmed to be higher in tumors from mice treated with CSPG4-CAR.CIK as compared with those from NTD.CIK-treated or vehicle-treated mice (Fig. 20B).
Of note, we did not observe any macroscopic evidence of toxicity or side effect in mice receiving CSPG4-CAR.CIK.
In selected experiments (N=2, HT1080 Fibrosarcoma and S1 UPS), we combined PD-1 blockade therapy with CSPG4-CAR.CIK immunotherapy. We treated dedicated cohorts of mice (n=3/cohort) with intraperitoneal anti-PD-1 antibody (200 μg/mouse) three times a week combined with intravenous infusion of $1x10^6$ CSPG4-CAR.CIK or unmodified NTD.CIK (Fig. 21A).
No significant synergism was observed treating mice with CSPG4-CAR.CIK or unmodified NTD.CIK therapy in combination with anti-PD-1 antibody ($p>0.05$) (Fig. 21B, C).

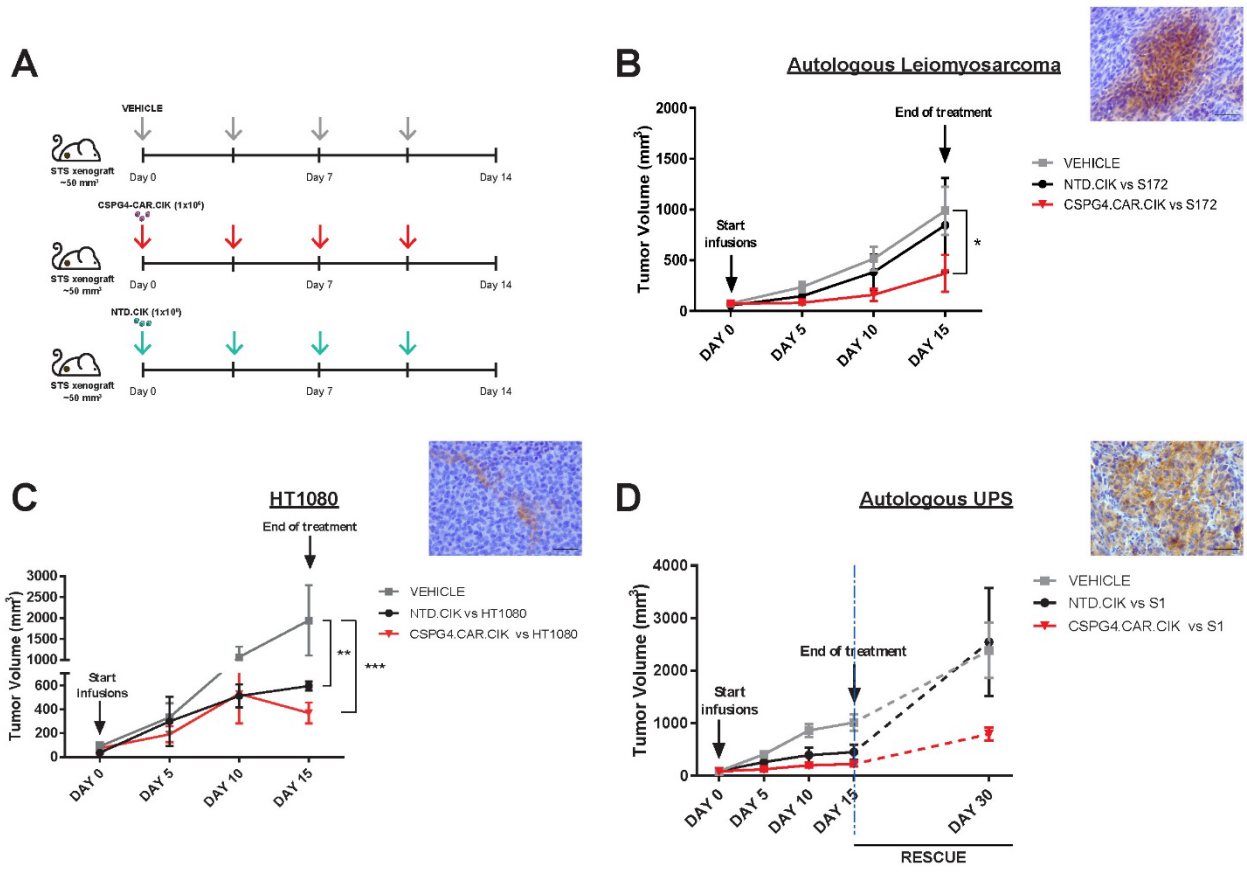

Figure 18. CSPG4-CAR.CIK are active against STS in xenograft models

Schematic representation of the STS xenografts and treatment with CSPG4-CAR.CIK (red arrows) and NTD.CIK (blue arrows). Vehicle-treated mice were infused with PBS (grey arrows). CIK were infused intravenously ($1x10^6$ cells/infusion) twice a week for 2 weeks **(A).** Autologous CSPG4-CAR.CIK caused a significant delay of the growth of the S172 leiomyosarcoma (CSPG4=72% and CSPG4 density=262 molecule/cell) as compared to unmodified NTD.CIK or vehicle-treated mice (n=6; $p<0.05$). IHC panel shows xenograft CSPG4 expression. **(B).** Autologous CSPG4-CAR.CIK caused a significant delay of the growth of the HT1080 fibrosarcoma (CSPG4=23% and CSPG4 density=521 molecule/cell) as compared to unmodified NTD.CIK or vehicle-treated mice (n=3, $p<0.001$). IHC panel shows xenograft CSPG4 expression. **(C).** Autologous CSPG4-CAR.CIK effectively delayed the growth of S1 UPS (CSPG4=95% and CSPG4 density=499 molecule/cell) as compared with controls (n=3, $p<0.0001$). IHC panel shows xenograft CSPG4 expression. **(D).** All results were analyzed by two-way ANOVA and the Bonferroni post-test; statistical significance is reported as * $P \leq 0.05$, ** $P \leq 0.01$, *** $P \leq 0.001$, and **** $P \leq 0.0001$.

Abbreviations: CIK: Cytokine Induced Killer cells; CSPG4: Chondroitin Sulfate Proteoglycan 4; CAR: Chimeric Antigen Receptor; NTD: Not Transduced; NOD/SCID: Non-obese diabetic/severe combined immunodeficiency mice; NSG: NOD/SCID gamma mice.

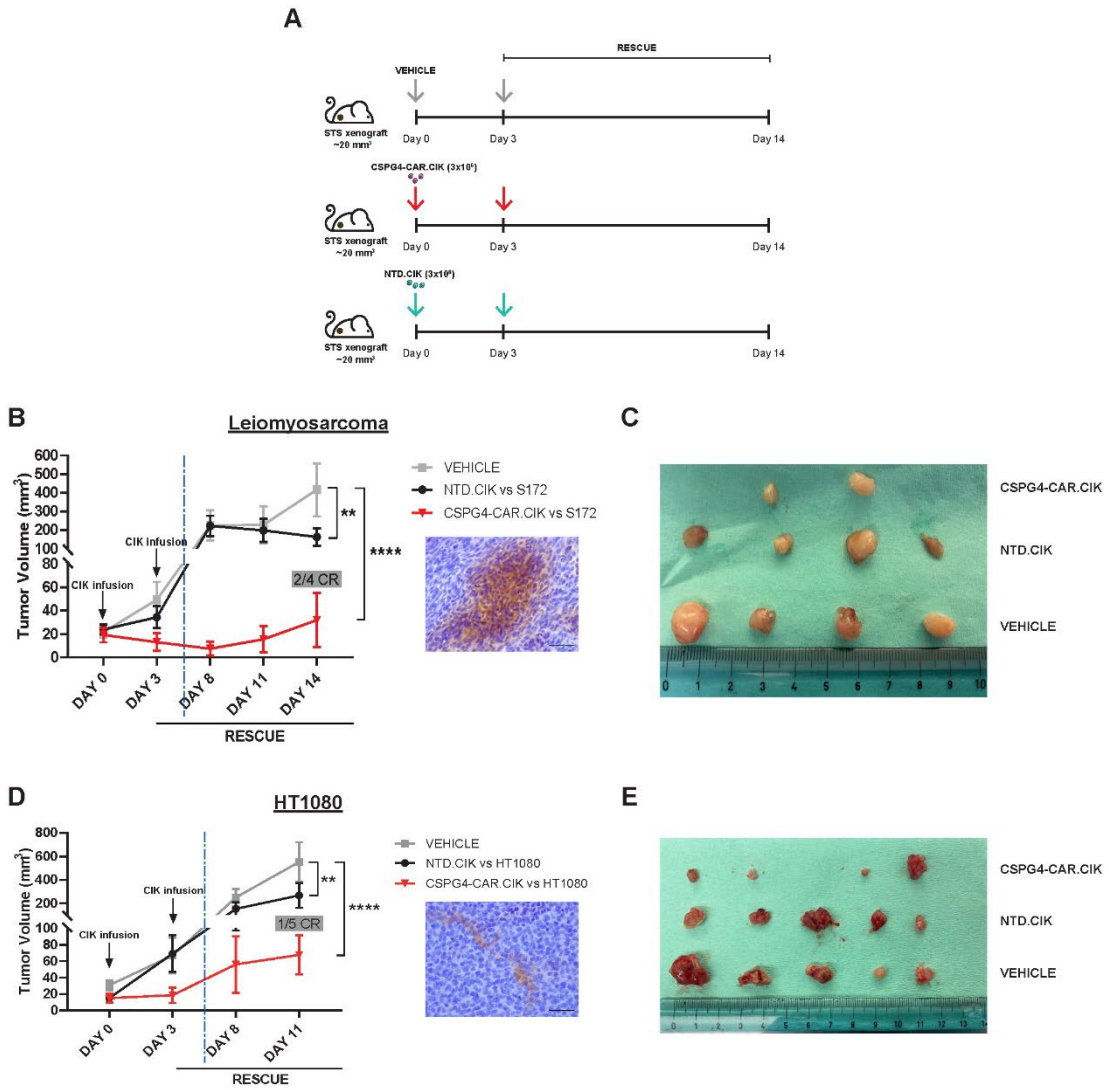

Figure 19. Enhanced tumor control by early CSPG4-CAR.CIK treatment

Schematic illustration of the treatment plan of STS xenografts with CSPG4-CAR.CIK (red arrows) and NTD.CIK (blue arrows). Vehicle-treated mice were infused with PBS (grey arrows). CIK were infused intravenously ($3x10^6$ cells/infusion) twice at day 0 and day 3 via tail vein in NOD/SCID mice. Tumor growth was monitored up to day 14 after the last dose of CIK **(A).** Antitumor activity by CSPG4-CAR.CIK (n=5) was observed in the HT1080 fibrosarcoma (23% $CSPG4^+$ and 521 molecule/cell) model (n=5). CSPG4-CAR.CIK delayed tumor growth up to 11 days after the end of treatments ($p<0.0001$). The antitumor effect was superior to that observed with paired unmodified NTD.CIK (n=5). In 1 out of 5 mice bearing the HT1080 fibrosarcoma (20%) and receiving CSPG4-CAR.CIK the tumor regressed. IHC panel shows xenograft CSPG4 expression. **(B, C).** CSPG4-CAR.CIK resulted in significant reduction of S172 leiomyosarcoma (72% $CSPG4^+$ and 262 molecule/cell) growth (n=4) as compared NTD.CIK (n=4, $p<0.05$) or vehicle treatment (n=4; $p<0.05$) up to day 8. In the following period CSPG4-CAR.CIK delayed tumor growth more efficiently as compared with unmodified NTD.CIK or vehicle-treated controls ($p<0.0001$). In 2 out of 4 mice nearing the S172 leiomyosarcoma (50%) and treated with CSPG4-CAR.CIK the tumor regressed. IHC panel shows xenograft CSPG4 expression. **(D, E).** All results were analyzed by two way ANOVA and Bonferroni's post test analysis, statistical significance is reported as * $P \leq 0.05$; ** $P \leq 0.01$; *** $P \leq 0.001$; **** $P \leq 0.0001$.

Abbreviations: CIK, Cytokine Induced Killer cells; CSPG4, Chondroitin Sulfate Proteoglycan 4; CAR Chimeric Antigen Receptor; NTD, Not Transduced; NOD/SCID, Non obese diabetic/severe combined immunodeficiency mice.

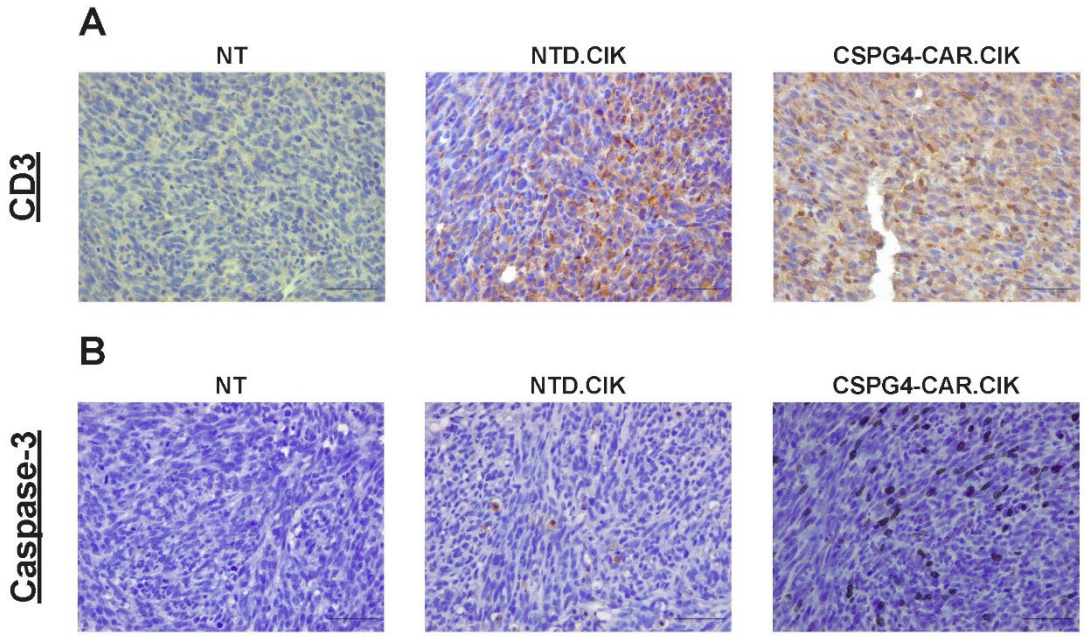

Figure 20. **CSPG4-CAR.CIK efficiently infiltrated and killed STS xenografts**
Tumor-homing of CSPG4-CAR.CIK and unmodified NTD.CIK was confirmed by IHC in explanted tumors using an anti-human CD3 antibody staining. Magnification: 40X; Scale bars: 50 µm **(A)**. Apoptotic tumor cells were visualized by detecting cleaved caspase 3 by IHC in explanted tumors **(B)**.
Abbreviations: CIK: Cytokine Induced Killer cells; CSPG4: Chondroitin Sulfate Proteoglycan 4; CAR: Chimeric Antigen Receptor; NTD: Not Transduced.

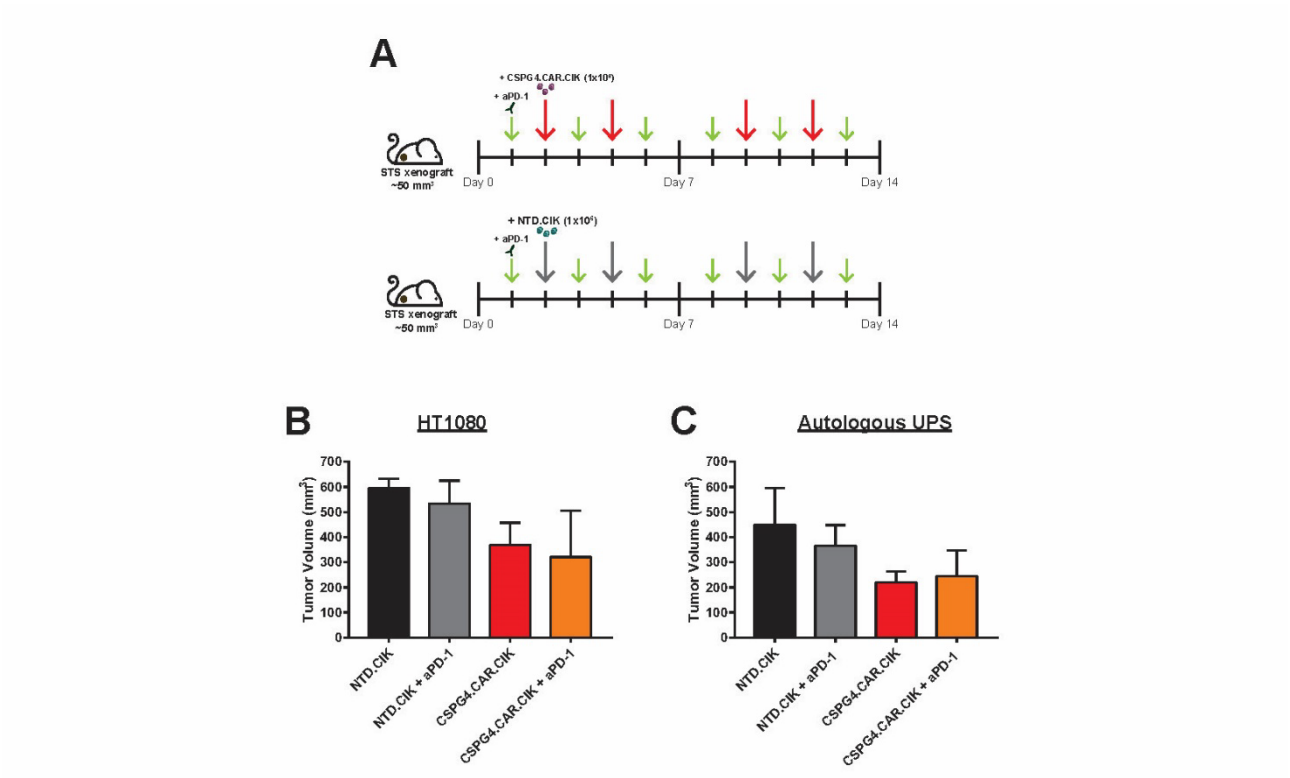

Figure 21. **PD-1 blockade did not enhance *in vivo* activity of CSPG4-CAR.CIK**
Schematic representation of the STS xenografts and treatment with CSPG4-CAR.CIK (red arrows) and NTD.CIK (blue arrows). CIK were infused intravenously ($1x10^6$ cells/infusion) twice a week for 2 weeks and anti-PD-1 (200 µg/mouse) was administrated intraperitoneally three times a week for 2 weeks **(A).** No significant synergism was

observed treating xenografts (HT1080 fibrosarcoma, S172 leiomyosarcoma) with CSPG4-CAR.CIK or unmodified NTD.CIK therapy in combination with anti-PD-1 antibody ($p>0.05$) **(B, C)**.

Abbreviations: CIK: Cytokine Induced Killer cells; CSPG4: Chondroitin Sulfate Proteoglycan 4; CAR: Chimeric Antigen Receptor; NTD: Not Transduced; NOD/SCID: Non-obese diabetic/severe combined immunodeficiency mice; NSG: NOD/SCID gamma mice.

Discussion and Future Perspective

Our data support CSPG4 as a valuable CAR-target and engineered CIK as a worthwhile platform for CAR-redirection aimed to the development and implementation of a novel and effective cellular immunotherapy for the treatment of patient with advanced/relapsed high grade STS.

We generated valuable data supporting the antitumor activity of CSPG4-CAR.CIK against STS derived from patients who relapsed after conventional treatments. Our experimental platform includes *in vitro* bi-dimensional assays, progressively more complex 3D models and 3 distinct *in vivo* STS xenografts.

STS are a heterogeneous group of mesenchymal diseases, characterized by multiple molecular and genomic features depending on the specific histotype. Currently, for the majority of patients with advanced STS the prognosis remains poor with conventional medical treatments

Various immunotherapies are considered for the treatment of sarcoma, either as single agent or in combination with chemotherapy or the molecular target agents. Emerging immunotherapy approaches expected to be effective against STS include immune checkpoint inhibitors and cellular immunotherapy. Among therapies with immune checkpoint inhibitors, PD-1 blockade (e.g. nivolumab and pembrolizumab) and CTLA-4 blockade (e.g. ipilimumab) have been the most investigated still with limited efficacy. Even if a complete understanding of STS resistance to checkpoint inhibitors is missing, it is possible to imagine that key roles are played by immunosuppressive TME elements, challenging metabolic conditions, low neo-antigen burden and defects in Ag presentation.

Among cellular immunotherapies, important results have been obtained with TCR-engineered T lymphocytes against NY-ESO-1 in patients with synovial sarcomas. Such approaches, tough extremely potent, are limited to selected histotypes and only to patients with precise HLA haplotypes. The future of cellular immunotherapy would require the definition of approaches with a broader applicability.

In this direction, CIK lymphocytes may represent an important resource to be explored.

CIK are T lymphocytes with enhanced cytokine activation during *ex vivo* expansion. CAR-engineered CIK may exploit dual MHC-independent anti-tumor killing potential, based on both the intrinsic CIK activity via NKG2D receptor and redirected CAR-activity.

Such feature may represent an added value in challenging settings like solid tumors. It increases the cytotoxic potential and counteracts tumor heterogeneity and escape mechanisms based on antigen loss and clonal selection.

We displayed that CIK transduction with CAR is feasible and retroviral engineering did not impair the expansion potential or phenotype of CIK, comparing with paired unmodified NTD.CIK. Clinical grade production retroviral engineered lymphocytes is complex, expensive and requires dedicated facilities compliant with very stringent regulatory issues. In the perspective of clinical development, alternative non-viral approaches for CAR transduction have been developed, such as Sleeping Beauty or PiggyBac transposon systems (*187, 188*). With this approach the efficient generation of CAR.CIK has been reported, and clinical protocols against haematological malignancies are ongoing (*67, 148, 189-191*). Such non–viral strategies may favourably promote the future effective clinical translation of CAR-based strategies with CIK lymphocytes to solid tumors.

Terminally differentiated effector memory (EM) is the most represented phenotype among mature CAR.CIK population. CIK are made by more terminally differentiated effectors compared to conventional T lymphocytes, resulting in a lower *in vivo* persistence (*145, 192*). It is possible to envision that in clinical settings, the short *in vivo* persistence requires multiple low-dose infusions of CAR.CIK to aim at disease control, differing from conventional CAR.T lymphocytes that may persist *in vivo* for longer time and are usually used in single infusion protocols. In regard to the safety profile, this same feature of CAR.CIK may turn out as favourable allowing a rapid control of potential side effects. Protocols for *ex vivo* expansion of CIK and CAR.CIK are very effective, easily allowing the obtainment of clinical relevant rates that can be cryopreserved for multiple clinical infusions.

Current crucial challenges for a successful application of CAR-therapy against sarcomas and solid tumors depends on *i) optimal target selection and antigen heterogeneity, ii) complex three-dimensional extracellular matrix architecture iii) metabolically-hostile and immunosuppressive TME.* In regard to these issues, our novel approach based on CSPG4-CAR.CIK may positively address effective results in this challenging field.

Several TAA have recently emerged for CAR.T cell therapy against sarcomas with encouraging results. These include HER2, GD2, IL-11R alpha, fibroblast activation protein, B7-H3, CD44v6, IGF1R and tyrosine kinase orphan-like receptor 1 (ROR1) (*97, 193*).

CSPG4 is involved in several signalling pathways associated with tumor cell proliferation, survival and migration and is expressed at high levels in various types of cancers with

minimal or no expression in normal tissues. This critical role as tumor promoting antigen makes it attractive for immunotherapy.

We found CSPG4 mRNA expression across multiple histotypes of STS included in TCGA database and we confirmed by flow cytometry CSPG4 protein expression on our patient-derived STS cell lines. CSPG4 expression was detected by the same antibody used to generate the anti-CSPG4 CAR, displaying an intense membrane density on STS with modest grade of heterogeneity. A potentially relevant mechanism of tumor immune escape is represented by antigen loss from surviving tumor cells. To this end, CAR.CIK may overcome antigen loss limitation by exploiting their double killer potential through the NKG2D mediated tumor killing. The density of CSPG4 resulted to be variable across distinct STS cell lines and in general higher than the value detected on normal keratinocytes.

We found a correlation between CSPG4 expression level and CSPG4-CAR.CIK anti-tumor activity with minimal activity against normal keratinocytes. These findings are consistent with data highlighting the importance of target density to trigger CAR activation (*194, 195*). In the perspective of a clinical application, our result support that a systematic confirmation of CSPG4 expression by IHC in STS would be required.

In selected experiments we could confirm that the observed efficient STS killing by CAR.CIK was not influenced by the possible HLA alloreactivity when CAR.CIK were generated by allogeneic donors, as the effect was fully comparable with autologous control. In the hypothesis of a clinical protocol, the source for CAR.CIK would be of course autologous, however our data are important to validate the experimental platform based on allogeneic CIK, as this is by far the most commonly available source in the majority of research experiments. The explored very low E:T ratios, within our tumor killing essays, reinforce the superiority of CAR.CIK especially in unfavorable conditions, that are likely to be more representative of realistic clinical scenarios.

To confirm the CAR-specificity, we showed that CSPG4-CAR.CIK and unmodified NTD.CIK similarly killed a control cell line not expressing CSPG4. This observation supports our original hypothesis that CAR.CIK may result as an appealing strategy against solid tumors, that often present with a heterogeneous expression of a given CAR-target.

In selected experiments, we reported that the preclinical activity of CAR.CIK was superior to paired CAR.T lymphocytes, supporting the underlying hypothesis that CAR.CIK exert a double and simultaneous anti-tumor capacity. Even if the numerosity of our experiments does not allow for definitive conclusions, we can at least be confident to consider these results as non-inferiority data for CAR.CIK as compared with more conventional CAR.T

lymphocytes. Extending the comparison to cytokine production, we report lower levels of IL6 and IL1β by CAR.CIK compared with conventional CAR.T lymphocytes. This observation induces intriguing speculations toward a safer profile by CAR.CIK, in terms of CRS risk providing rationale for dedicated preclinical studies to test this hypothesis.

CAR.CIK produced smilar levels of IFNγ and granzyme β as compared with paired conventional CAR.T lymphocytes and higher than unmodified NTD.CIK, confirming a strong Th1 type response. As additional speculation based on these data, CAR.CIK may be expected to favour important “bystander” immunological effects. The intense IFNγ secretion may enhance the expression of HLA-I molecules and the related antigen processing and presentation, potentially favouring both the innate and adaptive anti-tumor response. On the other hand, high rates of IFNγ may also increase PD-L1 expression at tumor sites with potential immunosuppressive effects, but also providing speculative rationale for synergism with checkpoint inhibitors.

It is well known that in solid tumors several biological variables may in principle reduce the clinical efficacy of adoptively transferred CAR-effectors even if these cells are equipped to efficiently kill tumor cells (*70*). Tumor cells can express inhibitory ligands (e.g. PD-L1/2) that can bind co-inhibitory receptor molecules on immune effector cells (e.g. PD-1). This engagement limits normal antitumor immune responses and promote the immune escape. Initial phase I/II clinical studies (NCT03190811, NCT03360630, NCT03393858, NCT03815630) based on combination of PD-1 blockade with DC-CIK immunotherapy against solid tumors are currently ongoing.

It is important to highlight that in these studies the protocol for *ex vivo* generation of CIK lymphocytes was different from our current procedures (*196*). In our hands, the expression of PD-1 on mature CAR.CIK is very modest, compared with conventional CAR.T lymphocytes and even our initial *in vivo* data do not suggest a great potential for synergisms between CAR.CIK and PD-1 blockade. Dedicated experiments will be required, and are actually part of our future plans, to explore the combination of CAR.CIK and PD-1 blockade, with paired CAR.T lymphocytes as control.

Besides PD-1 receptor, we noticed the intense expression of other immune checkpoints on CIK (e.g. TIM3, TIGIT) and successful combinatorial strategies may derive from synergism between CAR.CIK cellular immunotherapy and blocking of these checkpoints.

CSPG4-CAR.CIK anti-tumor activity was confirmed in 3 independent xenografts models. Tumor growth inhibition persisted for up to 2 weeks following the last administration of

CSPG4-CAR.CIK and complete tumor regressions were observed in mice bearing leiomyosarcoma (2 out of 4) and fibrosarcoma (1 out of 5).

The proposed approach is focused on STS but may be relevant also against other CSPG4$^+$ tumors.

Tumor homing, migration and ECM invasion should are key issues required for the success of CAR.CIK immunotherapy against STS and solid tumors. CSPG4-CAR.CIK showed a superior ability to effectively migrate towards, infiltrate and lyse 3D STS spheroids compared with unmodified NTD.CIK. Having in mind the future clinical translation of this strategy, we confirmed that such dynamic features were retained by CAR.CIK in metabolically challenging conditions, even simulating an efficient blood vessel “extravasation” process recapitulated by our 3D microfluidic system.

As already mentioned, the comprehension of TME complexity is a key issue to understand the mechanisms underlying the processes of both immune responses and immune resistance. Such knowledge would also be fundamental to design tailored immunotherapy strategies in challenging settings like that of STS. Cellular components of TME are often polarized to promote tumor growth, metastatization and immunosuppression, based on multiple mechanisms. Metabolic restrictions, often characterizing TME of solid tumors, may increase immunosuppressive MDSCs, T_{regs}, as well as the expression of inhibitory checkpoint molecules e on immune infiltrating cells such as PD-1 (*197-199*). Sarcomas are generally considered immune-quiescent tumors, although recent works proposed an immune-based classification of sarcomas on the basis of TME composition, identifying *immune-low*, *immune-high* and *highly vascularized* STS phenotypes (*62*). In our work, we successfully identified distinct TME immune elements in our cohort of surgical STS samples and PDO-STS spheroids. NK, NKT cells and MDSCs were on average the most abundant elements in STS TME. We could detect variable rates of infiltrating T lymphocytes, distinguishing cytotoxic, helper and T_{regs} subsets, reporting variable expression of PD-1 receptor.

These initial data are the basis for a proposed larger platform, aiming at annotating the rates, phenotype and architectural structure of TME elements in STS, along with the functional investigation of their interaction with the incoming CAR-engineered CIK.

A deeper comprehension of TME composition and the functional interactions with adoptively incoming lymphocytes will hopefully allow a more rationale designing of innovative immunotherapy clinical trials in STS.

Besides the cellular TME composition, a central issue of adoptive immunotherapies in solid tumors concerns the metabolic challenging features of TME. Nutrient availability in the TME shapes immune responses. The TME is often hypoxic, deprived of critical nutrients required for lymphocytes proliferation, enriched in immunosuppressive cytokines and products (e.g. prostaglandin E2, potassium electrolytes) and reactive oxygen species (ROS) that impair lymphocytes functions (*200-203*). A major challenge faced by the incoming anti-tumor lymphocytes is their possible acquisition of an exhausted functional profile.

Of note, CSPG4-CAR.CIK displayed an important adaptability *in vitro* to challenging metabolic conditions, representative of hostile TME. CSPG4-CAR.CIK functions were not significantly impaired by either glucose deprivation or hypoxia, preserving their viability, immunephenotype and efficient anti-tumor activity. Our findings are in line with studies on NK cells, suggesting potential mechanistic similarities with CIK lymphocytes (*204, 205*). CIK are endowed with a mixed T-NK phenotype and our data suggest that CIK metabolic reprogramming bears a time scale more similar to NK cells and different from T lymphocyte, strongly impaired by lack of glucose and low oxygen tension.

For instance, there are experimental proofs of concept that IL2 activated NK cells can overcome the adverse effects of hypoxia *in vitro (206).* CIK are *in vitro* expanded with high dose of IL2 and it could be speculated that IL2 stimulation supports the maintenance of their anti-tumor efficacy in challenging metabolic conditions. Dedicated experiments pairing CAR.CIK and CAR.T lymphocytes are required to compare their response to challenging metabolic conditions.

Immunecheckpoint ligand expression on STS cell was increased by challenging metabolic conditions, supporting a rational for enhanced tumor immune escape mechanisms. At the same time, we did not observe an increase of immunecheckpoint receptors on CAR.CIK cultured in the same challenging conditions.

As future perspective, we will research for the best CAR design strategy that allows to achieve rapid and sustained antitumor effects, which are supported by optimized molecular signalling and metabolic fitness of CAR-lymphocytes. An optimal T-cell co-stimulation is the first critical event to counteract the immunosuppressive TME of solid tumors. Co-stimulation provided by either CD28 or 4-1BB endo-domains are equally effective in promoting CAR anti-tumor activity however, the co-stimulation via CD28 allows an intense and rapid proliferation and activation while 4-1BB maintains long-term persistence of CAR.T lymphocytes (*207, 208*).

Parallel-dedicated experiments will be performed to explore the role of CD28 and 4-1BB co-stimulatory domains on CAR.CIK effector functions when challenged within hostile metabolic conditions.

Overall, our findings support the efficacy of CSPG4-CAR.CIK against currently incurable high grade STS. Taken together these results provide novel insights for the design of immunotherapeutic approaches for STS, such as CAR.CIK therapy, that may induce higher cytotoxic lymphocytes penetration within solid TME and may be more effective also in metabolically-challenging conditions. This study leads basis for dedicated exploration of this adoptive immunotherapy approach in clinical studies for patients with advanced STS of multiple histotypes.

References

1. O. Clemente *et al.*, Is immunotherapy in the future of therapeutic management of sarcomas? *J Transl Med* **19**, 173 (2021).
2. O. Ayodele, A. R. A. Razak, Immunotherapy in soft-tissue sarcoma. *Curr Oncol* **27**, 17-23 (2020).
3. J. Y. Hui, Epidemiology and Etiology of Sarcomas. *Surg Clin North Am* **96**, 901-914 (2016).
4. R. D. Lindberg, R. G. Martin, M. M. Romsdahl, H. T. Barkley, Conservative surgery and postoperative radiotherapy in 300 adults with soft-tissue sarcomas. *Cancer* **47**, 2391-2397 (1981).
5. A. López-Pousa *et al.*, SEOM Clinical Guideline of management of soft-tissue sarcoma (2016). *Clin Transl Oncol* **18**, 1213-1220 (2016).
6. M. Van Glabbeke *et al.*, Prognostic factors for the outcome of chemotherapy in advanced soft tissue sarcoma: an analysis of 2,185 patients treated with anthracycline-containing first-line regimens--a European Organization for Research and Treatment of Cancer Soft Tissue and Bone Sarcoma Group Study. *J Clin Oncol* **17**, 150-157 (1999).
7. J. Bajpai, D. Susan, Adjuvant chemotherapy in soft tissue sarcomas…Conflicts, consensus, and controversies. *South Asian J Cancer* **5**, 15-19 (2016).
8. V. Colia *et al.*, Activity of anthracycline- and ifosfamide-based chemotherapy in a series of patients affected by advanced myxofibrosarcoma. *Clin Sarcoma Res* **7**, 16 (2017).
9. R. Ratan, S. R. Patel, Chemotherapy for soft tissue sarcoma. *Cancer* **122**, 2952-2960 (2016).
10. J. Weitz, C. R. Antonescu, M. F. Brennan, Localized extremity soft tissue sarcoma: improved knowledge with unchanged survival over time. *J Clin Oncol* **21**, 2719-2725 (2003).
11. K. G. Billingsley *et al.*, Pulmonary metastases from soft tissue sarcoma: analysis of patterns of diseases and postmetastasis survival. *Ann Surg* **229**, 602-610; discussion 610-602 (1999).
12. V. Karavasilis *et al.*, Significant clinical benefit of first-line palliative chemotherapy in advanced soft-tissue sarcoma: retrospective analysis and identification of prognostic factors in 488 patients. *Cancer* **112**, 1585-1591 (2008).
13. F. Ducimetière *et al.*, Incidence of sarcoma histotypes and molecular subtypes in a prospective epidemiological study with central pathology review and molecular testing. *PLoS One* **6**, e20294 (2011).
14. S. Hirota *et al.*, Gain-of-function mutation at the extracellular domain of KIT in gastrointestinal stromal tumours. *J Pathol* **193**, 505-510 (2001).
15. M. C. Heinrich *et al.*, PDGFRA activating mutations in gastrointestinal stromal tumors. *Science* **299**, 708-710 (2003).
16. J. Verweij *et al.*, Progression-free survival in gastrointestinal stromal tumours with high-dose imatinib: randomised trial. *Lancet* **364**, 1127-1134 (2004).
17. C. D. Blanke *et al.*, Phase III randomized, intergroup trial assessing imatinib mesylate at two dose levels in patients with unresectable or metastatic gastrointestinal stromal tumors expressing the kit receptor tyrosine kinase: S0033. *J Clin Oncol* **26**, 626-632 (2008).
18. D. Hanahan, R. A. Weinberg, Hallmarks of cancer: the next generation. *Cell* **144**, 646-674 (2011).
19. M. J. Nathenson, A. P. Conley, E. Sausville, Immunotherapy: A New (and Old) Approach to Treatment of Soft Tissue and Bone Sarcomas. *Oncologist*, (2017).
20. D. Mitsis, V. Francescutti, J. Skitzki, Current Immunotherapies for Sarcoma: Clinical Trials and Rationale. *Sarcoma* **2016**, 9757219 (2016).
21. S. P. D'Angelo, W. D. Tap, G. K. Schwartz, R. D. Carvajal, Sarcoma immunotherapy: past approaches and future directions. *Sarcoma* **2014**, 391967 (2014).
22. P. W. Kantoff *et al.*, Sipuleucel-T immunotherapy for castration-resistant prostate cancer. *N Engl J Med* **363**, 411-422 (2010).
23. A. Morales, D. Eidinger, A. W. Bruce, Intracavitary Bacillus Calmette-Guerin in the treatment of superficial bladder tumors. *J Urol* **116**, 180-183 (1976).
24. D. M. Maurer, L. H. Butterfield, L. Vujanovic, Melanoma vaccines: clinical status and immune endpoints. *Melanoma Res* **29**, 109-118 (2019).

25. A. Raza *et al.*, Unleashing the immune response to NY-ESO-1 cancer testis antigen as a potential target for cancer immunotherapy. *J Transl Med* **18**, 140 (2020).
26. I. D. Davis *et al.*, Recombinant NY-ESO-1 protein with ISCOMATRIX adjuvant induces broad integrated antibody and CD4(+) and CD8(+) T cell responses in humans. *Proc Natl Acad Sci U S A* **101**, 10697-10702 (2004).
27. S. M. Pollack *et al.*, NY-ESO-1 is a ubiquitous immunotherapeutic target antigen for patients with myxoid/round cell liposarcoma. *Cancer* **118**, 4564-4570 (2012).
28. S. M. Pollack *et al.*, NYESO-1/LAGE-1s and PRAME are targets for antigen specific T cells in chondrosarcoma following treatment with 5-Aza-2-deoxycitabine. *PLoS One* **7**, e32165 (2012).
29. K. Odunsi *et al.*, Epigenetic potentiation of NY-ESO-1 vaccine therapy in human ovarian cancer. *Cancer Immunol Res* **2**, 37-49 (2014).
30. C. Kadoch, G. R. Crabtree, Reversible disruption of mSWI/SNF (BAF) complexes by the SS18-SSX oncogenic fusion in synovial sarcoma. *Cell* **153**, 71-85 (2013).
31. S. Kawaguchi *et al.*, SYT-SSX breakpoint peptide vaccines in patients with synovial sarcoma: a study from the Japanese Musculoskeletal Oncology Group. *Cancer Sci* **103**, 1625-1630 (2012).
32. S. Kawaguchi *et al.*, Phase I vaccination trial of SYT-SSX junction peptide in patients with disseminated synovial sarcoma. *J Transl Med* **3**, 1 (2005).
33. T. Tsukahara *et al.*, Prognostic significance of HLA class I expression in osteosarcoma defined by anti-pan HLA class I monoclonal antibody, EMR8-5. *Cancer Sci* **97**, 1374-1380 (2006).
34. D. Chowell *et al.*, Patient HLA class I genotype influences cancer response to checkpoint blockade immunotherapy. *Science* **359**, 582-587 (2018).
35. S. J. Luk *et al.*, PRAME and HLA Class I expression patterns make synovial sarcoma a suitable target for PRAME specific T-cell receptor gene therapy. *Oncoimmunology* **7**, e1507600 (2018).
36. H. Yabe *et al.*, Prognostic significance of HLA class I expression in Ewing's sarcoma family of tumors. *J Surg Oncol* **103**, 380-385 (2011).
37. M. El Beaino, D. M. Araujo, A. J. Lazar, P. P. Lin, Synovial Sarcoma: Advances in Diagnosis and Treatment Identification of New Biologic Targets to Improve Multimodal Therapy. *Ann Surg Oncol* **24**, 2145-2154 (2017).
38. N. Somaiah *et al.*, First-in-Class, First-in-Human Study Evaluating LV305, a Dendritic-Cell Tropic Lentiviral Vector, in Sarcoma and Other Solid Tumors Expressing NY-ESO-1. *Clin Cancer Res* **25**, 5808-5817 (2019).
39. R. G. Maki *et al.*, A Pilot Study of Anti-CTLA4 Antibody Ipilimumab in Patients with Synovial Sarcoma. *Sarcoma* **2013**, 168145 (2013).
40. H. A. Tawbi *et al.*, Pembrolizumab in advanced soft-tissue sarcoma and bone sarcoma (SARC028): a multicentre, two-cohort, single-arm, open-label, phase 2 trial. *Lancet Oncol* **18**, 1493-1501 (2017).
41. L. Paoluzzi *et al.*, Response to anti-PD1 therapy with nivolumab in metastatic sarcomas. *Clin Sarcoma Res* **6**, 24 (2016).
42. E. Ben-Ami *et al.*, Immunotherapy with single agent nivolumab for advanced leiomyosarcoma of the uterus: Results of a phase 2 study. *Cancer* **123**, 3285-3290 (2017).
43. V. Monga *et al.*, A Retrospective Analysis of the Efficacy of Immunotherapy in Metastatic Soft-Tissue Sarcomas. *Cancers (Basel)* **12**, (2020).
44. S. P. D'Angelo *et al.*, Nivolumab with or without ipilimumab treatment for metastatic sarcoma (Alliance A091401): two open-label, non-comparative, randomised, phase 2 trials. *Lancet Oncol* **19**, 416-426 (2018).
45. P. F. Robbins *et al.*, Tumor regression in patients with metastatic synovial cell sarcoma and melanoma using genetically engineered lymphocytes reactive with NY-ESO-1. *J Clin Oncol* **29**, 917-924 (2011).
46. C. Yee, The use of endogenous T cells for adoptive transfer. *Immunol Rev* **257**, 250-263 (2014).
47. D. Sangiolo, G. Mesiano, L. Gammaitoni, M. Aglietta, G. Grignani, Activity of cytokine-induced killer cells against bone and soft tissue sarcoma. *Oncoimmunology* **3**, e28269 (2014).
48. K. Ratnavelu *et al.*, Autologous immune enhancement therapy against an advanced epithelioid sarcoma: A case report. *Oncol Lett* **5**, 1457-1460 (2013).
49. C. H. June, R. S. O'Connor, O. U. Kawalekar, S. Ghassemi, M. C. Milone, CAR T cell immunotherapy for human cancer. *Science* **359**, 1361-1365 (2018).

50. S. S. Chandran *et al.*, Treatment of metastatic uveal melanoma with adoptive transfer of tumour-infiltrating lymphocytes: a single-centre, two-stage, single-arm, phase 2 study. *Lancet Oncol* **18**, 792-802 (2017).
51. C. M. Balch *et al.*, Patterns of human tumor-infiltrating lymphocytes in 120 human cancers. *Arch Surg* **125**, 200-205 (1990).
52. J. E. Mullinax *et al.*, Expanded Tumor-infiltrating Lymphocytes From Soft Tissue Sarcoma Have Tumor-specific Function. *J Immunother* **44**, 63-70 (2021).
53. M. D. Kraus, L. Guillou, C. D. Fletcher, Well-differentiated inflammatory liposarcoma: an uncommon and easily overlooked variant of a common sarcoma. *Am J Surg Pathol* **21**, 518-527 (1997).
54. C. Kuhnen *et al.*, Dedifferentiated liposarcoma with extensive lymphoid component. *Pathol Res Pract* **201**, 347-353 (2005).
55. M. Boxberg *et al.*, PD-L1 and PD-1 and characterization of tumor-infiltrating lymphocytes in high grade sarcomas of soft tissue - prognostic implications and rationale for immunotherapy. *Oncoimmunology* **7**, e1389366 (2018).
56. S. Rusakiewicz *et al.*, Immune infiltrates are prognostic factors in localized gastrointestinal stromaltumors. *Cancer Res* **73**, (2013).
57. S. W. Sorbye *et al.*, Prognostic impact of lymphocytes in soft tissue sarcomas. *PLoS One* **6**, e14611 (2011).
58. W. W. Tseng *et al.*, Analysis of the intratumoral adaptive immune response in well differentiated and dedifferentiated retroperitoneal liposarcoma. *Sarcoma* **2015**, 547460 (2015).
59. S. Movva *et al.*, Multi-platform profiling of over 2000 sarcomas: identification of biomarkers and novel therapeutic targets. *Oncotarget* **6**, 12234-12247 (2015).
60. S. P. D'Angelo *et al.*, Prevalence of tumor-infiltrating lymphocytes and PD-L1 expression in the soft tissue sarcoma microenvironment. *Hum Pathol* **46**, 357-365 (2015).
61. G. Bindea *et al.*, Spatiotemporal dynamics of intratumoral immune cells reveal the immune landscape in human cancer. *Immunity* **39**, 782-795 (2013).
62. F. Petitprez *et al.*, B cells are associated with survival and immunotherapy response in sarcoma. *Nature* **577**, 556-560 (2020).
63. I. Ramachandran *et al.*, Systemic and local immunity following adoptive transfer of NY-ESO-1 SPEAR T cells in synovial sarcoma. *J Immunother Cancer* **7**, 276 (2019).
64. M. M. van Loenen *et al.*, Mixed T cell receptor dimers harbor potentially harmful neoreactivity. *Proc Natl Acad Sci U S A* **107**, 10972-10977 (2010).
65. I. Dufait *et al.*, Retroviral and lentiviral vectors for the induction of immunological tolerance. *Scientifica (Cairo)* **2012**, (2012).
66. Z. Izsvák, P. B. Hackett, L. J. Cooper, Z. Ivics, Translating Sleeping Beauty transposition into cellular therapies: victories and challenges. *Bioessays* **32**, 756-767 (2010).
67. C. F. Magnani *et al.*, Transposon-Based CAR T Cells in Acute Leukemias: Where are We Going? *Cells* **9**, (2020).
68. J. Wagner, E. Wickman, C. DeRenzo, S. Gottschalk, CAR T Cell Therapy for Solid Tumors: Bright Future or Dark Reality? *Mol Ther* **28**, 2320-2339 (2020).
69. C. H. June, M. Sadelain, Chimeric Antigen Receptor Therapy. *N Engl J Med* **379**, 64-73 (2018).
70. G. Dotti, S. Gottschalk, B. Savoldo, M. K. Brenner, Design and development of therapies using chimeric antigen receptor-expressing T cells. *Immunol Rev* **257**, 107-126 (2014).
71. S. Rafiq *et al.*, Targeted delivery of a PD-1-blocking scFv by CAR-T cells enhances anti-tumor efficacy *in vivo*. *Nat Biotechnol* **36**, 847-856 (2018).
72. A. A. Hombach, H. Abken, Costimulation by chimeric antigen receptors revisited the T cell antitumor response benefits from combined CD28-OX40 signalling. *Int J Cancer* **129**, 2935-2944 (2011).
73. M. R. Collinson-Pautz *et al.*, Constitutively active MyD88/CD40 costimulation enhances expansion and efficacy of chimeric antigen receptor T cells targeting hematological malignancies. *Leukemia* **33**, 2195-2207 (2019).
74. S. Guedan *et al.*, ICOS-based chimeric antigen receptors program bipolar TH17/TH1 cells. *Blood* **124**, 1070-1080 (2014).

75. S. Nair *et al.*, Functional Improvement of Chimeric Antigen Receptor Through Intrinsic Interleukin-15Rα Signaling. *Curr Gene Ther* **19**, 40-53 (2019).
76. T. Shum *et al.*, Constitutive Signaling from an Engineered IL7 Receptor Promotes Durable Tumor Elimination by Tumor-Redirected T Cells. *Cancer Discov* **7**, 1238-1247 (2017).
77. M. Mata *et al.*, Inducible Activation of MyD88 and CD40 in CAR T Cells Results in Controllable and Potent Antitumor Activity in Preclinical Solid Tumor Models. *Cancer Discov* **7**, 1306-1319 (2017).
78. L. Cherkassky *et al.*, Human CAR T cells with cell-intrinsic PD-1 checkpoint blockade resist tumor-mediated inhibition. *J Clin Invest* **126**, 3130-3144 (2016).
79. M. Chmielewski, H. Abken, TRUCKs: the fourth generation of CARs. *Expert Opin Biol Ther* **15**, 1145-1154 (2015).
80. R. D. Guest *et al.*, The role of extracellular spacer regions in the optimal design of chimeric immune receptors: evaluation of four different scFvs and antigens. *J Immunother* **28**, 203-211 (2005).
81. R. G. Majzner *et al.*, Tuning the Antigen Density Requirement for CAR T-cell Activity. *Cancer Discov* **10**, 702-723 (2020).
82. M. Hudecek *et al.*, Receptor affinity and extracellular domain modifications affect tumor recognition by ROR1-specific chimeric antigen receptor T cells. *Clin Cancer Res* **19**, 3153-3164 (2013).
83. S. E. James *et al.*, Antigen sensitivity of CD22-specific chimeric TCR is modulated by target epitope distance from the cell membrane. *J Immunol* **180**, 7028-7038 (2008).
84. J. Feucht *et al.*, Calibration of CAR activation potential directs alternative T cell fates and therapeutic potency. *Nat Med* **25**, 82-88 (2019).
85. D. Wijewarnasuriya, C. Bebernitz, A. V. Lopez, S. Rafiq, R. J. Brentjens, Excessive Costimulation Leads to Dysfunction of Adoptively Transferred T Cells. *Cancer Immunol Res* **8**, 732-742 (2020).
86. S. Guedan *et al.*, Single residue in CD28-costimulated CAR-T cells limits long-term persistence and antitumor durability. *J Clin Invest* **130**, 3087-3097 (2020).
87. A. H. Long *et al.*, 4-1BB costimulation ameliorates T cell exhaustion induced by tonic signaling of chimeric antigen receptors. *Nat Med* **21**, 581-590 (2015).
88. D. Gomes-Silva *et al.*, Tonic 4-1BB Costimulation in Chimeric Antigen Receptors Impedes T Cell Survival and Is Vector-Dependent. *Cell Rep* **21**, 17-26 (2017).
89. W. Xiong *et al.*, Immunological Synapse Predicts Effectiveness of Chimeric Antigen Receptor Cells. *Mol Ther* **26**, 963-975 (2018).
90. A. J. Davenport *et al.*, Chimeric antigen receptor T cells form nonclassical and potent immune synapses driving rapid cytotoxicity. *Proc Natl Acad Sci U S A* **115**, E2068-E2076 (2018).
91. Y. Murayama *et al.*, Effectiveness of 4-1BB-costimulated HER2-targeted chimeric antigen receptor T cell therapy for synovial sarcoma. *Transl Oncol* **14**, 101227 (2021).
92. A. Englisch, B. Altvater, S. Kailayangiri, W. Hartmann, C. Rossig, VEGFR2 as a target for CAR T cell therapy of Ewing sarcoma. *Pediatr Blood Cancer* **67**, e28313 (2020).
93. M. Lehner *et al.*, Redirecting T cells to Ewing's sarcoma family of tumors by a chimeric NKG2D receptor expressed by lentiviral transduction or mRNA transfection. *PLoS One* **7**, e31210 (2012).
94. X. Huang *et al.*, IGF1R- and ROR1-Specific CAR T Cells as a Potential Therapy for High Risk Sarcomas. *PLoS One* **10**, e0133152 (2015).
95. K. Hsu *et al.*, Chimeric Antigen Receptor-modified T cells targeting EphA2 for the immunotherapy of paediatric bone tumours. *Cancer Gene Ther* **28**, 321-334 (2021).
96. M. Charan *et al.*, GD2-directed CAR-T cells in combination with HGF-targeted neutralizing antibody (AMG102) prevent primary tumor growth and metastasis in Ewing sarcoma. *Int J Cancer* **146**, 3184-3195 (2020).
97. N. Ahmed *et al.*, Human Epidermal Growth Factor Receptor 2 (HER2) -Specific Chimeric Antigen Receptor-Modified T Cells for the Immunotherapy of HER2-Positive Sarcoma. *J Clin Oncol* **33**, 1688-1696 (2015).
98. M. H. Ravindranath, S. Muthugounder, N. Presser, Ganglioside signatures of primary and nodal metastatic melanoma cell lines from the same patient. *Melanoma Res* **18**, 47-55 (2008).
99. J. Portoukalian, S. Carrel, J. F. Doré, P. Rümke, Humoral immune response in disease-free advanced melanoma patients after vaccination with melanoma-associated gangliosides. EORTC Cooperative Melanoma Group. *Int J Cancer* **49**, 893-899 (1991).

100. J. Yu *et al.*, Anti-GD2/4-1BB chimeric antigen receptor T cell therapy for the treatment of Chinese melanoma patients. *J Hematol Oncol* **11**, 1 (2018).
101. C. Bonini *et al.*, HSV-TK gene transfer into donor lymphocytes for control of allogeneic graft-versus-leukemia. *Science* **276**, 1719-1724 (1997).
102. A. Di Stasi *et al.*, Inducible apoptosis as a safety switch for adoptive cell therapy. *N Engl J Med* **365**, 1673-1683 (2011).
103. K. C. Straathof *et al.*, An inducible caspase 9 safety switch for T-cell therapy. *Blood* **105**, 4247-4254 (2005).
104. M. Introna *et al.*, Genetic modification of human T cells with CD20: a strategy to purify and lyse transduced cells with anti-CD20 antibodies. *Hum Gene Ther* **11**, 611-620 (2000).
105. X. Wang *et al.*, A transgene-encoded cell surface polypeptide for selection, *in vivo* tracking, and ablation of engineered cells. *Blood* **118**, 1255-1263 (2011).
106. C. L. Bonifant, H. J. Jackson, R. J. Brentjens, K. J. Curran, Toxicity and management in CAR T-cell therapy. *Mol Ther Oncolytics* **3**, 16011 (2016).
107. B. S. Jones, L. S. Lamb, F. Goldman, A. Di Stasi, Improving the safety of cell therapy products by suicide gene transfer. *Front Pharmacol* **5**, 254 (2014).
108. M. Griffioen *et al.*, Retroviral transfer of human CD20 as a suicide gene for adoptive T-cell therapy. *Haematologica* **94**, 1316-1320 (2009).
109. E. Moghanloo *et al.*, Remote controlling of CAR-T cells and toxicity management: Molecular switches and next generation CARs. *Transl Oncol* **14**, 101070 (2021).
110. M. Ruella *et al.*, Dual CD19 and CD123 targeting prevents antigen-loss relapses after CD19-directed immunotherapies. *J Clin Invest* **126**, 3814-3826 (2016).
111. D. Schneider *et al.*, A tandem CD19/CD20 CAR lentiviral vector drives on-target and off-target antigen modulation in leukemia cell lines. *J Immunother Cancer* **5**, 42 (2017).
112. J. Wei, X. Han, J. Bo, W. Han, Target selection for CAR-T therapy. *J Hematol Oncol* **12**, 62 (2019).
113. C. C. Kloss, M. Condomines, M. Cartellieri, M. Bachmann, M. Sadelain, Combinatorial antigen recognition with balanced signaling promotes selective tumor eradication by engineered T cells. *Nat Biotechnol* **31**, 71-75 (2013).
114. E. Lanitis *et al.*, Chimeric antigen receptor T Cells with dissociated signaling domains exhibit focused antitumor activity with reduced potential for toxicity *in vivo*. *Cancer Immunol Res* **1**, 43-53 (2013).
115. K. T. Roybal *et al.*, Precision Tumor Recognition by T Cells With Combinatorial Antigen-Sensing Circuits. *Cell* **164**, 770-779 (2016).
116. K. T. Roybal *et al.*, Engineering T Cells with Customized Therapeutic Response Programs Using Synthetic Notch Receptors. *Cell* **167**, 419-432.e416 (2016).
117. V. D. Fedorov, M. Themeli, M. Sadelain, PD-1- and CTLA-4-based inhibitory chimeric antigen receptors (iCARs) divert off-target immunotherapy responses. *Sci Transl Med* **5**, 215ra172 (2013).
118. A. M. Huehls, T. A. Coupet, C. L. Sentman, Bispecific T-cell engagers for cancer immunotherapy. *Immunol Cell Biol* **93**, 290-296 (2015).
119. S. Yu, M. Yi, S. Qin, K. Wu, Next generation chimeric antigen receptor T cells: safety strategies to overcome toxicity. *Mol Cancer* **18**, 125 (2019).
120. C. Y. Wu, K. T. Roybal, E. M. Puchner, J. Onuffer, W. A. Lim, Remote control of therapeutic T cells through a small molecule-gated chimeric receptor. *Science* **350**, aab4077 (2015).
121. A. Juillerat *et al.*, Design of chimeric antigen receptors with integrated controllable transient functions. *Sci Rep* **6**, 18950 (2016).
122. R. Rotolo *et al.*, CAR-Based Strategies beyond T Lymphocytes: Integrative Opportunities for Cancer Adoptive Immunotherapy. *Int J Mol Sci* **20**, (2019).
123. D. Sangiolo, Cytokine induced killer cells as promising immunotherapy for solid tumors. *J Cancer* **2**, 363-368 (2011).
124. I. G. Schmidt-Wolf *et al.*, Phenotypic characterization and identification of effector cells involved in tumor cell recognition of cytokine-induced killer cells. *Exp Hematol* **21**, 1673-1679 (1993).
125. I. G. Schmidt-Wolf, R. S. Negrin, H. P. Kiem, K. G. Blume, I. L. Weissman, Use of a SCID mouse/human lymphoma model to evaluate cytokine-induced killer cells with potent antitumor cell activity. *J.Exp.Med.* **174**, 139-149 (1991).

126. P. H. Lu, R. S. Negrin, A novel population of expanded human CD3+CD56+ cells derived from T cells with potent *in vivo* antitumor activity in mice with severe combined immunodeficiency. *J.Immunol.* **153**, 1687-1696 (1994).
127. M. Introna *et al.*, Rapid and massive expansion of cord blood-derived cytokine-induced killer cells: an innovative proposal for the treatment of leukemia relapse after cord blood transplantation. *Bone Marrow Transplant.* **38**, 621-627 (2006).
128. P. Palmerini *et al.*, A serum-free protocol for the *ex vivo* expansion of Cytokine-Induced Killer cells using gas-permeable static culture flasks. *Cytotherapy* **22**, 511-518 (2020).
129. D. Sangiolo *et al.*, Alloreactivity and anti-tumor activity segregate within two distinct subsets of cytokine-induced killer (CIK) cells: implications for their infusion across major HLA barriers. *Int Immunol* **20**, 841-848 (2008).
130. G. Mesiano *et al.*, Cytokine Induced Killer cells are effective against sarcoma cancer stem cells spared by chemotherapy and target therapy. *Oncoimmunology* **7**, e1465161 (2018).
131. G. Mesiano *et al.*, Cytokine-induced killer (CIK) cells as feasible and effective adoptive immunotherapy for the treatment of solid tumors. *Expert Opin Biol Ther* **12**, 673-684 (2012).
132. D. Sangiolo *et al.*, Cytokine-induced killer cells eradicate bone and soft-tissue sarcomas. *Cancer Res* **74**, 119-129 (2014).
133. L. Gammaitoni *et al.*, Cytokine-Induced Killer Cells Kill Chemo-surviving Melanoma Cancer Stem Cells. *Clin Cancer Res*, (2016).
134. S. Capellero *et al.*, Preclinical immunotherapy with Cytokine-Induced Killer lymphocytes against epithelial ovarian cancer. *Sci Rep* **10**, 6478 (2020).
135. L. Gammaitoni *et al.*, Effective Activity of Cytokine Induced Killer Cells against Autologous Metastatic Melanoma including Cells with Stemness Features. *Clin Cancer Res*, (2013).
136. A. Dalla Pietà *et al.*, Innovative therapeutic strategy for B-cell malignancies that combines obinutuzumab and cytokine-induced killer cells. *J Immunother Cancer* **9**, (2021).
137. R. Sommaggio *et al.*, Adoptive cell therapy of triple negative breast cancer with redirected cytokine-induced killer cells. *Oncoimmunology* **9**, 1777046 (2020).
138. E. Cappuzzello, A. Tosi, P. Zanovello, R. Sommaggio, A. Rosato, Retargeting cytokine-induced killer cell activity by CD16 engagement with clinical-grade antibodies. *Oncoimmunology* **5**, e1199311 (2016).
139. P. Olioso *et al.*, Immunotherapy with cytokine induced killer cells in solid and hematopoietic tumours: a pilot clinical trial. *Hematol Oncol*, (2009).
140. C. Wu, J. Jiang, L. Shi, N. Xu, Prospective study of chemotherapy in combination with cytokine-induced killer cells in patients suffering from advanced non-small cell lung cancer. *Anticancer Res* **28**, 3997-4002 (2008).
141. D. Hui, L. Qiang, W. Jian, Z. Ti, K. Da-Lu, A randomized, controlled trial of postoperative adjuvant cytokine-induced killer cells immunotherapy after radical resection of hepatocellular carcinoma. *Dig Liver Dis* **41**, 36-41 (2009).
142. D. S. Weng *et al.*, Minimally invasive treatment combined with cytokine-induced killer cells therapy lower the short-term recurrence rates of hepatocellular carcinomas. *J Immunother* **31**, 63-71 (2008).
143. M. Shi *et al.*, Autologous cytokine-induced killer cell therapy in clinical trial phase I is safe in patients with primary hepatocellular carcinoma. *World J.Gastroenterol.* **10**, 1146-1151 (2004).
144. L. Liu *et al.*, Randomized study of autologous cytokine-induced killer cell immunotherapy in metastatic renal carcinoma. *Clin Cancer Res* **18**, 1751-1759 (2012).
145. V. Leuci *et al.*, CD44v6 as innovative sarcoma target for CAR-redirected CIK cells. *Oncoimmunology* **7**, e1423167 (2018).
146. L. C. Schmeel, F. C. Schmeel, C. Coch, I. G. Schmidt-Wolf, Cytokine-induced killer (CIK) cells in cancer immunotherapy: report of the international registry on CIK cells (IRCC). *J Cancer Res Clin Oncol* **141**, 839-849 (2015).
147. R. Nishimura *et al.*, *In vivo* trafficking and survival of cytokine-induced killer cells resulting in minimal GVHD with retention of antitumor activity. *Blood* **112**, 2563-2574 (2008).
148. M. C. Rotiroti *et al.*, Targeting CD33 in Chemoresistant AML Patient-Derived Xenografts by CAR-CIK Cells Modified with an Improved SB Transposon System. *Mol Ther* **28**, 1974-1986 (2020).

149. I. Pizzitola *et al.*, Chimeric antigen receptors against CD33/CD123 antigens efficiently target primary acute myeloid leukemia cells *in vivo*. *Leukemia* **28**, 1596-1605 (2014).
150. S. Tettamanti *et al.*, Targeting of acute myeloid leukaemia by cytokine-induced killer cells redirected with a novel CD123-specific chimeric antigen receptor. *Br J Haematol* **161**, 389-401 (2013).
151. M. Merker *et al.*, Generation and characterization of ErbB2-CAR-engineered cytokine-induced killer cells for the treatment of high-risk soft tissue sarcoma in children. *Oncotarget* **8**, 66137-66153 (2017).
152. M. Merker *et al.*, ERBB2-CAR-Engineered Cytokine-Induced Killer Cells Exhibit Both CAR-Mediated and Innate Immunity Against High-Risk Rhabdomyosarcoma. *Front Immunol* **11**, 581468 (2020).
153. Y. Wang, C. Geldres, S. Ferrone, G. Dotti, Chondroitin sulfate proteoglycan 4 as a target for chimeric antigen receptor-based T-cell immunotherapy of solid tumors. *Expert Opin Ther Targets* **19**, 1339-1350 (2015).
154. R. J. Brentjens *et al.*, Safety and persistence of adoptively transferred autologous CD19-targeted T cells in patients with relapsed or chemotherapy refractory B-cell leukemias. *Blood* **118**, 4817-4828 (2011).
155. R. A. Morgan *et al.*, Case report of a serious adverse event following the administration of T cells transduced with a chimeric antigen receptor recognizing ERBB2. *Mol Ther* **18**, 843-851 (2010).
156. A. Oldberg, P. Antonsson, E. Hedbom, D. Heinegård, Structure and function of extracellular matrix proteoglycans. *Biochem Soc Trans* **18**, 789-792 (1990).
157. C. Geldres *et al.*, T lymphocytes redirected against the chondroitin sulfate proteoglycan-4 control the growth of multiple solid tumors both *in vitro* and *in vivo*. *Clin Cancer Res* **20**, 962-971 (2014).
158. C. Visus *et al.*, Targeting ALDH(bright) human carcinoma-initiating cells with ALDH1A1-specific $CD8^+$ T cells. *Clin Cancer Res* **17**, 6174-6184 (2011).
159. A. Barrantes-Freer *et al.*, Human glioma-initiating cells show a distinct immature phenotype resembling but not identical to NG2 glia. *J Neuropathol Exp Neurol* **72**, 307-324 (2013).
160. M. Kusche-Gullberg, L. Kjellén, Sulfotransferases in glycosaminoglycan biosynthesis. *Curr Opin Struct Biol* **13**, 605-611 (2003).
161. A. E. Faassen *et al.*, A cell surface chondroitin sulfate proteoglycan, immunologically related to CD44, is involved in type I collagen-mediated melanoma cell motility and invasion. *J Cell Biol* **116**, 521-531 (1992).
162. J. Yang *et al.*, Melanoma chondroitin sulfate proteoglycan enhances FAK and ERK activation by distinct mechanisms. *J Cell Biol* **165**, 881-891 (2004).
163. I. T. Makagiansar, S. Williams, T. Mustelin, W. B. Stallcup, Differential phosphorylation of NG2 proteoglycan by ERK and PKCalpha helps balance cell proliferation and migration. *J Cell Biol* **178**, 155-165 (2007).
164. M. Chekenya *et al.*, The progenitor cell marker NG2/MPG promotes chemoresistance by activation of integrin-dependent PI3K/Akt signaling. *Oncogene* **27**, 5182-5194 (2008).
165. T. Kageshita *et al.*, Association of high molecular weight melanoma-associated antigen expression in primary acral lentiginous melanoma lesions with poor prognosis. *Cancer Res* **53**, 2830-2833 (1993).
166. N. C. Hsu, P. Y. Nien, K. K. Yokoyama, P. Y. Chu, M. F. Hou, High chondroitin sulfate proteoglycan 4 expression correlates with poor outcome in patients with breast cancer. *Biochem Biophys Res Commun* **441**, 514-518 (2013).
167. R. Warta *et al.*, Reduced promoter methylation and increased expression of CSPG4 negatively influences survival of HNSCC patients. *Int J Cancer* **135**, 2727-2734 (2014).
168. A. Svendsen *et al.*, Expression of the progenitor marker NG2/CSPG4 predicts poor survival and resistance to ionising radiation in glioblastoma. *Acta Neuropathol* **122**, 495-510 (2011).
169. R. O. Schlingemann, F. J. Rietveld, R. M. de Waal, S. Ferrone, D. J. Ruiter, Expression of the high molecular weight melanoma-associated antigen by pericytes during angiogenesis in tumors and in healing wounds. *Am J Pathol* **136**, 1393-1405 (1990).
170. M. S. Lord, J. M. Whitelock, Recombinant production of proteoglycans and their bioactive domains. *FEBS J* **280**, 2490-2510 (2013).
171. X. Wang *et al.*, Functional characterization of an scFv-Fc antibody that immunotherapeutically targets the common cancer cell surface proteoglycan CSPG4. *Cancer Res* **71**, 7410-7422 (2011).

172. J. Wang *et al.*, Targeting the NG2/CSPG4 proteoglycan retards tumour growth and angiogenesis in preclinical models of GBM and melanoma. *PLoS One* **6**, e23062 (2011).
173. X. Wang *et al.*, CSPG4 in cancer: multiple roles. *Curr Mol Med* **10**, 419-429 (2010).
174. X. Wang *et al.*, CSPG4 protein as a new target for the antibody-based immunotherapy of triple-negative breast cancer. *J Natl Cancer Inst* **102**, 1496-1512 (2010).
175. Z. Rivera *et al.*, CSPG4 as a target of antibody-based immunotherapy for malignant mesothelioma. *Clin Cancer Res* **18**, 5352-5363 (2012).
176. H. Torisu-Itakura *et al.*, Redirected lysis of human melanoma cells by a MCSP/CD3-bispecific BiTE antibody that engages patient-derived T cells. *J Immunother* **34**, 597-605 (2011).
177. R. V. Iozzo, L. Schaefer, Proteoglycan form and function: A comprehensive nomenclature of proteoglycans. *Matrix Biol* **42**, 11-55 (2015).
178. M. A. Price *et al.*, CSPG4, a potential therapeutic target, facilitates malignant progression of melanoma. *Pigment Cell Melanoma Res* **24**, 1148-1157 (2011).
179. W. B. Stallcup, The NG2 antigen, a putative lineage marker: immunofluorescent localization in primary cultures of rat brain. *Dev Biol* **83**, 154-165 (1981).
180. S. Pellegatta *et al.*, Constitutive and TNFα-inducible expression of chondroitin sulfate proteoglycan 4 in glioblastoma and neurospheres: Implications for CAR-T cell therapy. *Sci Transl Med* **10**, (2018).
181. V. Leuci, C. Donini *et al.*, CSPG4-Specific CAR.CIK Lymphocytes as a Novel Therapy for the Treatment of Multiple Soft-Tissue Sarcoma Histotypes. *Clin Cancer Res*, (2020).
182. W. Luo *et al.*, Differential immunogenicity of two peptides isolated by high molecular weight-melanoma-associated antigen-specific monoclonal antibodies with different affinities. *J Immunol* **174**, 7104-7110 (2005).
183. J. Vera *et al.*, T lymphocytes redirected against the kappa light chain of human immunoglobulin efficiently kill mature B lymphocyte-derived malignant cells. *Blood* **108**, 3890-3897 (2006).
184. Y. Wang, F. Sabbatino, X. Wang, S. Ferrone, Detection of chondroitin sulfate proteoglycan 4 (CSPG4) in melanoma. *Methods Mol Biol* **1102**, 523-535 (2014).
185. J. Deng *et al.*, CDK4/6 Inhibition Augments Antitumor Immunity by Enhancing T-cell Activation. *Cancer Discov* **8**, 216-233 (2018).
186. A. R. Aref *et al.*, 3D microfluidic *ex vivo* culture of organotypic tumor spheroids to model immune checkpoint blockade. *Lab Chip* **18**, 3129-3143 (2018).
187. D. Morita *et al.*, Enhanced Expression of Anti-CD19 Chimeric Antigen Receptor in. *Mol Ther Methods Clin Dev* **8**, 131-140 (2018).
188. H. Singh, H. Huls, P. Kebriaei, L. J. Cooper, A new approach to gene therapy using Sleeping Beauty to genetically modify clinical-grade T cells to target CD19. *Immunol Rev* **257**, 181-190 (2014).
189. C. F. Magnani *et al.*, Immunotherapy of acute leukemia by chimeric antigen receptor-modified lymphocytes using an improved Sleeping Beauty transposon platform. *Oncotarget* **7**, 51581-51597 (2016).
190. P. Kebriaei *et al.*, Phase I trials using Sleeping Beauty to generate CD19-specific CAR T cells. *J Clin Invest* **126**, 3363-3376 (2016).
191. C. F. Magnani *et al.*, Sleeping Beauty-engineered CAR T cells achieve antileukemic activity without severe toxicities. *J Clin Invest* **130**, 6021-6033 (2020).
192. M. Franceschetti *et al.*, Cytokine-induced killer cells are terminally differentiated activated CD8 cytotoxic T-EMRA lymphocytes. *Exp Hematol* **37**, 616-628 e612 (2009).
193. Y. Pang, X. Hou, C. Yang, Y. Liu, G. Jiang, Advances on chimeric antigen receptor-modified T-cell therapy for oncotherapy. *Mol Cancer* **17**, 91 (2018).
194. R. G. Majzner *et al.*, CAR T Cells Targeting B7-H3, a Pan-Cancer Antigen, Demonstrate Potent Preclinical Activity Against Pediatric Solid Tumors and Brain Tumors. *Clin Cancer Res* **25**, 2560-2574 (2019).
195. H. Du *et al.*, Antitumor Responses in the Absence of Toxicity in Solid Tumors by Targeting B7-H3 via Chimeric Antigen Receptor T Cells. *Cancer Cell* **35**, 221-237.e228 (2019).
196. Z. Yuan, H. Yang, Y. Wei, Combined induction with anti-PD-1 and anti-CTLA-4 antibodies provides synergistic antitumor effects in DC-CIK cells in renal carcinoma cell lines. *Int J Clin Exp Pathol* **12**, 123-132 (2019).

197. M. Fane, A. T. Weeraratna, How the ageing microenvironment influences tumour progression. *Nat Rev Cancer* **20**, 89-106 (2020).
198. Q. Duan, H. Zhang, J. Zheng, L. Zhang, Turning Cold into Hot: Firing up the Tumor Microenvironment. *Trends Cancer* **6**, 605-618 (2020).
199. M. Binnewies *et al.*, Understanding the tumor immune microenvironment (TIME) for effective therapy. *Nat Med* **24**, 541-550 (2018).
200. R. J. DeBerardinis, Tumor Microenvironment, Metabolism, and Immunotherapy. *N Engl J Med* **382**, 869-871 (2020).
201. S. K. Vodnala *et al.*, T cell stemness and dysfunction in tumors are triggered by a common mechanism. *Science* **363**, (2019).
202. K. A. Gelderman, M. Hultqvist, J. Holmberg, P. Olofsson, R. Holmdahl, T cell surface redox levels determine T cell reactivity and arthritis susceptibility. *Proc Natl Acad Sci U S A* **103**, 12831-12836 (2006).
203. S. Cemerski, A. Cantagrel, J. P. Van Meerwijk, P. Romagnoli, Reactive oxygen species differentially affect T cell receptor-signaling pathways. *J Biol Chem* **277**, 19585-19593 (2002).
204. M. P. Keppel, N. Saucier, A. Y. Mah, T. P. Vogel, M. A. Cooper, Activation-specific metabolic requirements for NK Cell IFN-γ production. *J Immunol* **194**, 1954-1962 (2015).
205. S. E. Keating *et al.*, Metabolic Reprogramming Supports IFN-γ Production by CD56bright NK Cells. *J Immunol* **196**, 2552-2560 (2016).
206. S. Sarkar *et al.*, Hypoxia induced impairment of NK cell cytotoxicity against multiple myeloma can be overcome by IL-2 activation of the NK cells. *PLoS One* **8**, e64835 (2013).
207. Z. Zhao *et al.*, Structural Design of Engineered Costimulation Determines Tumor Rejection Kinetics and Persistence of CAR T Cells. *Cancer Cell* **28**, 415-428 (2015).
208. C. Sun *et al.*, THEMIS-SHP1 Recruitment by 4-1BB Tunes LCK-Mediated Priming of Chimeric Antigen Receptor-Redirected T Cells. *Cancer Cell* **37**, 216-225.e216 (2020).

Acknowledgements

I would like to express my sincere gratitude to my tutor, Prof. Dario Sangiolo, who supported my scientific growth, assisting and guiding me throughout my academic career.

I would like to show my profound appreciation to my co-tutor Dr. Valeria Leuci, who deeply helped me to finalize this thesis and our research projects.

I would also like to thank Dr. Ramona Rotolo for her complicity and all the essential advices.

I wish to acknowledge all the member of the Experimental Cell Therapy Lab for the lovely time spent together.

My special thanks go to my family and friends for their continuous support and unconditional love.